Doctoral Dissertation

Failure Mechanism of Lithium–Oxygen Batteries with a Redox Mediator

Seongmin Ha

Department of Energy Engineering

(Battery Science and Technology)

Graduate School of UNIST

2018

Failure Mechanism of Lithium–Oxygen Batteries with a Redox Mediator

Seongmin Ha

Department of Energy Engineering
(Battery Science and Technology)

Graduate School of UNIST

ULSAN NATIONAL INSTITUTE OF SCIENCE AND TECHNOLOGY

Failure Mechanism of Lithium–Oxygen Batteries with a Redox Mediator

A dissertation
submitted to the Graduate School of UNIST
in partial fulfillment of the requirements
for the degree of Doctor of Philosophy in Energy Engineering

Seongmin Ha

12 / 28 / 2017

Approved by

Advisor
Sung You Hong

Advisor
Kyu Tae Lee

ULSAN NATIONAL INSTITUTE OF SCIENCE AND TECHNOLOGY

Failure Mechanism of Lithium–Oxygen Batteries with a Redox Mediator

Seongmin Ha

This certifies that the dissertation of Seongmin Ha is approved.

12 / 28 / 2017

signature

Advisor: Sung You Hong

signature

Advisor: Kyu Tae Lee

signature

Nam–Soon Choi

signature

Yoon Seok Jung

signature

Seok Ju Kang

Abstract

Lithium–oxygen ($Li–O_2$) batteries are receiving large attention as a promising energy storage system for electrically powered mobile devices from mobile phone to electric vehicles due to their high energy density. However, the practical utilization of $Li–O_2$ batteries remain insufficient due to several drawbacks such as poor energy efficiency and cycle performance. Solid catalysts are suggested for reduced polarization of $Li–O_2$ batteries, resulting in the improving energy efficiency. However, solid catalysts exhibit the limited performance of $Li–O_2$ batteries due to the spatial limitation. The redox mediators as soluble catalysts has been introduced for not only improving energy efficiency, but also surmounting spatial constraint of solid catalysts for $Li–O_2$ batteries. The redox mediators effectively decreases the polarization for oxygen evolution reactions (OER) in the $Li–O_2$ batteries, leading to improving electrochemical performance. On the other hand, the reduced polarization by redox mediators gradually reverts to original high polarization over a certain number of cycles owing to a continuous loss of their catalytic activity as cycle number increasing. The shuttle effect for redox mediators has been considered to be associated with the degradation of $Li–O_2$ batteries with redox mediators, however, the failure mechanism does not fully elucidate the increasing polarization and loss of capacity observed with $Li–O_2$ batteries.

In this dissertation, it is demonstrated that the $Li–O_2$ cells involved redox mediator deteriorates due to low compatibility between redox mediator and cell components, such as electrolyte solvent and Li metal anode. The electrolyte solvents influence on the electrochemical reversibility and radical stability of redox mediator. It is demonstrated that the radical stability of redox mediator dominantly influence on the cycle performance of $Li–O_2$ batteries with redox mediator, whereas the electrochemical reversibility of redox mediator is hardly related with that of $Li–O_2$ batteries. Therefore, the appropriate solvent for the redox mediator promotes the stability of redox mediator radical, resulting in the enhanced performance of $Li–O_2$ batteries. Furthermore, the side reaction of redox mediator aggravates the electrochemical performance of Li metal and exhausts the redox mediators simultaneously. This unexpected reaction arises even though protective layer on the Li surface, which consists of lithium oxides formed by the oxygen contained in the electrolytes, covers the surface of Li metal. However, the introducing of $LiNO_3$ as a salt, which can act two roles, such as the fast protective layer generator and a capturer for the redox mediator radicals, alleviates the side reaction, resulting in the improved cycle performance of $Li–O_2$ batteries. Therefore, the optimization of electrolyte and the protection of Li metal anode for redox mediator strongly influence on the improving performance of $Li–O_2$ batteries with a redox mediator. To clarify the failure mechanism of $Li–O_2$ batteries containing redox mediators, 10–methylphenothiazine (MPT) is selected as a model redox mediator.

Keywords: Lithium oxygen batteries, Failure mechanism, Redox mediator, Electrolyte, Lithium metal anode

Contents

List of Figures

List of Table

Abbreviations

Abbreviation	Full name	Abbreviation	Full name
AN	Acceptor number	ccp	Cubic close–packed structure
$Co(Terp)_2$	Cobalt bis(terpyridine)	CV	Cyclic voltammetry
CW X–band	Continuous–wave X–band	Diglyme, G2	1–Methoxy–2–(2–methoxyethoxy)ethnae
DMAc	*N*,*N*–dimethylacetamide	DMC	Dimethyl carbonate
DME, monoglyme, G1	1,2–dimethoxyethane	DMF	Dimethylformamide
DMPZ	5,10–dihydro–5,10–dimethylphenazine	DMSO	dimethyl sulfoxide
DN	Donor number	EC	Ethylene carbonate
EDS	Energy dispersive X–ray spectroscopy	EES	Electrochemical energy storage
EMC	Ethyl methyl carbonate	EMS	Ethyl methyl sulfone
EPR	Electron paramagnetic resonance	ESR	Electron spin resonance

EV	Electric vehicles	FePc	Iron phthalocyanine
^{1}H NMR	^{1}H Nuclear magnetic resonance	HSAB	Pearson's hard–soft acid–bases theory
ICE	Initial Coulombic efficiency	IPA	Isopropanol
KB	Ketjenblack	LED	Low electron detector
LIBs	Lithium–ion (Li–ion) batteries	LOBs	Lithium–oxygen (Li–O_2) batteries
LSBs	Lithium–sulfur (Li–S) batteries	MPT	10–methylphenothiazine
$MPT^{\bullet+}$	Oxidized MPT, MPT radical	NMP	1–Methylpyrrolidin–2–one
OER	Oxygen evolution reaction	OLO	Over–lithiated oxide (Lithium– and manganese–rich oxide)
ORR	Oxygen reduction reaction	PC	Propylene carbonate
PLIBs	Post lithium–ion batteries	PTFE	Poly(tetrafluoroethylene)
SEI	Solid–electrolyte interphase	SEM	Scanning electron microscope

TDPA	Tris(4–(diethylamino)phenyl)amine	TEGDME, Tetraglyme, G4	2,5,8,11,14–Pentaoxapentadecane
TEMPO	2,2,6,6–tetramethyl–1–piperidinyloxy	TM	Transition metal
TMS	Tetramethylsilane	TOF–SIMS	Time–of–flight secondary ion mass spectrometry
Triglyme, G3	1,2–Bis(2–methoxyethoxy)ethane	TTF	Tetrathiafulvalene
XRD	X–ray diffraction		

1. Introduction

1.1 Next generation rechargeable batteries

Since industrial revolution, the technologies of humanity have developed steadily to enrich our life. Various and large amount of electronic devices have been supplied to the worldwide from household to industries due to their usability. However, this development has brought us many concerns. Among them, global warming and the depletion of fossil fuels are strongly influencing on our life, for example, rapid climate change, global air pollution, and increasing energy cost. The simple method to prevent the crises is reducing energy consumption. However, because we cannot easily give up our developed and convenient life, the electrification of overall industries from small portable devices to smart electricity grid has been adopted as an irreplaceable global strategy for addressing these serious global issues. Electric vehicle (EV), smart grid involving electrochemical energy storage (EES), and renewable energy generation has been introduced to solve two problems simultaneously. However, the requirements, such as high specific energy and/or energy density, high energy efficiency, long cycle life, low cost per energy and maintenance cost, and eco–friendly, of electrochemical energy storage devices must be enhanced than conventional rechargeable batteries. For example, to facilitate a driving range of more than 500 km for EV, it must be supplied the rechargeable batteries with a practical specific energy in cell level of above 350 Wh kg^{-1} at least as shown in Figure 1.1a.[1-2] Contrastively, the state–of–the–art lithium–ion batteries (LIBs) only exhibit practical specific energy of 256 Wh kg^{-1} as shown in Figure 1.1b.[3] Therefore, various next generation rechargeable batteries have are suggested to deviate from the fossil fuel industry and for realizing the zero emission of greenhouse effect gases.

Since commercialization in 1991,[4] the performance of LIBs have been improved steadily by the development of materials and cell preparing process. LIBs is widely using from mobile phone to EES due to their highest practical specific energy and energy density than other conventional rechargeable batteries. However, even though the performance of LIBs achieves the value similar to their theoretical specific energy or energy density, the LIBs are deficient to satisfy demands for high performance mobile devices, EV, and EES. Therefore, the post lithium–ion batteries (PLIBs) has been introduced for overcoming the insufficiency. One approaches for the improvement are the development of electrode materials with higher capacity for LIBs, such as nickel–rich and over–lithiated (lithium– and manganese–rich) layered oxide as a cathode, and silicon and lithium metal as an anode. (part 1.1.1) The other approaches are the introducing and developing the new electrochemical energy storage system, such as sulfur–based (lithium–sulfur batteries, part 1.1.2) and oxygen–based (lithium–oxygen batteries, part 1.2). Because the prior approaches are based on the LIBs technologies, it has already been introduced partially in commercial products or may be commercialized within the 10 years. On the other hands, the latter approaches are still in laboratory stage; therefore, it needs to investigate intensively.

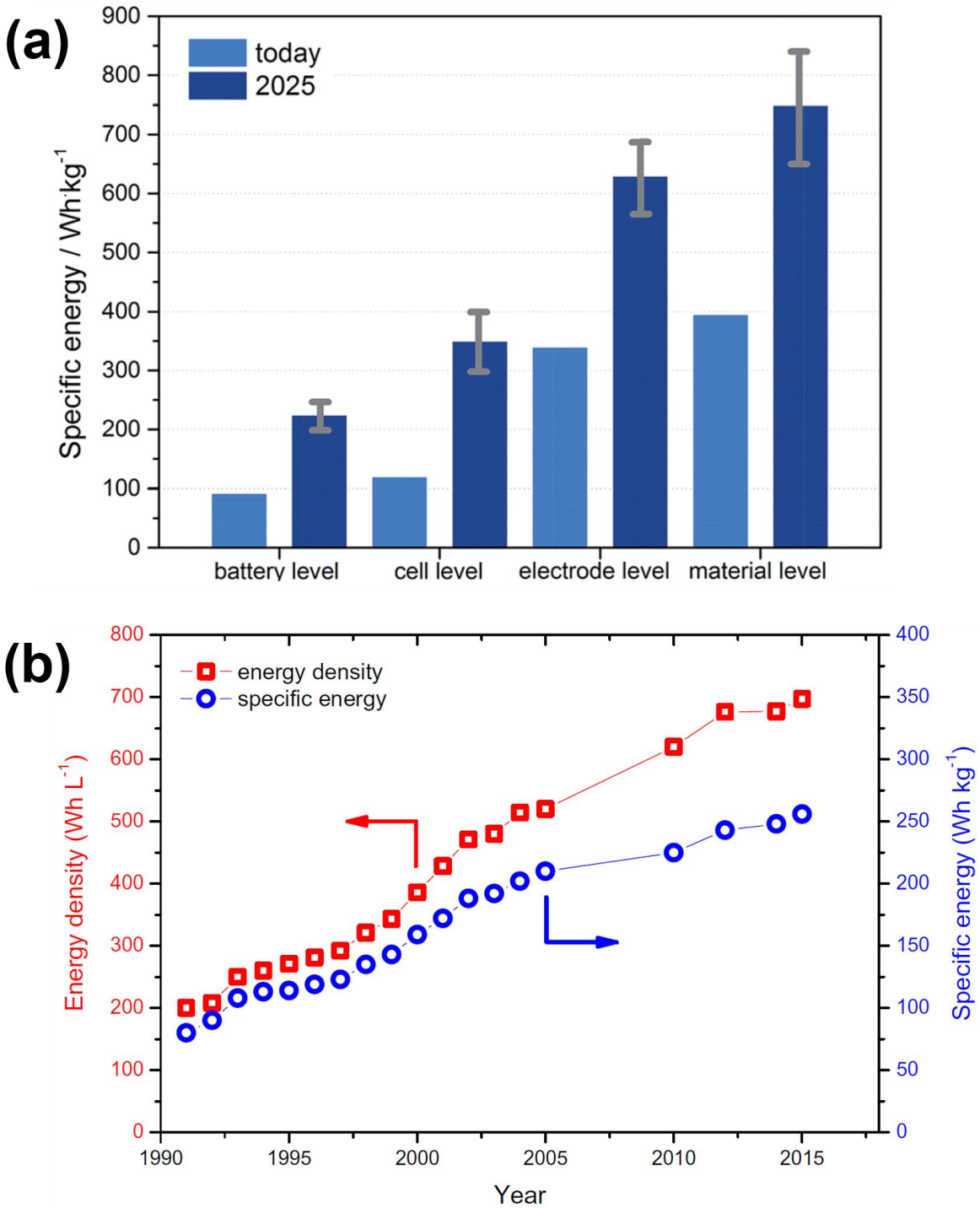

Figure 1.1 (a) The present value and target value (for 500 km per charge) of specific energy for the present and future generation of battery pack, cell, electrodes, and cathode active materials. Reprinted by permission from ref. 2. Copyright 2015 Royal Society of Chemistry. (b) Improvement of the specific energy and energy density of cell level Li–ion batteries (LIBs) from 1991 to 2017. Reprinted by permission from ref. 3. Copyright 2017 Springer Nature.

1.1.1 Post lithium–ion batteries (PLIBs)

Ni–rich layered oxide as a cathode material

The first commercialized LIBs consisted of lithium cobalt oxide ($LiCoO_2$) as a cathode (positive electrode), coke (soft carbon) as an anode (negative electrode), and non–aqueous electrolyte, which was achieved with 80 Wh kg^{-1}, 200 Wh l^{-1}, and the cell voltage of 3.7 V *vs*. Li/Li^+.[4-5] To enhance the performance and decrease the cost of LIBs, the cobalt metal in the $LiCoO_2$ of layered oxide structure was substituted other transition metal, such as nickel, manganese, and aluminum. Firstly, $LiNi_{1/3}Co_{1/3}Mn_{1/3}O_2$ was suggested for improving capacity, higher reversibility, and thermal stability.[6-7] However, the 1/3 layered oxide exhibited a low degree of increased capacity (*ca.* 153 mA g^{-1}),[7-8] and the content of cobalt must be reduced in the composition of transition metal due to their high cost. Among layered oxide with various composition of transition metal, nickel–rich layered oxide materials, $LiNi_xCo_yM_zO_2$ (M = Mn or Al, $x + y + z = 1$, $x \geq 0.5$) as shown in Figure 1.2a, is attracting an attention, the origin of which can be traced to the early works by the Dahn's group.[9] In fact, $LiNi_{0.8}Co_{0.15}Al_{0.05}O_2$ as thermally stabilized nickel–rich oxide by aluminum are already commercialized.[10] All of layered materials have an alternately repeated slabs consisting of Li and transition metal (TM) in the cubic close–packed (ccp) frame of oxygen atoms as shown in Figure 1.2b. The octahedral sites between oxygen frames contain Li and TM ions, in which form the corresponding slab. In addition, there is scattered some Li–TM mixing sites throughout the host structure due to the cation size similarity between Li and Ni ions. The Ni–rich oxide have higher specific capacity owing to their electronic structure; the e_g band of TM separates from 2p band of oxygen in contrast with those of $LiCoO_2$, allowing in a higher degree of oxidation without oxygen evolution. As a result, Ni–rich oxide have a higher capacity of 180 ~ 200 Wh kg^{-1} than that of $LiCoO_2$.[11-12] Despite high capacity of Ni–rich oxide, the layered oxide is suffering from the low cyclability, arising from structural and surface change. Crystallographically, because of the cation size similarity, the TM cation in TM slab preferentially migrates to octahedral site in Li slab during delithiation, resulting in transformation of crystal structure from layered to electrochemically inactive spinel–like and/or cubic (NiO, MnO) structure depending on the degree of delithiation as shown in Figure 1.3a.[13-14] This partial structural change occurs during cycling, arising the dropping redox potential, slower rate capability, and capacity fading due to partial shrinkage of c–axis for crystal structure.[12-13] Moreover, this change influences on the interfacial instability of Ni–rich oxide. The rock salt cubic structure grows form surface to bulk at initial stage delithiation, and then, this disordered layer maintain the thickness of tens of nanometer over further cycles as shown in Figure 1.3b.[12, 15] Despite maintaining the thin thickness, this layer on the surface impedes the lithiation/delithiation process. In addition, this surface deformation also arises the dissolution of TM ions into the electrolyte, resulting in the decreasing reversible capacity and forming electrochemically inactive interfacial compounds.[12, 16-17] This interfacial compounds also increases the

impedance of the Ni–rich oxide. Some strategies, for example, TM doping,[10, 18-24] surface coating with chemically/electrochemically stable materials,[25-31] and introducing of spinel phases near the surface of oxide or concentration gradient structures,[32-33] have been suggested to mitigate the failure of Ni–rich oxide. The developing progress may be a rough journey because thermodynamically preferred phase transition arises the failure of Ni–rich oxide, nonetheless, the developments is expected to continue for searching outstanding solutions owing to their relatively higher possibility of realization.

Li– and Mn– rich (over–lithiated) layered oxide as a cathode material

Li– and Mn–rich (over–lithiated) layered oxide (OLO) originates from the early works by the Thackeray groups.[34] They exhibited that the Li_2MnO_3 as a layered rock–salt structure can have electrochemically activity with respect to Li insertion/deinsertion process by acid treatment or electrochemical charging over a high potential of 4.5 V *vs*. Li/Li^+ accompanying with oxygen evolution.[35-37] Li_2MnO_3 can also be represented the layered $LiMO_2$ notated as $Li[Li_{1/3}Mn_{2/3}]O_2$, where consists of interslab octahedral sites occupied by Li^+ only and slab octahedral sites occupied by Li^+ and Mn^{4+} (in an atomic ratio of 1:2) as shown in Figure 1.4a. The structure of OLO has described as a single phase solid solution (notation: $Li[Li_{a/3}Ni_{b/3}Co_{c/3}Mn_{d/3}]O_2$ (a + b + c + d = 3)) or a composite of two phase (notation: $xLi_2MnO_3 \cdot (1\text{-}x)LiNi_aCo_bMn_cO_2$ (a + b + c = 1)); the rhombohedral phase ($R\bar{3}m$, $LiMO_2$) and monoclinic phase (C2/m, Li_2MnO_3).[35, 38-39] The delithiation/lithiation process consists of 3 steps in case of electrochemical activation as shown in Figure 1.4b:[40] Li^+ is extracted from the Li^+ only interslab site during the first delithiation until *ca.* 4.4 V *vs*. Li/Li^+. Until the end of voltage plateau of *ca.* 4.5 V *vs*. Li/Li^+, the lithium oxide (Li_2O) and oxygen gases (O_2) releases from the materials, resulting in the formation of MnO_2, which could be intercalated subsequently Li^+. Beyond activation, above 4.6 V *vs*. Li/Li^+, Li^+ is extracted from the TM slab, and TM ions migrates to the Li only slab. During discharge, as shown in Figure 1.4c, Li^+ firstly inserts into the TM slab at high potential. The insertion of Li^+ into the Li slab gardually occurs at below 3.5 V (*vs.* Li/Li^+). After the activation, the layered oxide possesses reversible capacity of above 250 mA h g^{-1} depending on the type of TM. The migration of TM ions into the Li slabs in order to the charge compensation for oxygen causes a voltage hysteresis between delithiation and lithiation.[14, 41] In addition, this TM ions gradually make inactive sites and traps the Li^+ in the Li slabs during cycle, indicating the capacity and voltage fading of OLO. Furthermore, TM ions trapped sites in the Li slabs impedes the diffusion of Li^+ into the TM slab sites, resulting in the structure change from layered to spinel leading to the decreasing redox potential.[42-43] TM dissolution also degrades the capacity of OLO owing to the HF attack, which is easily formed at high potential.[44] To mitigate the voltage and capacity degradation, the optimization of electrochemical operating condition was introduced, for example, electrochemical activation at low temperature and stepwise potential activation, resulting in the decreased capacity fading due to the interface modification.[45-47] The use of alternative electrolyte and additives was also evaluated for the suppressing TM dissolution and surface

reorganization.[44] The surface coating and doping, similar to the case for Ni–rich oxide, also exhibited a promising possibility for improved performance of OLO.[18, 22-23, 27] In contrast to the Ni–rich oxide, the understanding of the failure mechanism of OLO is in laboratory stage and the relatively cost–effective approaches for the layered oxide are less available for OLO, leading to slower progress towards commercialization.[8]

Silicon material as an anode material

The enhanced specific energy and/or energy density of PLIBs can be achieved when the specific energy and/or energy density of not only cathode, but also anode is improved. Especially, the alternative anode, such as silicon and lithium metal, must be adopted for satisfying to the demand for EV with the operating range of above 500 km.[2, 48] Since the Argonne National Laboratory and General Motors examined the silicon (Si) as anode for lithium–metal sulfide batteries in the 1970s,[49-50] Si material have been attracting an intensive attention due to not only their high theoretical specific capacity of above 4000 mA h g^{-1}, but also the low operating voltage of *ca.* 0.3 V *vs.* Li/Li^+.[8, 51] In contrast to the layered oxide or graphite, the lithiation/delithiation process of Si is based on the alloying process via following reaction:

$$4.4Li + Si \leftrightarrow Li_{4.4}Si$$

This process is accompanying with the huge volumetric change of above 400 %.[51] This volume expansion cause the severe drawbacks, such as pulverization, delamination from current collector, and the thick formation of solid–electrolyte interphase (SEI), which interrupts the commercialization of Si anode for PLIBs as shown in Figure 1.5a.[8, 51-52] At the initial stage of research toward Si materials, nanostructured, carbon composite electrode, and effective binder capable of accommodating huge volume change have been introduced to reduce the pulverization and delamination as shown in Figure 1.5b.[52-66] Moreover, the new designed electrolyte has been also suggested to maintain the stable SEI.[67-69] In spite of the significant improved performance of Si used with the solutions, the silicon monoxide (SiO_x, $x \approx 1$) has been adopted for the battery industry instead of the above mentioned solutions owing to their more reasonable price and reliable production quality as shown in Figure 1.6a.[70-71] However, because the poor initial Coulombic efficiency (ICE), SiO_x has been only used less 5 wt% in a blended form with graphite. The low ICE requires the additional cathode materials, leading to the loss in the specific energy and/or energy density of the entire cell. In this context, attempts to the manufacturing the prelithiated Si anode using solution or electrochemical process has been increasing as shown in Figure 1.6b.[72-74] Combining the prior method, such as nanostructured electrode, binder tolerant to volume change, electrolyte forming stable SEI, and pre–lithiated Si, could be achieved the high ICE, reversible capacity, and cyclability of Si anode. However, the specific energy and energy density of this

system is still insufficient to satisfy the demands for EV.

Lithium metal as an anode material

Since Stanley Whittingham at Exxon was conceptually introduced for the Li–TiS_2 system in 1970s,[75] Li metal anode had been intensively for Li batteries. When the Li batteries containing a Li metal anode and a MoS_2 cathode was commercialized firstly in the late 1980s by Moli Energy,[76-77] this cylindrical–type cells exhibited a hundreds of cycle performance, therefore, millions of cells were sold to the market. However, this batteries became notorious for safety issues, including frequent and severe fires arose from the dendrite formation, to the public.[78-79] At that time, Sony launched the Li–ion batteries containing carbonaceous anodes to replace Li metal successfully, and this cell has been exhibited high reliability until now.[4] As a result, the entire Li batteries using Li metal anode was recalled and disappeared without any trace from the market, furthermore, the research related with Li metal anode has also been drastically reduced. Nowadays, the increasing demands for higher specific energy and/or energy density of rechargeable batteries is revitalizing the research on the Li metal anode again owing to their highest theoretical capacity (3860 mA h g^{-1}, 2061 mA h cm^{-3}) and lowest electrochemical potential (-3.04 V *vs*. SHE) than all possible alkali metal. To become a viable technology, the Li anode is need to surmount the tremendous drawbacks: dendrite growth and unstable interface, which is complicate correlation with the failure of Li metal anode as shown in Figure 1.7a.[78-81] The dendrite growth is related with inhomogeneous dissolution and plating, arose from the non–uniform native oxide and current density on the Li metal surface. This dendrite grows on the Li metal surface during the Li stripping/plating, resulting in the internal short circuit and the vigorous morphological change, such as porous surface structure and dead lithium. Furthermore, this morphological change leads to the formidable decomposition of electrolyte, resulting in the thick passivation retarding the Li^+ diffusion and depletion of electrolyte. The volume change of Li metal anode also impedes the stable cyclability due to their reaction mechanism analogous to conversion and alloying materials, in contrast to intercalation materials. To deal with these issues, it need to obtain a profound insight toward interfacial chemistries, stripping/plating behavior of Li, and the entangled interaction among them. To understand the interfacial chemistry, ever since Emanuel Peled and Doron Aurbach as a pioneer have firstly studied toward component of interfacial layer, the SEI on the Li metal has been investigated with various electrolyte.[82-85] The passivation by the 'mosaic structured' SEI suppresses the continuous decomposition of electrolyte and make it available to stably operate a Li metal containing cell under a highly reductive circumstance as shown in Figure 1.7b. However, the passivation is vulnerable to considerable interface fluctuation, leading to continuously forming SEI on the Li metal and exhausting the electrolyte. To resolve the unstable interface, various electrolyte engineering has been introduced, for example, ether–based electrolyte,[86-94] salt and gaseous form additive,[95-103] fluorinated or organic compound,[103-112] self–healing electrostatic shield as shown in Figure 1.8a,[112-113] and high salt concentration.[114-115] Instead of

the consumable techniques, the permanent protective layer has been also introduced, such as artificial SEI,[102-103, 116-123] artificial layer for isolating and controlling the interface between Li metal and electrolyte as shown in Figure 1.8a,[124-132] scaffolds or morphological change for guiding the Li stripping/plating,[133-138] and solid electrolyte.[139-143] Despite these suggested technologies for use of Li metal as an anode in Li–based batteries are enhanced the performance of Li metal anode, it need to verify the safety and performance corresponding to the level of industries to prevent the prior misstep. However, the investigation and improvement toward Li metal anode must be retained owing to being beneficial in the long run for not only Li–metal batteries but also new Li–based battery systems, such as lithium–sulfur (Li–S) and lithium–oxygen (Li–O_2) batteries.

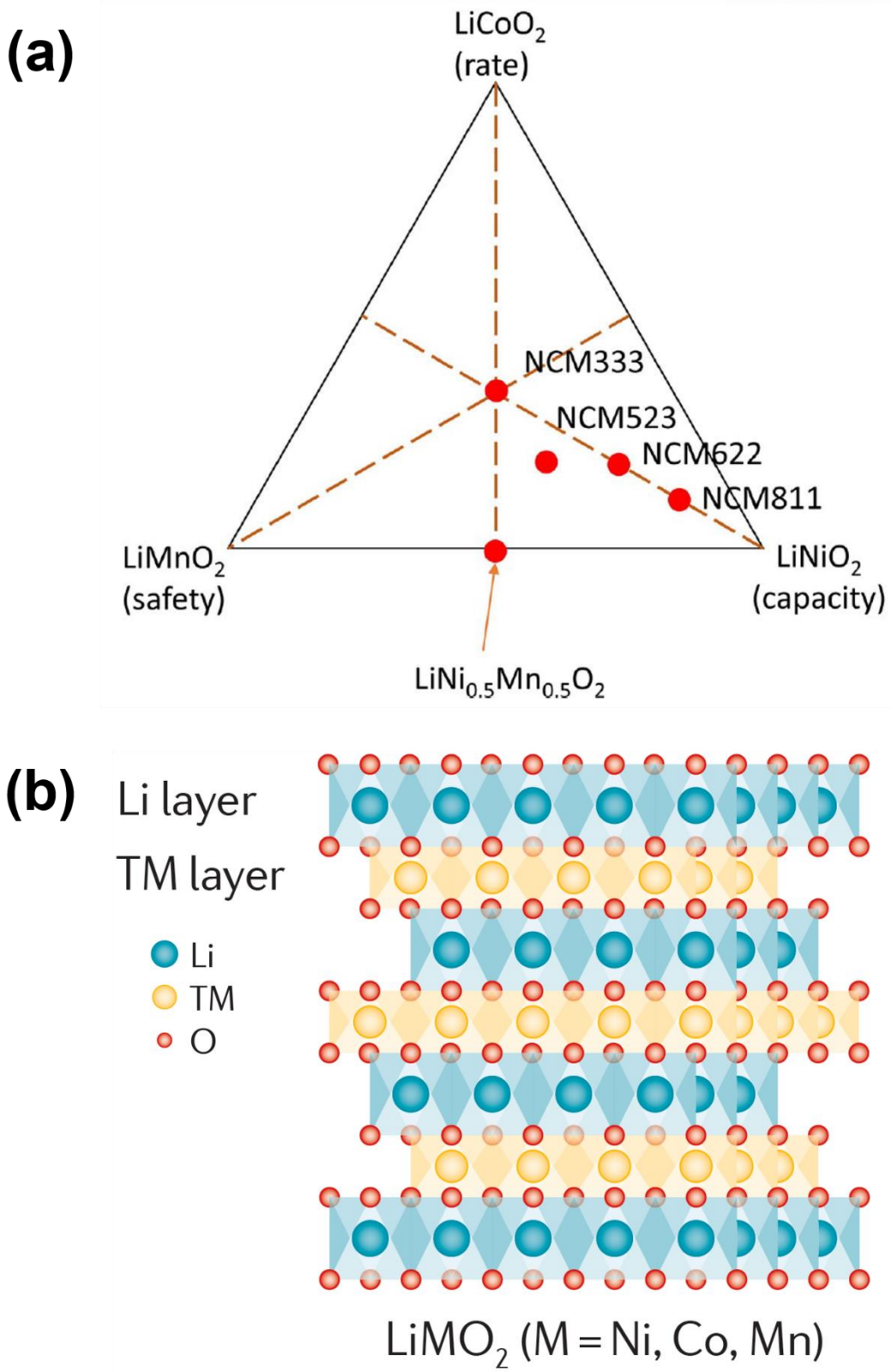

Figure 1.2 (a) Phase diagram of the ternary system between $LiNiO_2$, $LiCoO_2$, and $LiMnO_2$ with some representative composition. Reprinted by permission from ref. 12. Copyright 2017 The Electrochemical Society. (b) Crystal structure of layered $LiMO_2$ (M = Ni, Co, and/or Mn). Reprinted by permission from ref. 8. Copyright 2016 Springer Nature.

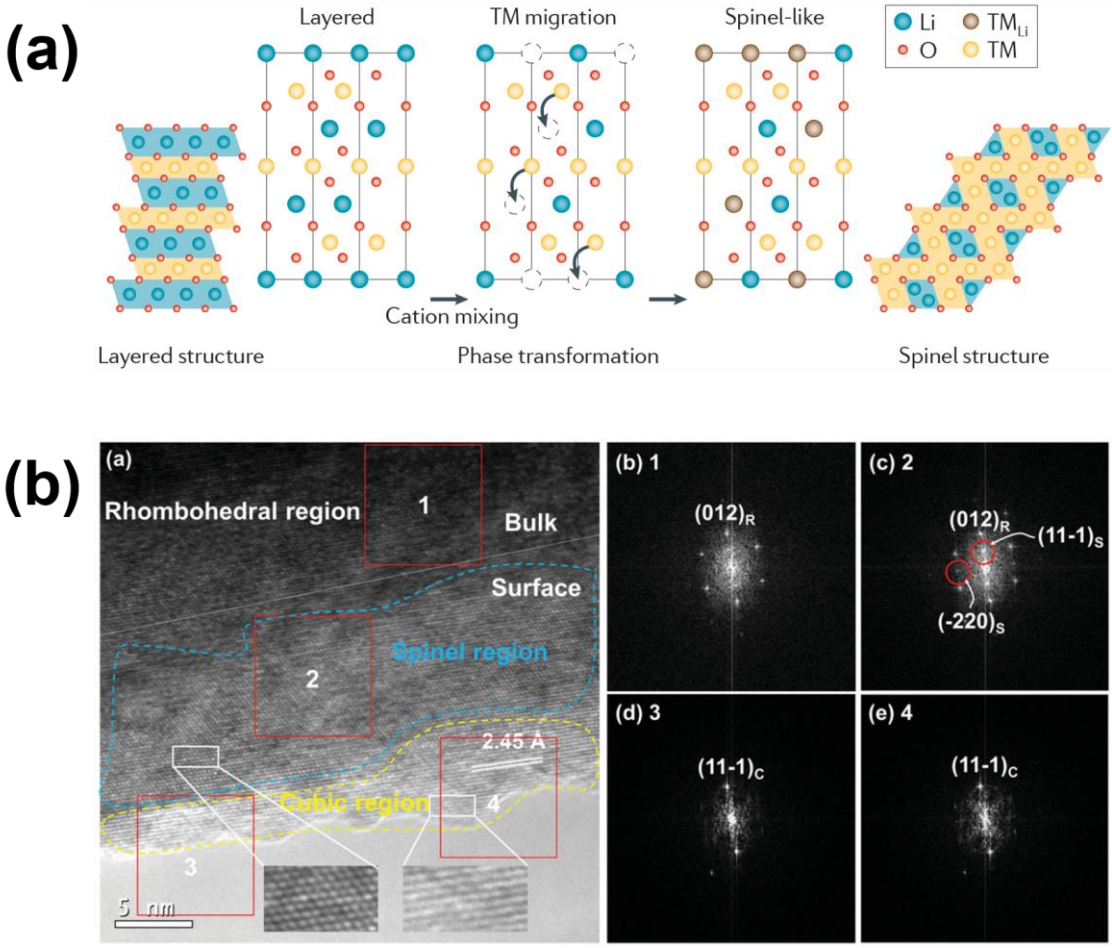

Figure 1.3 (a) Proposed phase transition process from layered to spinel–like structure of TM over charging. Reprinted by permission from ref. 8. Copyright 2016 Springer Nature. (b) Partial crystal structure change of $LiNi_{0.5}Co_{0.2}Mn_{0.3}O_2$ on the surface region after 50 cycles. Reprinted by permission from ref. 15. Copyright 2013 John Wiley & Sons, Inc..

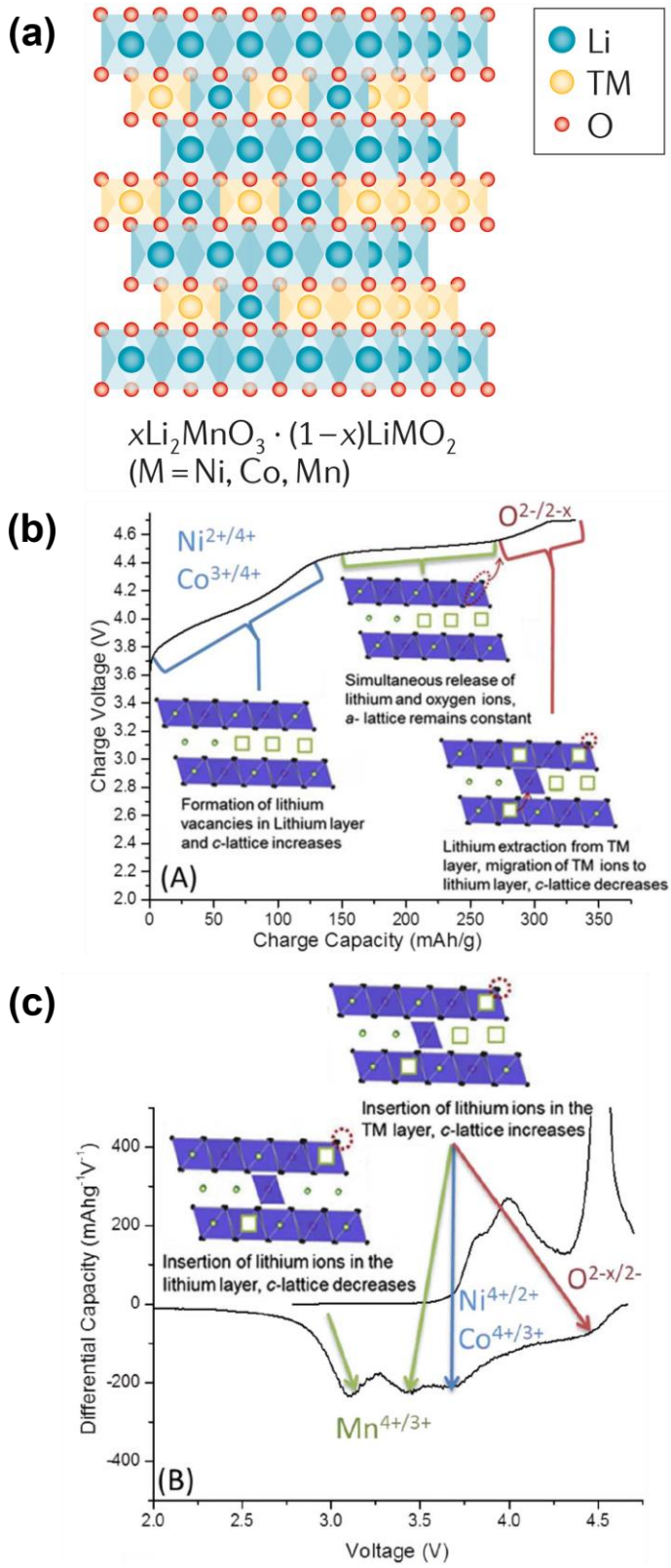

Figure 1.4 (a) Crystal structure of over–lithiated oxide (OLO). Reprinted by permission from ref. 8. Copyright 2016 Springer Nature. (b) Voltage profile during charge and (c) dQ/dV plot during discharge of 1st cycle for $0.35LiMn_2O_3 \cdot 0.65Li(Ni_{0.35}Co_{0.20}Mn_{0.45})O_2$. Reprinted by permission from ref. 12. Copyright 2017 The Electrochemical Society.

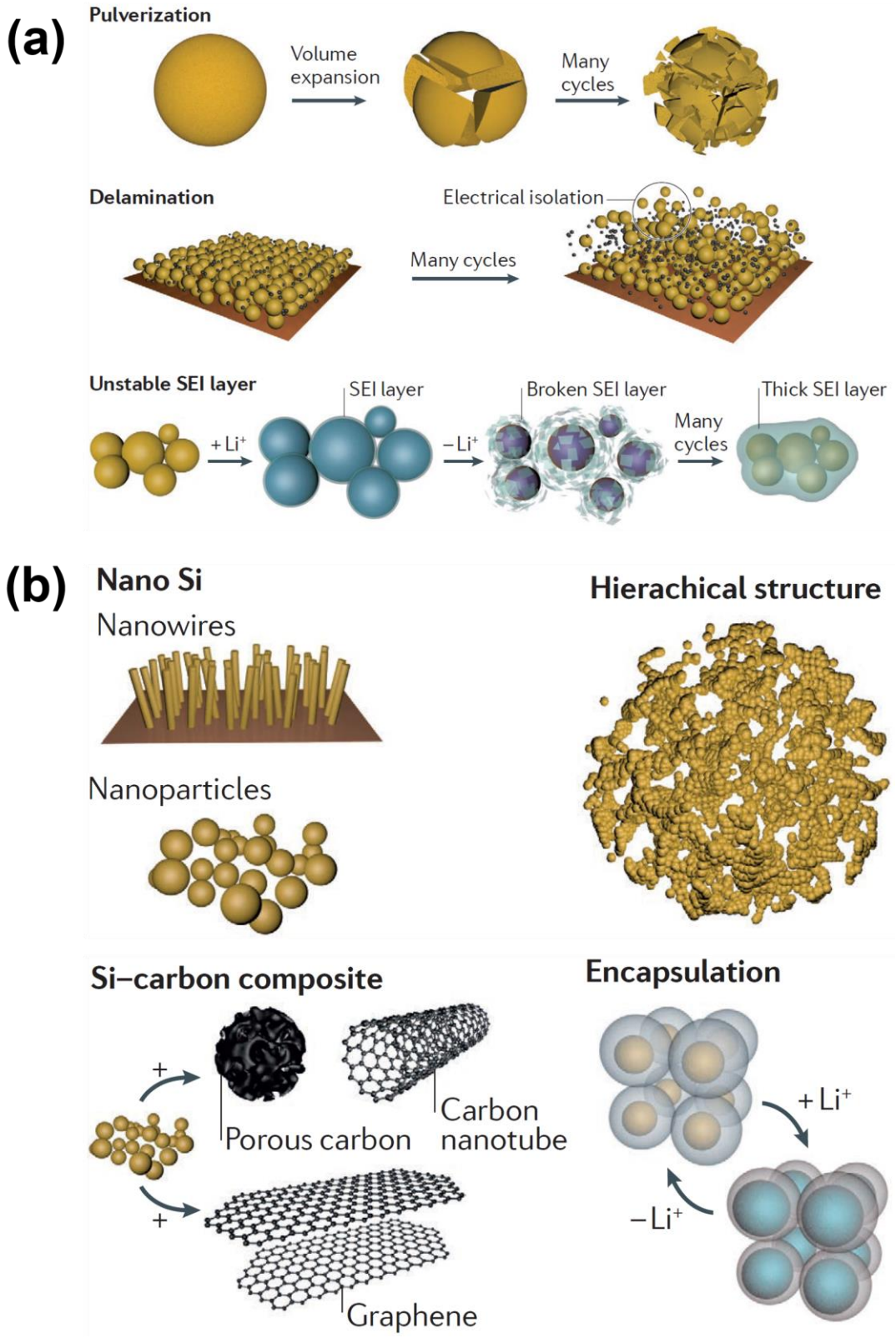

Figure 1.5 Schematic diagrams (a) for the failure mechanism of Si anode and (b) of nanostructured Si anodes and their composites. Reprinted by permission from ref. 8. Copyright 2016 Springer Nature.

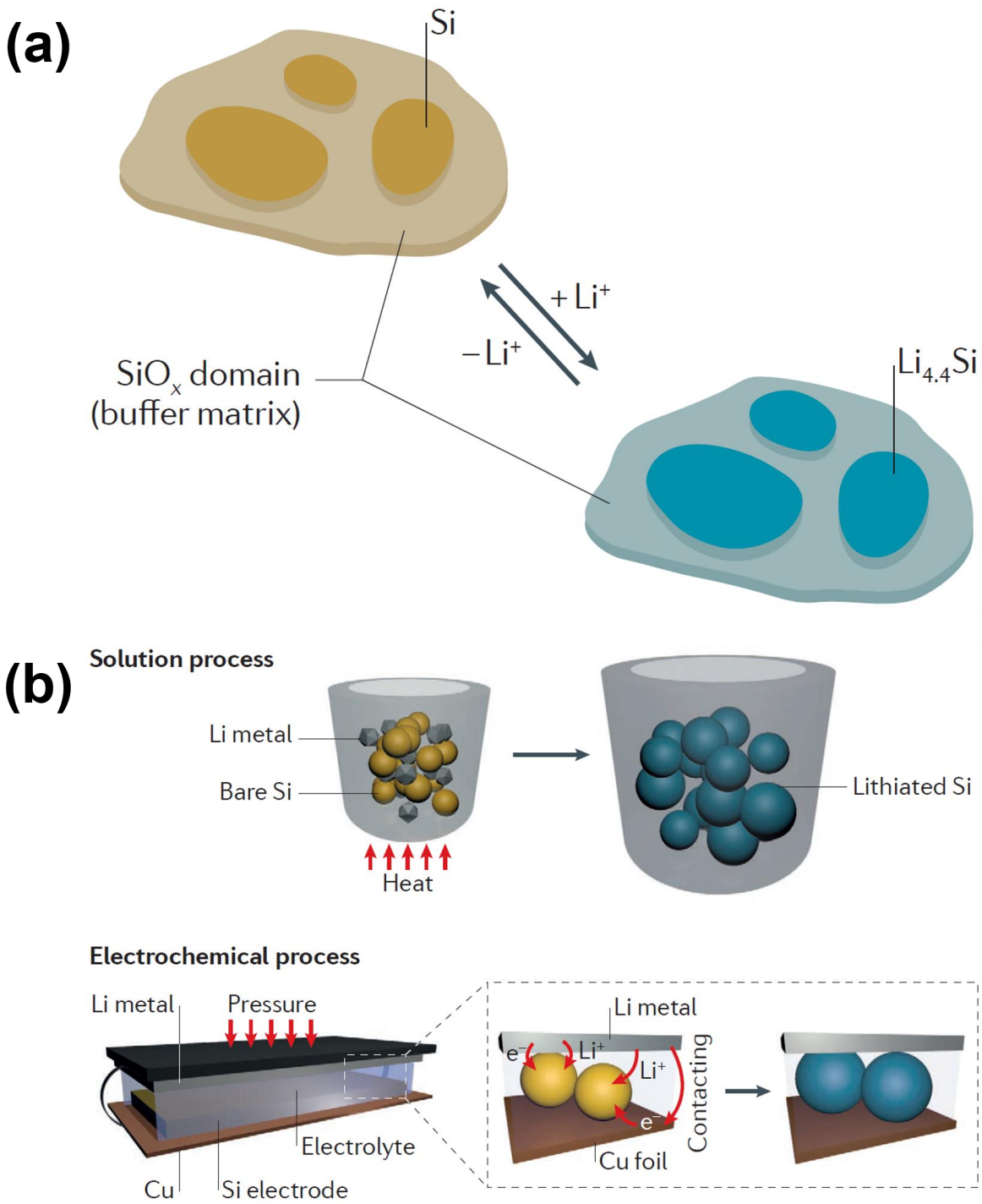

Figure 1.6 Schematic diagrams of (a) reaction process toward SiO_x anode and (b) pre–lithiated Si anodes via a solution and electrochemical processes. Reprinted by permission from ref. 8. Copyright 2016 Springer Nature.

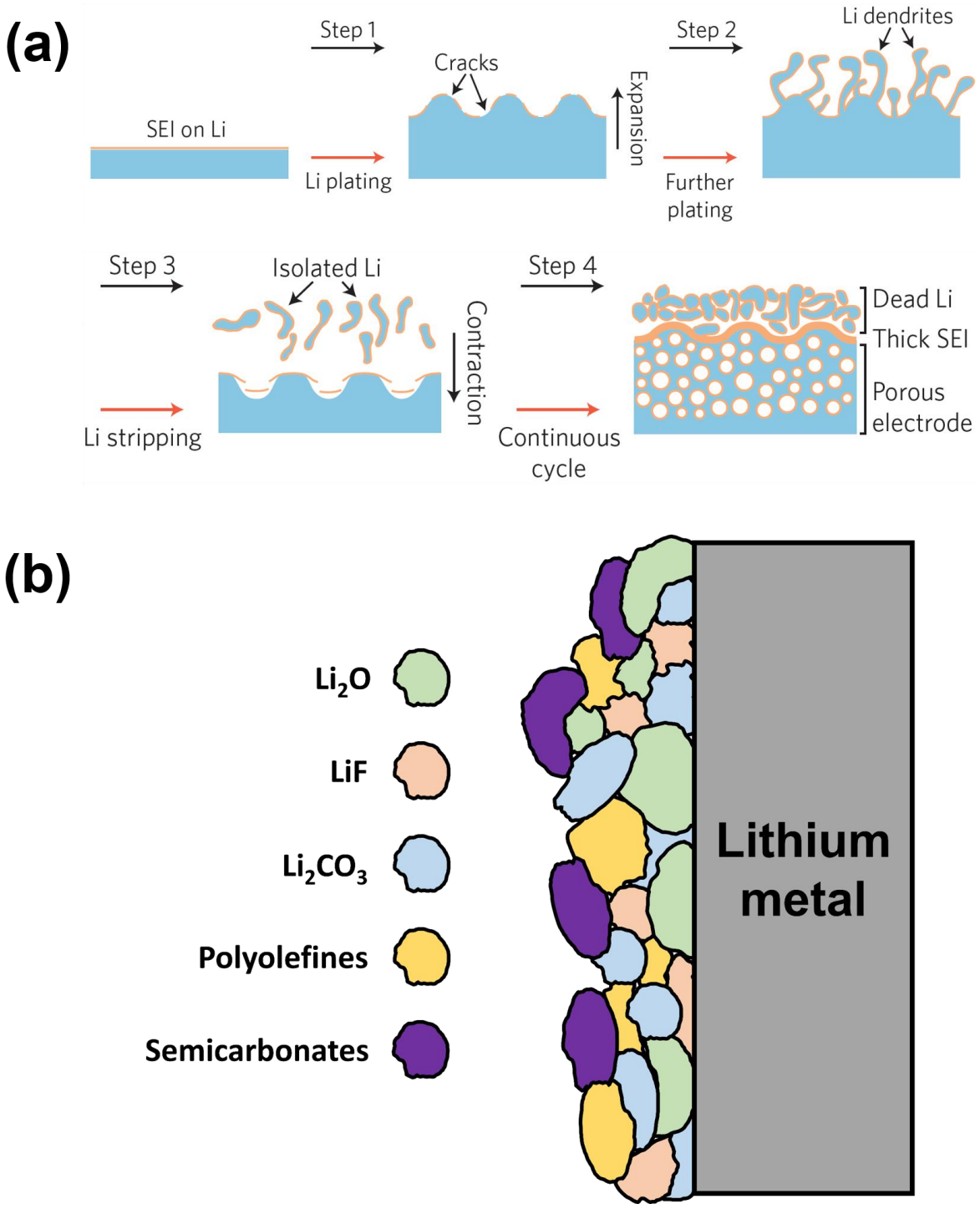

Figure 1.7 Schematic diagrams of (a) the failure mechanism toward Li metal during cycling. Reprinted by permission from ref. 79. Copyright 2017 Springer Nature. (b) Schematic cross–section diagram of the "mosaic" morphology of solid–electrolyte interphase (SEI) on the Li metal.

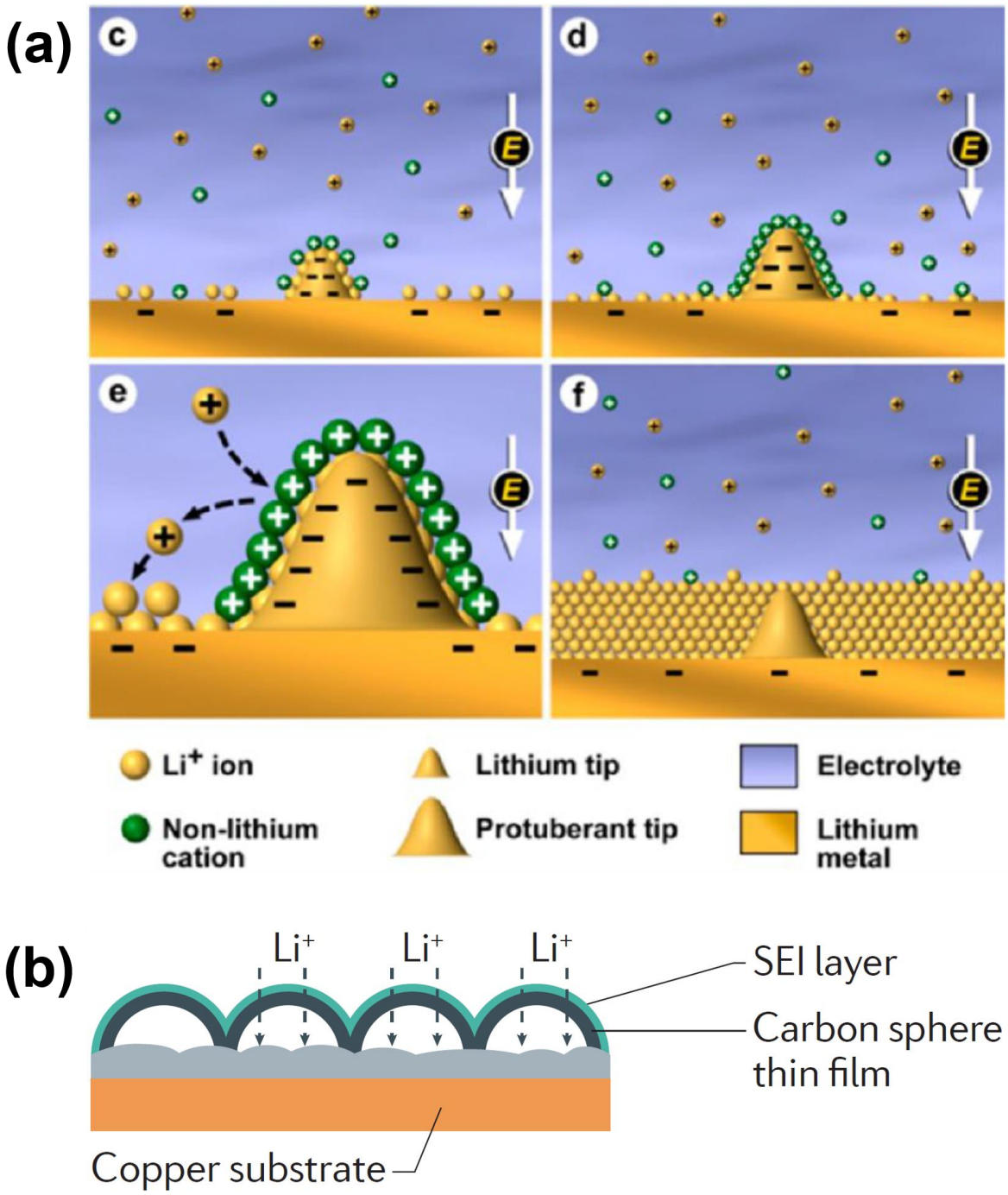

Figure 1.8 Schematic diagram of (a) the self–healing electrostatic shield (SHES) mechanism toward Li metal during cycling. Reprinted by permission from ref. 113. Copyright 2013 American Chemical Society. (b) Schematic cross–section diagram of the artificial layer for isolating and controlling the interface between Li metal and electrolyte. Reprinted by permission from ref. 8. Copyright 2016 Springer Nature.

1.1.2 Sulfur–based batteries (Li–S batteries)

To surpass the limiting specific energy of LIBs, the weight of active materials and inactive materials, such as host materials and conductive carbon, must be reduced. In this context, lighter elements as a redox center have been considered to electrode material for new electrochemical energy storage system. Among these new electrochemical energy storage system to replace the Li–ion batteries, sulfur–based batteries is one of the most promising energy storage system owing to their high theoretical specific energy, low cost, and abundant reserves. Ever since Herbet and Ulam at Electric Tech Corp. introduced the sulfur as a cathode for electrochemical cell conceptually in 1962,[144] alkali metal–sulfur energy storage system, such as sodium–sulfur (Na–S) and lithium–sulfur (Li–S) batteries,[145-146] had been investigated but were abandoned soon. However, since the demand for the high energy storage system has begun to increase, the intensive research toward Li–S batteries (LSBs) has been revitalized. The reason is that the cell operates at room temperature in contrast to Na–S batteries to operate at a temperature of 300–350 °C and have the theoretical specific and energy density of 2500 W h kg^{-1} and 2800 W h l^{-1}.[147] Especially, PolyPlus and Sion Power Corporation are developing the proto–type LSBs for unmanned vehicles and military–purpose devices. However, LSBs has been still not materialized the promising energy storage devices to overtake commercialized LIBs owing to their several limitation inherent in the reaction chemistry:[8, 147] (1) insulating nature of sulfur leading to poor reversibility and low rate capability; (2) soluble polysulfide intermediates (Li_2S_x, $3 \leq x \leq 6$) leading to the shuttle phenomenon; and (3) unstable interface between Li and electrolyte. One approaches to dissolution of polysulfides is the designing sulfur cathode structure. The encapsulating technique with conductive porous materials to sulfur has been introduced to resolve the sulfur cathode related two problems simultaneously.[148-151] The conductive materials, for example, mesoporous activated carbon fibers or nano–sized assemblies, not only provide the electron conducting path for insulating sulfur, but also reduce the dissolution of polysulfide as shown in Figure 1.9a. This dissolution suppressing progresses via the depleting contact area between polysulfide and electrotype or the enhancing binding affinity to polysulfides. The introducing $LiNO_3$ in the electrolyte can be exhibited not only the inhibiting effect of the dissolution, but also catalytic effect for the redox reaction of sulfur.[95, 152] Moreover, the SEI formed on the sulfur filling in micropore can be prevented the dissolution as shown in Figure 1.9b.[153-154] The appropriate content of sulfur in micropore excludes accessing other electrolyte solvent molecules to the micropore, leading to the redox reaction of polysulfides in solid phase, so called the quasi–solid–state reaction with desolvated Li^+. The relatively insoluble small sulfur allotrope and chemically bound sulfur to polymer can be also suppress the dissolution.[155-157] In a practical point of view, the low energy density arose from the low density and loading amount of sulfur must be surpassed by designing high density electrode accompanying with alleviating polysulfide dissolution. Furthermore, the limitation of Li metal as above mentioned can be also considered for the commercialization of LSBs. However, despite the

drawbacks of LSBs will be resolved, the specific energy and/or energy density of LSBs in full package scale of batteries may be still insufficient to satisfy the demand for high energy needed devices.

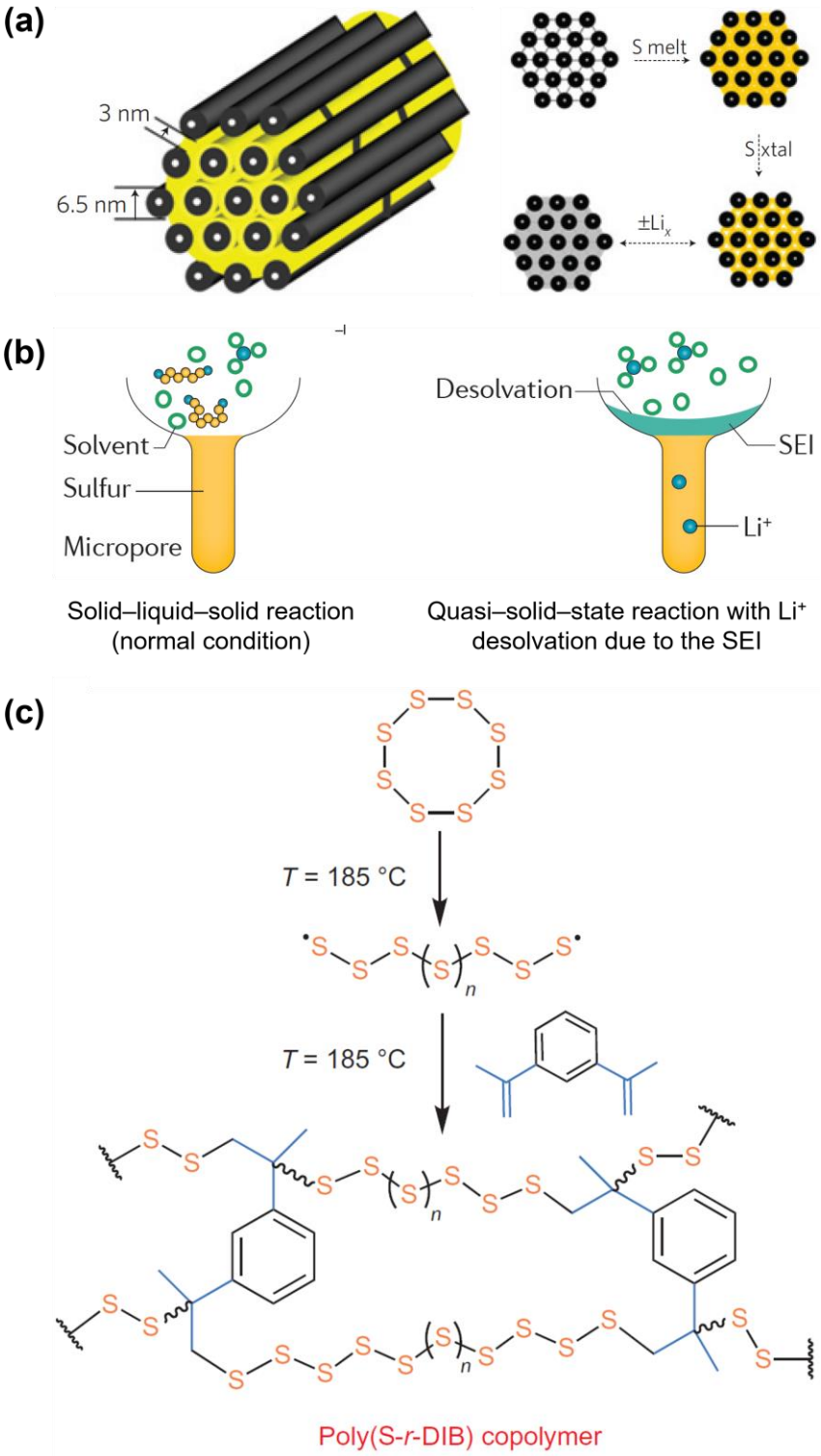

Figure 1.9 (a) Schematic diagram of the carbon encapsulated S (yellow) electrode. Reprinted by permission from ref. 148. Copyright 2009 Springer Nature. (b) Schematic diagram for comparison of lithiation reaction in Li–S batteries (LSB) depending on Li^+ desolvation. Reprinted by permission from ref. 8. Copyright 2016 Springer Nature. (c) Synthetic process diagram for copolymerization of S_8 with 1,3–diisopro–penylbenzene (DIB) to form chemically stable sulfur polymer. Reprinted by permission from ref. 156. Copyright Springer Nature.

1.2 Lithium–Oxygen batteries ($Li–O_2$ batteries)

Lithium–oxygen ($Li–O_2$) batteries has been received large attention as the most attractive energy storage device due to their high theoretical energy density (*ca.* 11 kW kg^{-1}) which is superior to that of any other next generation rechargeable batteries.[158-159] The $Li–O_2$ batteries is typically comprised of a Li metal anode, oxygen electrode with high surface area, and Li–ion conducting electrolyte as shown in Figure 11.1a. The $Li–O_2$ batteries has been classified into four categories based on the electrolyte; non–aqueous, aqueous, hybrid, and all–solid–state batteries depending on the type of electrolyte as shown in Figure 11.1b. This classification depending on the electrolytes is used because the electrolyte influence on the reaction kinetics and reaction process of $Li–O_2$ batteries. Among them, liquid–state electrolyte–based $Li–O_2$ batteries including non–aqueous and aqueous systems have been investigated intensively due to their higher ionic conductivity than that of solid electrolyte–based system. Between the liquid electrolytes, the non–aqueous electrolyte for $Li–O_2$ batteries is more feasible than aqueous electrolyte to use of Li metal at the anode without safety issue. Moreover, the $Li–O_2$ batteries with non–aqueous electrolyte has higher theoretical energy density than that of $Li–O_2$ batteries with aqueous electrolyte because of the electrolyte participated in the reaction of $Li–O_2$ batteries.

The reaction mechanism of $Li–O_2$ batteries showing the voltage profile as shown in Figure 1.11c is based on the oxidation reaction of Li metal via following reaction with a redox potential of 2.96 V *vs*. Li/Li^+:[160]

Anode (oxidation during discharge): $2Li\ (solid) \leftrightarrow 2Li^+ + 2e^-$

Cathode (reduction during discharge): $O_2\ (gas) + 2e^- \leftrightarrow O_2^{2-}$

Overall reaction: $2Li\ (solid) + O_2\ (gas) \leftrightarrow Li_2O_2\ (solid)$

This reaction is in case of $Li–O_2$ batteries with non–aqueous electrolyte. The forward reaction to form lithium peroxide (Li_2O_2) is named as oxygen reduction reaction (ORR) and the backward reaction for the decomposition of Li_2O_2 is named as oxygen evolution reaction (OER). These two processes are main process that governing the electrochemical performance of $Li–O_2$ batteries. The non–aqueous electrolyte do not directly participates the reaction of the $Li–O_2$ batteries in contrast with the aqueous electrolyte, but strongly influences on the reaction process. Consequently, the electrochemical process of $Li–O_2$ batteries is governed by the properties of electrolyte. In the non–aqueous electrolyte, the electrochemical process of forming Li_2O_2 occurs via two routes: the surface route and the solution route as shown in Figure 1.11a.[161-162] On the first stage of discharge, a lithium superoxide (LiO_2) forms after the electrochemical reduction of oxygen. This LiO_2 is slightly soluble into the non–aqueous solvent; therefore, the solubility of LiO_2, which is according to Pearson's hard–soft acid–bases (HSAB) theory, determines the pathway of further reaction to form a Li_2O_2. A LiO_2 is less soluble into the solvent with

low donor number (DN), therefore, the adsorbed LiO_2 onto the oxygen electrode surface is mainly reduces to Li_2O_2 by electrochemical process. On the other hands, in the solvent with high DN, LiO_2 is more soluble into the solvent due to enhanced stability of the complex (Li^+–$(solvent)_n$–O_2^-) by the high DN solvents, and disproportionate themselves into Li_2O_2.[163] In addition, because the polarization and surface area of oxygen electrode less influence on the solution process, high DN solvents improve the discharge capacity of Li–O_2 batteries as shown in Figure 1.11b.[161-162] Interestingly, the Li salt anion with high DN can also increases the DN of solvent having relatively low DN, leading to being as if the properties of high DN solvent.[162, 164] Moreover, the contents of water in the Li–O_2 batteries influences the discharge reaction mechanism that determines the large toroidal formation leading to the high discharge capacity.[162, 165-166] However, the electrolytes possessing the high DN is not always good for the enhanced performance of Li–O_2 batteries due to the needs for the considering other properties of electrolytes simultaneously. The non–aqueous electrolyte is needed to the following attributes for the ideal reaction of Li–O_2 batteries:[160]

(a) High chemical stability against reactive oxygen derivatives, such as superoxide (O_2^-), peroxide (O_2^{2-}), its adduct (LiO_2 and Li_2O_2), and various additives
(b) High electrochemical stability
(c) High oxygen solubility
(d) High diffusivity of oxygen and Li^+
(e) Low volatility and high boiling point for minimizing evaporation
(f) Sufficiently high conductivity for desired rate capability

To achieve high electrochemical performance of Li–O_2 batteries, the various non–aqueous electrolytes have been investigated for appropriate solvents, salts, and additives. The carbonate–based solvents, such as dimethyl carbonate (DMC), ethyl methyl carbonate (EMC), ethylene carbonate (EC), and propylene carbonate (PC), were firstly used as an electrolyte solvent for Li–O_2 batteries.[167] However, these solvents exhibited the low stability against reactive oxygen derivatives, as a results, the reaction of Li–O_2 batteries with carbonate–based electrolytes mainly forms lithium carbonate (Li_2O_3) and lithium alkylcarbonate (RO–(C=O)–OLi) rather than the Li_2O_2.[168] To substitute the carbonate–based electrolyte, ether–based electrolytes were suggested and exhibited the enhanced electrochemical performance of Li–O_2 batteries than that of Li–O_2 batteries with carbonate–based electrolyte. The ether–based electrolyte is mainly used 1,2–dimethoxyethane (DME, monoglyme, G1), 1–Methoxy–2–(2–methoxyethoxy)ethnae (diglyme, G2), 1,2–Bis(2–methoxyethoxy)ethane (triglyme, G3), or 2,5,8,11,14–Pentaoxapentadecane (TEGDME, tetraglyme, G4).[169-170] These solvent as an electrolyte for Li–O_2 batteries have been widely used due to their stability against reactive oxygen species, high oxidation stability (up to 4 V *vs*. Li/Li^+), low volatility except to the case of monoglyme, and good

wetting property for electrodes. However, although the Li–O_2 batteries with ether–based electrolyte showed the operation over numerous cycles and the ether is relatively insensitive toward nucleophilic O_2^- attack than the carbonates, the ether–base solvent were not completely inert toward reactive oxygen species. The high DN solvent, such as dimethylformamide (DMF),[171] *N*,*N*–dimethylacetamide (DMAc),[172-173] dimethyl sulfoxide (DMSO),[163, 174-175] and ethyl methyl sulfone (EMS),[176] as a electrolyte solvent for Li–O_2 batteries have been suggested and demonstrated outstanding performance of Li–O_2 batteries. However, these solvents still suffer from the necleophilic O_2^- attack, instability against Li_2O_2, or side reaction with Li metal.[171, 176-185] Unfortunately, in spite of intensive research toward the ideal electrolyte, the chemical stability against reactive oxygen derivatives still remain the key challenging issue.

The main drawbacks of Li–O_2 batteries is two: chemical/electrochemical stability related with the prior mentioned electrolyte and reaction kinetic related with ORR and OER. Especially, the high polarization of Li–O_2 batteries is main issue for achieving longer cycle performance due to sluggish kinetics of the OER. Furthermore, the high charging potential accelerates the decomposition of electrolyte and oxygen electrode corrosion, resulting in poor cycle performance of Li–O_2 batteries. To overcome the limitation, various solid catalysts have been suggested to facilitate the OER reaction as shown in Figure 1.12a and b. These catalysts, such as noble metals,[186-188] transition metal oxides,[189-192] noble metal–metal oxide or organometallic composite,[193-196] and modified carbon–based catalysts,[197-198] decrease the charging overpotential than that of pristine porous carbon electrode. In spite of their usefulness, solid catalysts encounter the two drawbacks: the spatial constraint and unexpected reaction.[186] The solid catalysts reacts only at the interfaces between catalyst surface and the solid Li_2O_2, therefore, a large amount of catalyst is required. In addition, some catalysts not only accelerates the decomposition of desired discharge products, but also the cell components like the electrolyte. Therefore, attempt to surmount the limitation of solid catalysts, the red–ox mediator as a soluble catalyst has been introduced in the electrolytes of Li–O_2 batteries as shown in Figure 1.12c and d. A tetrathiafulvalene (TTF) was first reported and could decrease the polarization of OER in Li–O_2 batteries.[199] Furthermore, the various redox mediator has been suggested, such as redox organic material [5,10–dihydro–5,10–dimethylphenazine (DMPZ), 10–methylphenothiazine (MPT), tris(4–(diethylamino)phenyl)amine (TDPA), 2,2,6,6–tetramethyl–1–piperidinyloxy (TEMPO) and its derivatives],[200-205] halide–based inorganic salt (cesium iodide (CsI), indium iodide (InI_3), lithium bromide (LiBr), lithium iodide (LiI)],[206-210] and metal–organic compound [cobalt bis(terpyridine) ($Co(Terp)_2$) and iron phthalocyanine (FePc)],[211-212] as a desirable soluble catalysts for OER in the Li–O_2 batteries. These redox mediators decreased the overpotential efficiently and exhibited extended cycle performance of Li–O2 batteries. However, the redox mediator is also faced with the limitation; their catalytic activity gradually degrades as cycles progress, leading to a progressively increasing polarization as cycle number increasing. This increasing polarization in the Li–O_2 batteries with a redox

mediator has been regarded to arise from the shuttle effect, which charge transfer phenomena via the electrolyte by shuttle agent.[210, 213-214] This effect influences on the concentration of redox mediator radicals near to the oxygen electrode, resulting in increasing the polarization. Therefore, the redox mediator for the Li–O_2 batteries still requires further enhancement.

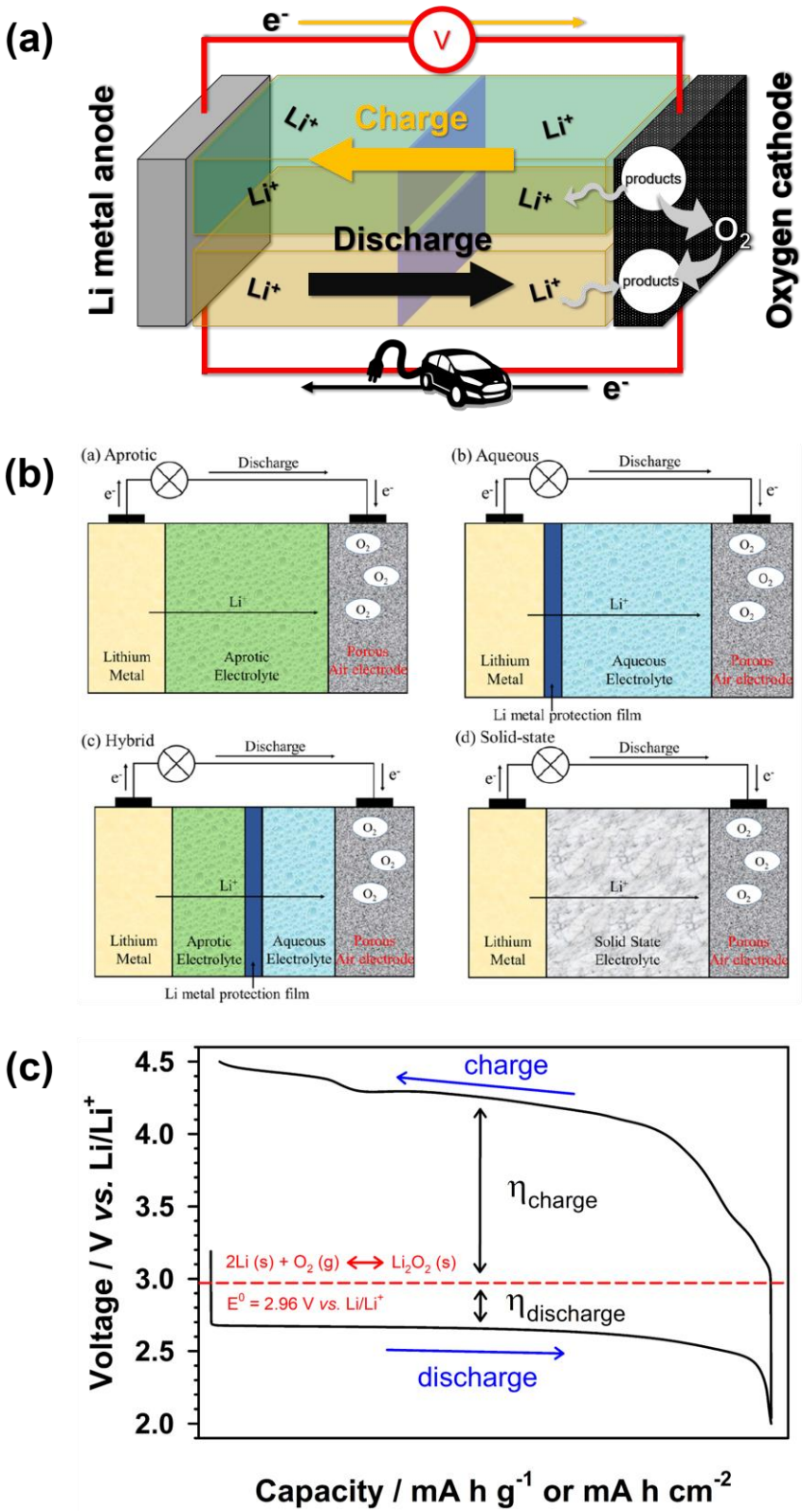

Figure 1.10 (a) Schematic diagram of Li–O_2 batteries with the reaction process during discharge/charge. (b) Schematic diagram of the various type of Li–O_2 batteries depending on the electrolyte system. Reprinted by permission from ref. 159. Copyright 2014 American Chemical Society. (c) Typical galvanostatic voltage profile of Li–O_2 batteries.

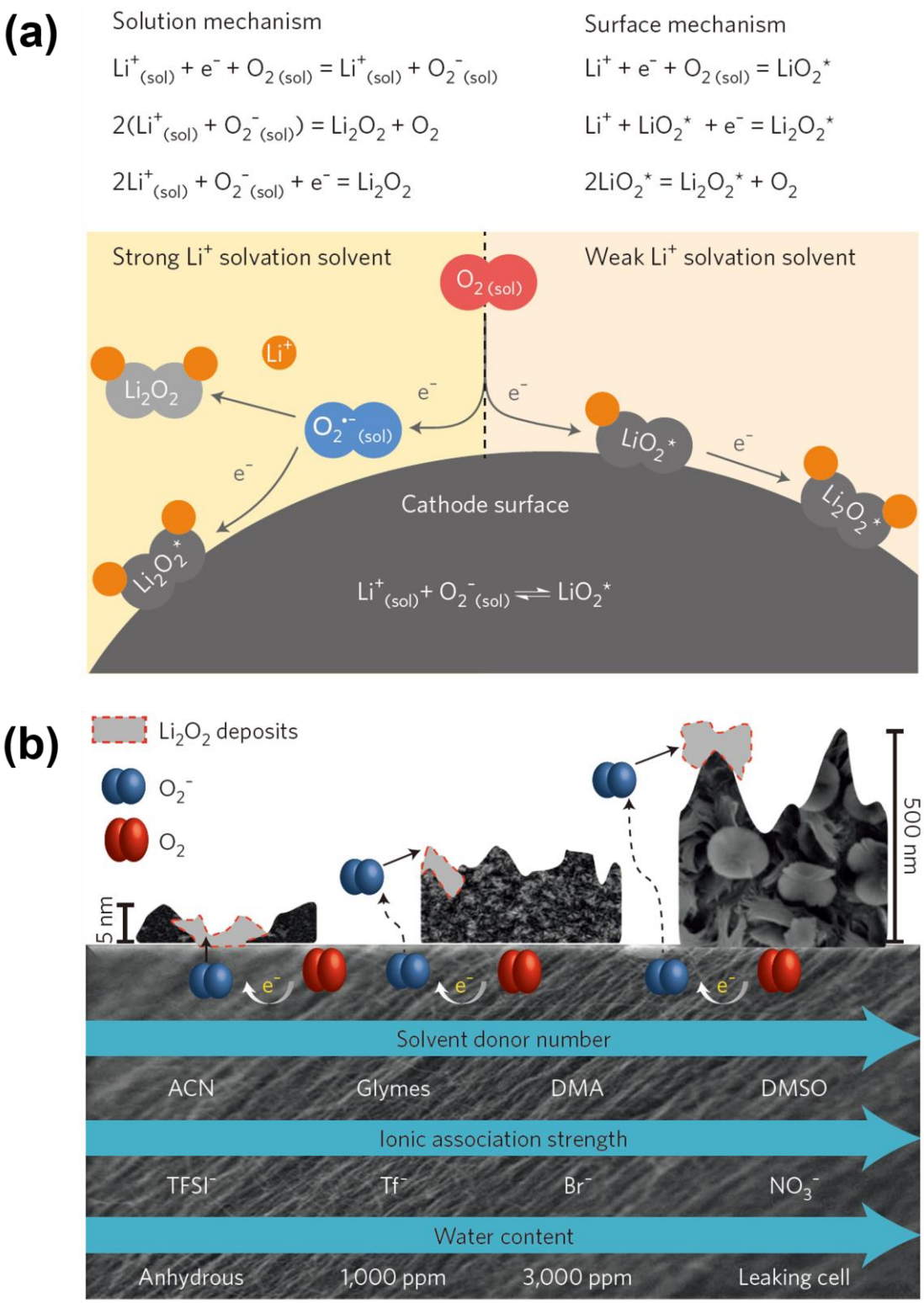

Figure 1.11 Schematic diagrams of (a) reduction mechanism in the Li–O_2 batteries at low overpotential and (b) the mechanisms of surface and solution growth in the Li–O_2 batteries depending on the electrolyte solvents. Reprinted by permission from ref. 162. Copyright 2016 Springer Nature.

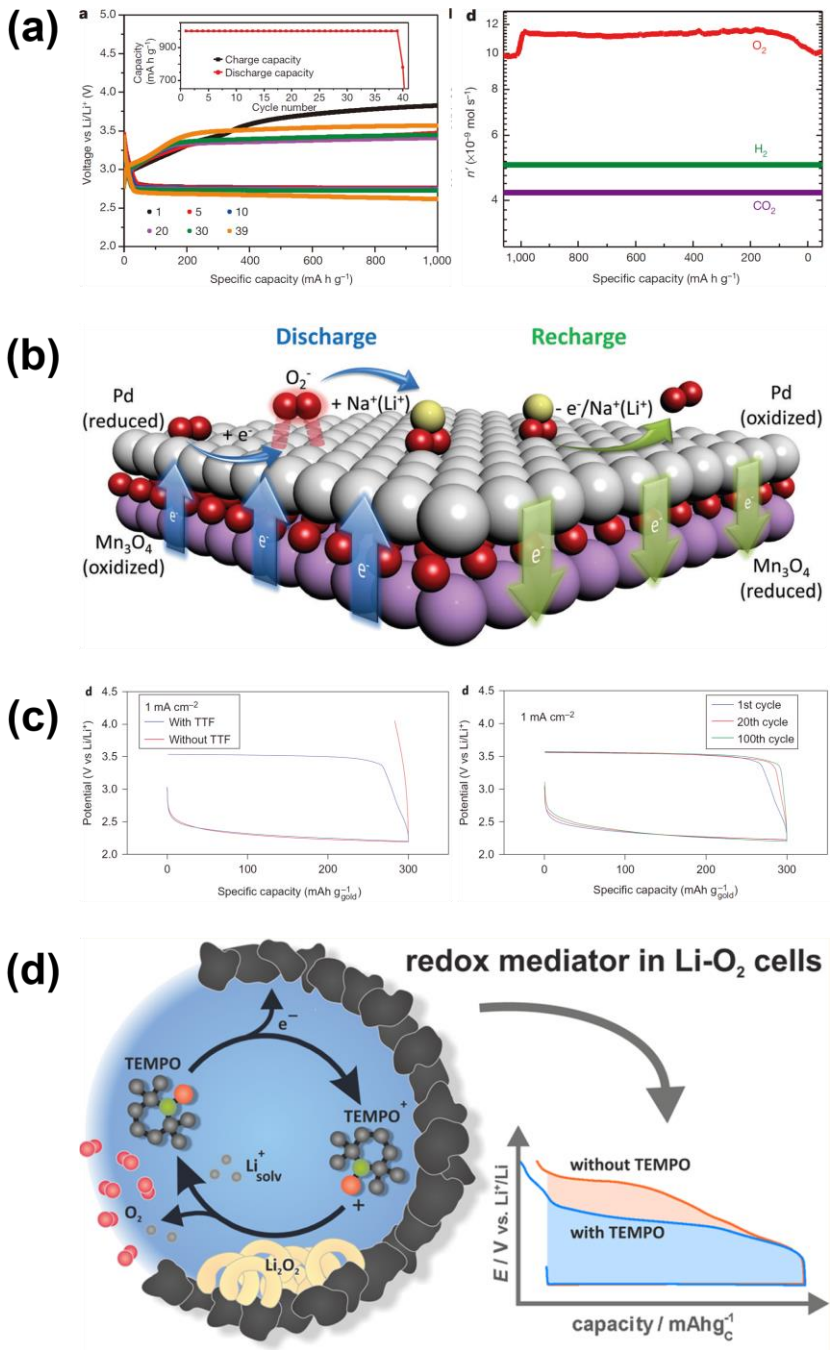

Figure 1.12 (a) Galvanonstatic voltage profile (left) and differential electrochemical mass spectroscopy (DEMS, right) analysis of Li–O_2 cell loaded Ir/rGO catalysts. Reprinted by permission from ref. 195. Copyright 2016 Springer Nature. (b) Schematic diagram for the reaction mechanism of the Li–O_2 cell loaded Mn_3O_4/Pd catalysts. Reprinted by permission from ref. 196. Copyright 2013 Royal Society of Chemistry. (c) Galvanostatic voltage profile of Li–O_2 cell containing TTF as a redox mediator for OER or TTF–free at 1st cycle (left), and of Li–O_2 cell containing TTF during cycling (right). Reprinted by permission from ref. 199. Copyright 2013 Springer Nature. (d) Schematic diagram for the reaction mechanism of the Li–O_2 cell containing TEMPO as a redox mediator. Reprinted by permission from (d) ref. 201. Copyright 2014 American Chemical Society.

1.3 Research motivation

This doctoral dissertation is focused on the study of failure mechanism of the non–aqueous Li–O_2 batteries with redox mediator. Especially, this dissertation is dealing with how to degrade the electrochemical activity of redox mediator in the electrolyte for Li–O_2 batteries, furthermore, suggests the method of sustaining electrochemical activity of redox mediator in the Li–O_2 batteries based on the analyzed results. The shuttle effect concept is not sufficient to explain the gradually increasing overpotential of Li–O_2 batteries over the cycling. The polarization of Li–O_2 batteries with redox mediator is almost correlated with the redox potential of redox mediator, because the redox mediator in the electrolyte for Li–O_2 batteries firstly oxidizes during electrochemical process. Therefore, the increasing polarization is related with the electrochemically inert passivation of electrode or the loss of electro–active species by side reaction. In addition, during shuttling phenomenon, there is no loss of electrochemical species: redox mediator radicals produced on the oxygen electrode diffuse out to Li metal anode, and are reverted to the previous form of redox mediator by Li metal anode. The returned redox mediators then diffuse back to the oxygen electrode. Although there is the charge shuttling via the redox mediator in the electrolyte, the shuttle agents maintain their electro–activity and concentration on the oxygen electrode. In case of lithium–sulfur batteries (Li–S batteries), the potential of Li–S batteries remain a constant during shuttle effect. One possibility to losing redox mediator activity or concentration is the side reaction of redox mediator on the oxygen electrode, which related with electrochemical reversibility and/or radical stability of redox mediator. The redox mediator may losses their electrochemical activity due to the side reaction arisen from high reactivity of their radical or exposure to highly reactive oxygen derivatives. The other possibility is the side reaction on the Li metal anode. In case of some redox mediators, such as FePc[211] and TEMPO[214], the clues of side reaction toward Li metal anode were observed without precise explain toward failure mechanism. These two origin for the failure of Li–O_2 batteries with a redox mediator arose from the cell components can also observed from comparing the electrochemical performance of Li–O_2 batteries with a TTF.[199, 201] The Li–O_2 batteries with TTF using nanoporous gold, DMSO, and LFP as an oxygen cathode, electrolyte, and anode, respectively, shows the stable performance, whereas the increasing polarization of charging potential was observed in the Li–O_2 batteries using porous carbon, 1–Methoxy–2–(2–methoxyethoxy)ethnae (diglyme), and Li metal as an oxygen cathode, electrolyte, and anode, respectively.

Therefore, this dissertation analyzes the correlation between redox mediator and cell components, such as electrolyte solvent and Li metal, and is proved that the side reaction between them strongly influences on the failure of Li–O_2 batteries with a redox mediator.

1.4 Characterization

Electron spin resonance (ESR) or electron paramagnetic resonance (EPR)

Ever since Zavoisky was observed the electron spin signal of $CuCl_2 \cdot 2H_2O$ in 1944 as the experimental evidence toward the concept of quantum mechanics,[215] the Electron spin resonance (ESR) has been used for the analyzing the paramagnetic properties of materials. In early stage on the development of the magnetic analysis, research using ESR had been progressed more than that using nuclear magnetic resonance (NMR) due to their higher sensitivity toward the magnetic resonance. However, because the analysis of ESR only works at the situation with unpaired electron, NMR has been widely adopted for various analysis of materials instead of ESR. Moreover, the time resolution of spectroscope for ESR is needed the scale of nano–seconds, leading to the requirement of high level technologies. However, the demand for ESR has increased to analyze the reaction mechanism and properties of materials as the science and technologies evolve owing to being the exclusive equipment for analysis of unpaired electron state.

The motion of charge on an atomic or sub–atomic scale leads to the magnetism. The electron having negative charge also spins itself, resulting in the magnetic moment. Therefore, electron also respond with the external magnetic field, leading to the change of electron energy state. This phenomenon, which is the energy difference induced the interaction between unpaired electron and external magnetic field, is called "Zeeman effect".[216] The electron is placed on the lower energy state when their magnetic moment is parallel to the external magnetic field, whereas the electron is placed on the higher energy state when opposite direction to the external magnetic field. As the selection rule, the electron have only two state, such as - $\frac{1}{2}$ for parallel state and $+\frac{1}{2}$ for opposite state to external magnetic field. These energy state of electron is as the following equation:[216]

$$\mathrm{E} = m_s g \mu_B B_0 = \pm \frac{1}{2} g \mu_B B_0$$

m_s: electron spin quantum number, g: g–factor, B_0: external magnetic field

μ_B: Bohr magneton $\left(\mu_B = \frac{e\hbar}{2m_e} = 9.27400968 \times 10^{-24} \quad J/T = A \cdot m^2\right)$

Therefore, the energy gap between two states of electron is as the following equation:

$$\Delta\mathrm{E} = g \mu_B B_0$$

This equation indicates two characteristic of energy state for electron spin: two state of electron spin is same each other when the external magnetic field do not exist, and the energy gap between two states

is proportion to the intensity of external magnetic field. Based on quantum mechanics and Planck's law, when the energy of incident electromagnetic wave on the electron is equal to the energy gap of electron transition, the electron absorbs its microwave. In this context, when the microwave incident to the electron, the electron absorbs the microwave of specific wavelength which is equal to the energy gap as shown in Figure 1.13a. This absorption is as the following equation:[216]

$$\Delta E = g\mu_B B_0 = h\upsilon$$

h: Planck constant $(h = 6.626070040 \times 10^{-34} \ J \cdot s)$, υ: wavelength of microwave

For ESR, the microwave in range of GHz is used. There are two method for obtaining ESR signal: one is the change of microwave frequency at constant magnetic field, the other is the change of magnetic field at constant microwave frequency. In general, the latter method has been used widely due to the technical difficulty of controlling microwave. The g–factor as a proportional constant is associated with the properties of electron, therefore, the information of electronic structure in the materials is obtained from the g–factor.

However, the information from the g–factor is limitative to obtain detailed data toward the geometrical structure of electron distribution. This information can be obtained from the "hyperfine interaction" between the nuclei and electron analogous to the NMR. The nuclei also have a charge and spin itself, as a result, the nuclei has a magnetic moment. This magnetic moment generates the magnetic field, leading to the influence on the magnetic moment of electron. This effect of nuclei magnetic field further subdivides the energy level of electron spin, resulting in the splitting of ESR signal as shown in Figure 1.13b. The energy level of the electron, which have the electron spin quantum number of S and the nuclear spin quantum number of I is as the following equation:[216]

$$E = m_s g\mu_B B_0 + m_s g_N \mu_N B_0 + m_s m_I A$$

g_N: nuclear g–factor, m_I: nuclear spin quantum number, A: the hyperfine coupling constant

μ_N: nuclear magneton $\left(\mu_N = \frac{e\hbar}{2m_P} = 5.050783699 \times 10^{-27} \ J/T\right)$

The degree of ESR signal splitting is related with the hyperfine coupling constant. The hyperfine coupling shows the detailed information near the unpaired electron, such as type and quantity of atom consisting the molecules or ions and the geometrical structure of electron states in the molecules or ions.

In this dissertation, the change of radical signal depending on the time was measured to analyze the life time of radical. For the analysis, the 3–electrode cell was introduced for the formation of radical electrochemically.

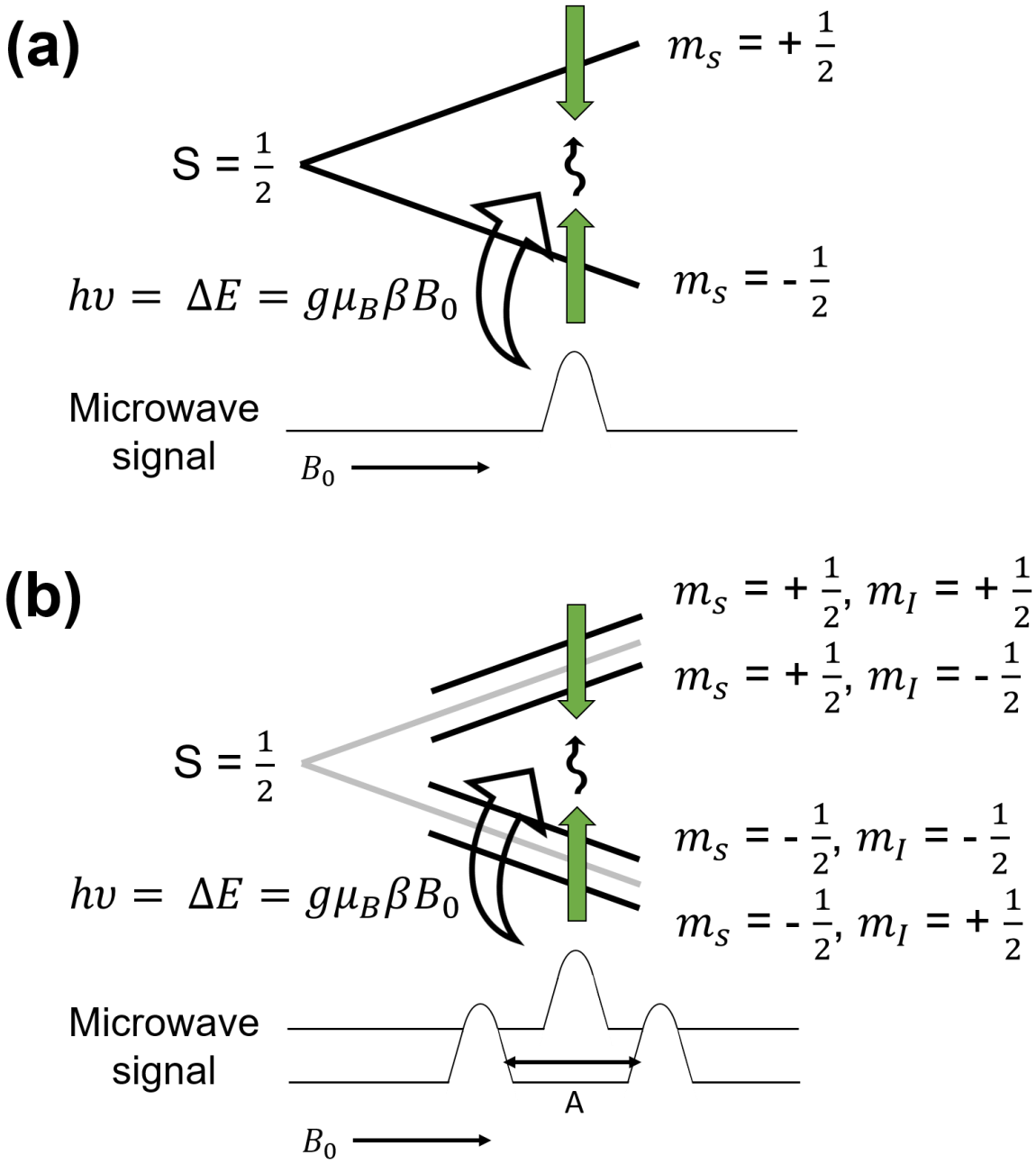

Figure 1.13 The change of electron energy level and spectrum of microwave in the system including (a) only the electron with the spin quantum number of 1/2 and (b) the electron with the spin quantum number of 1/2 and the nuclear quantum number of 1/2.

2. 10–methlyphenothiazine (MPT) as a redox mediator for facilitating oxygen evolution reaction of Li–O_2 batteries

2.1 Introduction

To effectively facilitate the catalyst reaction, the catalyst or reactant must possess the freely moving phase, such as liquid or gas which has high collision frequency. In this context, the catalyst of gas or liquid phase is more suitable for the redox reaction of Li–O_2 batteries which forms the solid state products as a reaction products or reactant. Therefore, the redox mediator as a pseudo liquid phase facilitates the decomposition of the discharge products rather than the solid catalyst. The reaction mechanism of redox mediator for the Li–O_2 batteries is also quite differed from that of solid catalyst depending on catalytic reaction process as shown in Figure 2.1.[217] In case of catalyst–free, the polarization of Li–O_2 batteries leads the expected electrochemical redox reaction to higher potential. If redox mediator dissolves in the electrolyte, the electrochemical reaction of redox mediator firstly occurs before the electrochemical reaction of the reactant, such as O_2 or Li_2O_2. As a result of the electrochemical reaction of redox mediator, the redox mediator radicals form in the electrolyte and freely move around. These redox mediator radicals decompose the discharge product in case of OER or facilitate the reduction of O_2 in case of ORR, which originate from the difference of redox potential between redox mediator and reactant. In summary, as shown in Figure 2.2, the catalytic process of redox mediator consists of two process: the one is electrochemical process, the other is catalytic process. To select the effective redox mediator for Li–O_2 batteries, it must be considered following conditions:

For electrochemical process

(a) Slightly higher (for OER) or lower (for ORR) redox potential of redox mediator than that of Li_2O_2
(b) Higher electrochemical reversibility of redox mediator
(c) Higher stability of redox mediator against the discharge products, such as LiO_x and Li_2O_2

For catalytic process

(a) Faster kinetics between redox mediator and discharge products rather than other chemical species
(b) Higher stability (longer life time) of redox mediator radicals

In this dissertation, 10–methylphenothiazine (MPT) has been adopted as a model redox mediator for Li–O_2 batteries. Because MPT was suggested as an overcharge protection for Li–ion batteries (LIBs),[218] this redox mediator possesses high electrochemical reversibility and stability in Li–ion containing

electrolytes. The redox potential of MPT is 3.5 V (*vs.* Li/Li^+) in the carbonate electrolytes, which is higher than that of $Li–O_2$ batteries. Moreover, Zhou's group has been introduced MPT as a redox mediator for $Li–O_2$ batteries.[203] Therefore, MPT as a redox mediator may be suitable for $Li–O_2$ batteries.

In this chapter, the electrochemical performance of MPT for $Li–O_2$ batteries is examined to evaluate the suitability of MPT as a redox mediator by cyclic voltammetry, galvanostatic discharge–charge, *ex situ* X–ray diffraction (XRD), and scanning electron microscope (SEM). The electrochemical performance of MPT is excellent, but their performance shows the limitation in the $Li–O_2$ batteries. This indicates that the electrochemical performance of MPT also degrades in the $Li–O_2$ batteries and is suitable as a model redox mediator to analyze the failure mechanism of $Li–O_2$ batteries.

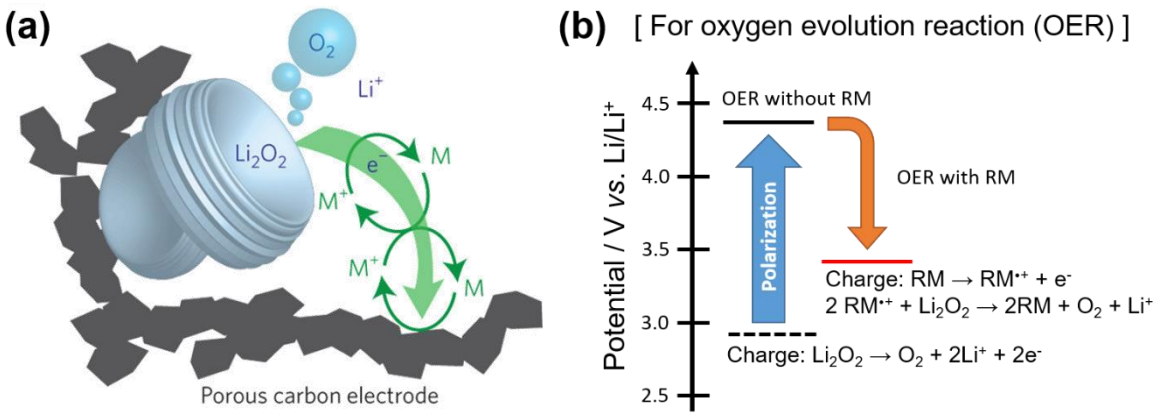

Figure 2.1 (a) The graphical diagram for the reaction process of redox mediator. Reprinted by permission from ref. 217. Copyright 2016 Springer Nature. (b) Schematic diagram toward the reaction mechanism of redox mediator labeled with the scale of potential *vs.* Li/Li^+ in case of the oxygen evolution reaction (OER).

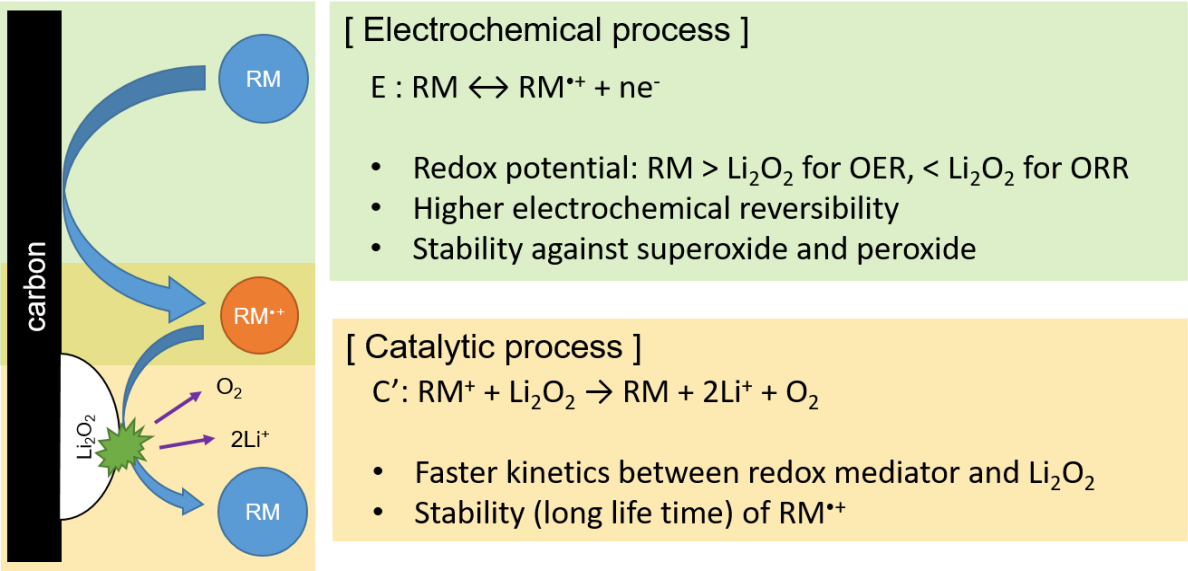

Figure 2.2 A schematic diagram toward the reaction process of redox mediator in case of the oxygen evolution reaction (OER) and the desirable characteristics thereof.

2.2 Experimental details

2.2.1 Materials

To minimize the side reaction by trace water, the water contents of tetraethylene glycol dimethyl ether (tetraglyme, Alfa Aesar, 99.69%) were controlled at less than 10 ppm via purifying with activated 4 Å molecular sieves (Alfa Aesar) before use. This value of water contents for the solvents was measured by Karl–Fischer titration (SP150, Metrohm). Moreover, Lithium trifluoromethanesulfonate ($LiSO_3CF_3$, Sigma–Aldrich, 99.995%) were dehydrated at 150 °C for 24 h in a vacuum oven before use. The 10–methylphenothiazine (MPT, Alfa Aesar, 99.9%) was also dehydrated at 60 °C for 48 h in a vacuum oven before use. After completely drying, all salts was dissolved in the solvents at a 1 molarity, for example, 1 *M* $LiSO_3CF_3$ in tetraglyme. MPT was also dissolved in the solvents at a 0.05 molarity. All chemicals were handled under an 99.9999 % Ar atmosphere.

2.2.2 Electrode preparation

The oxygen cathode were prepared by slurry casting onto a carbon paper (TGP–H–030, Toray) as a current collect. The slurry consisted of 90 wt % Ketjenblack (KB), 10 wt % poly(tetrafluoroethylene) (PTFE, Sigma–Aldrich), and the mixture solvents of isopropanol (IPA, 99.9 %, Alfa Aesar, 80 v/v %) and deionized water (20 v/v %). A KB of *ca.* 254 μg (0.4 ± 0.05 mg cm^{-2}) loaded on the electrode with a 9 mm diameter, and the electrode were dehydrated at 120 °C for 12 hrs in a vacuum oven.

2.2.3 Electrochemical characterization

All voltammetry techniques were performed using a SP150 potentiostat (BioLogic Science Instruments) with the homemade three–electrode cells consisting of a glassy carbon rod (area = 0.03 cm^2, Alfa Aesar), 316 SUS mesh (area = 2.01 cm^2, 200 mesh), and Li metal foil (thickness = 700 μm, Honjo Metal) as the working, counter, and reference electrodes, respectively. The cyclic voltammetry for the evaluating the electrochemical performance of redox mediator was conducted at a scan rate of 50 mV s^{-1} in the voltage range of 2.0 ~ 4.5 V (*vs*. Li/Li^+) up to 200 cycles.

All galvanostatic experiments were performed with two–electrode system using WBCS3000 galvanostat (WonATech). The oxygen cathode, Li metal anode (diameter = 11 mm), and glass fiber separator (Whatman® GF/C, Sigma–Aldrich, diameter = 12 mm) comprised the Li–O_2 batteries. The various electrolyte, such as tetraglyme electrolyte containing 1 *M* $LiSO_3CF_3$ + 50 *mM* MPT or MPT–free, was added to the Li–O_2 cell with an amount of 120 μL. The galvanostatic experiments of Li–O_2 batteries were performed at a current density of 300 mA g^{-1}_{KB}, a constant capacity of 1000 mA h g^{-1}_{KB}, and sealed cell chamber with a static pressure of 1 bar after purging with 99.999% O_2. The purging

process was performed with a flow rate of 40 mL min^{-1} for 5 min and a pressure of 2 bar. Instead of continuous O_2 flowing, the Li–O_2 cell was purged with O_2 after every 33 cycles.

2.2.4 Characterization

The *ex situ* X–ray diffraction (XRD) patterns of collected oxygen electrodes from Li–O_2 cells after cycling were obtained using a Bruker D2 PHASER with Cu K_α radiation (λ = 1.5418 Å) operated in the 2θ range of 10 to 80° with the sweep step of 3455 and step time of 4 s per step. The electrodes were sealed with Be window of 100 μm thickness and Kapton® tape (Dupont) in the Ar–filled glove box for prohibiting exposure to air. The *ex situ* scanning electron microscope (SEM) images and energy dispersive X–ray spectroscopy (EDS) spectra of collected oxygen electrodes from Li–O_2 cells after cycling were obtained using a JEOL JSM–7800F Prime and Oxford Instruments X–Max^N with an acceleration voltage of 15 keV and low electron detector (LED) mode. The electrodes for SEM were prepared in the Ar–filled glove and minimize to exposure to air using the sealing vial.

2.3 Result and Discussion

10–methylphenothiazine (MPT) as a redox mediator for Li–O_2 batteries

MPT as a redox mediator was first evaluated the validity for Li–O_2 batteries by investigating its electrochemical properties. Figure 2.3 exhibits the cyclic voltammograms of MPT under Ar and O_2 atmospheres, with 1.0 *M* $LiSO_3CF_3$ in tetraglyme as an electrolyte. The oxidation and reduction peaks of MPT were observed at 4.2 and 3.5 V (*vs*. Li/Li^+), respectively,[202-203, 218] indicating that MPT is capable of redox mediator, which has the higher redox potential than that of Li_2O_2. Furthermore, reversible redox reaction of MPT was also observed over 200 cycles in both Ar and O_2 atmospheres, implying that there is no side reaction between MPT and O_2 dissolved in the electrolyte. To analyze the influence of MPT on the reversible decomposition of Li_2O_2, the ex situ XRD analysis of Li–O_2 cells after 1st cycle is demonstrated in Figure 2.4. The Li–O_2 cell with MPT–free electrolyte showed a larger polarization during charge than Li–O_2 cells with MPT containing electrolyte, whereas both cells exhibited the similar capacity and polarization during discharge as shown in Figure 2.4a. However, the Li_2O_2 as a main discharge product (arrow sign: Li_2O_2 related peak in the range of 30 to 40°) formed and disappeared reversibly in the both cell during 1st cycle as shown in Figure 2.4b, indicating that the MPT in the Li–O_2 batteries play a role well as a redox mediator for the decomposition of Li_2O_2 without severe side reaction during discharge in accordance with the prior cyclic voltammetry results and Feng's results.[203]

The influence of MPT on the electrochemical performance of Li–O_2 cells is demonstrated in Figure 2.5. The MPT–free Li–O_2 cell exhibited poor cycle performance accompanying with a large polarization and unexpected capacity fading within 10 cycles; this is associated with the pore clogging on the cathode due to the accumulation of Li_2O_2 and Li_2CO_3, when ethereal electrolytes were adopted.[177-178, 180, 182-183, 219] As shown in the surface morphologies of the porous cathodes after 10 cycles charged, it was obvious the clogging of pore in case of MPT–free (Figure 2.5a). Moreover, this clogged pores were filled with high oxygen–containing particles as shown in Figure 2.6c and Table 2.1, indicating that a large amount of discharge products or side products remain on the oxygen cathode in spite of charged state of oxygen electrode. However, less pore clogging and oxygen composition on the oxygen electrode was observed in the Li–O_2 cell with MPT as shown in Figure 2.6b, 2.6d, and Table 2.1. The MPT dissolved in the electrolyte brought about an improved cycle performance with smaller polarization of the Li–O_2 cell, involving no capacity fading until 35 cycles. The redox reaction between $MPT^{\bullet+}$ and Li_2O_2 influenced on the low charging potential at *ca.* 3.5 V (*vs*. Li/Li^+) as shown in Figure 2.5c, which demonstrates the successful decomposition of Li_2O_2 during charging by MPT.[203] In spite of their effective functioning, the charging potential gradually increased as the number of cycles increase, in consistent with the behaviors of other previously suggested redox mediators; $Co(Terp)_2$, CsI, FePc, InI, LiI, LiBr, TDPA, TEMPO, and TTF.[201, 204, 206-207, 210-212] This demonstrates that the concentration of electrochemically active MPT also gradually decreases during cycling, leading to an increased

polarization.

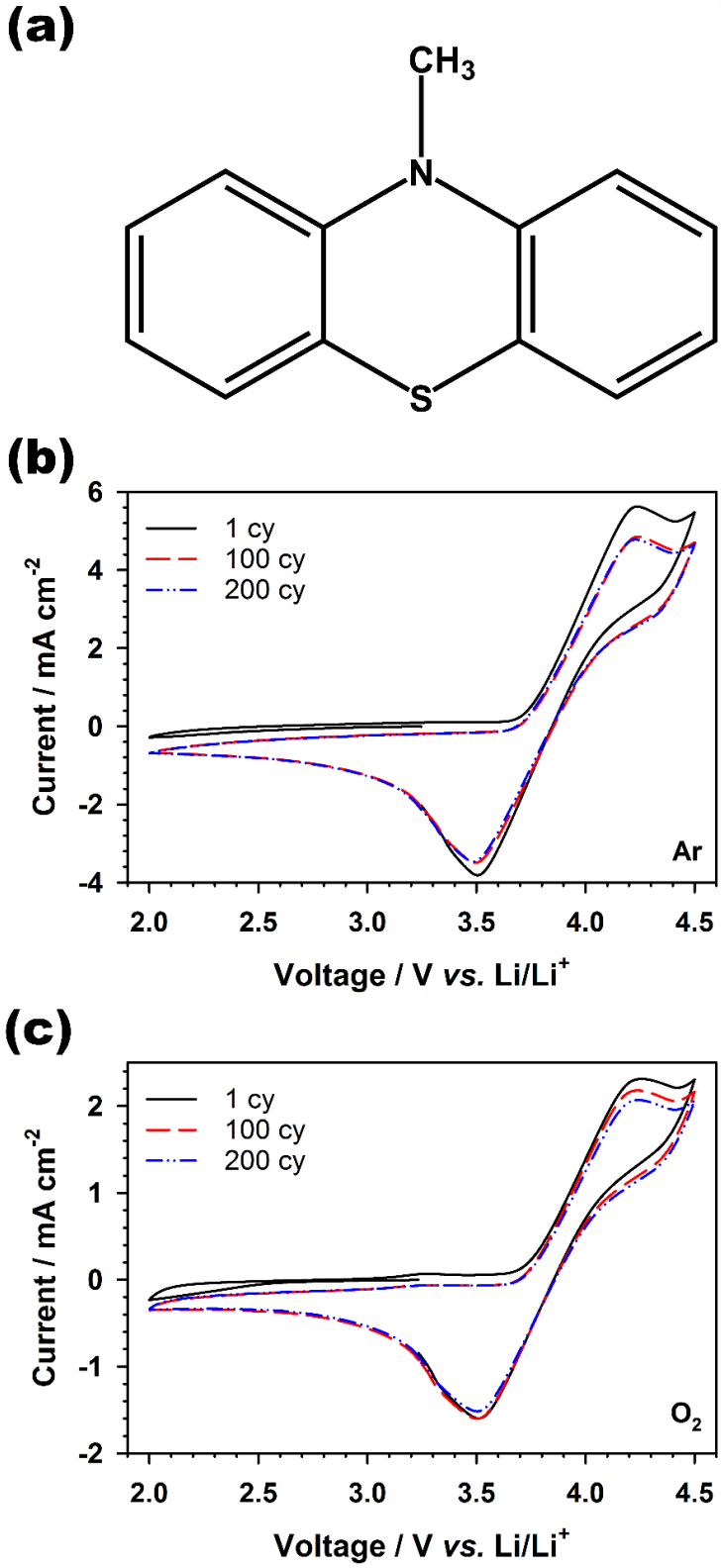

Figure 2.3 (a) A molecular structure of 10–methylphenothiazine (MPT). Cyclic voltammograms of MPT under (b) Ar and (c) O_2 atmospheres at a scan rate of 50 mV s^{-1} in the voltage range between 2.0 and 4.5 V *vs*. Li/Li^+.

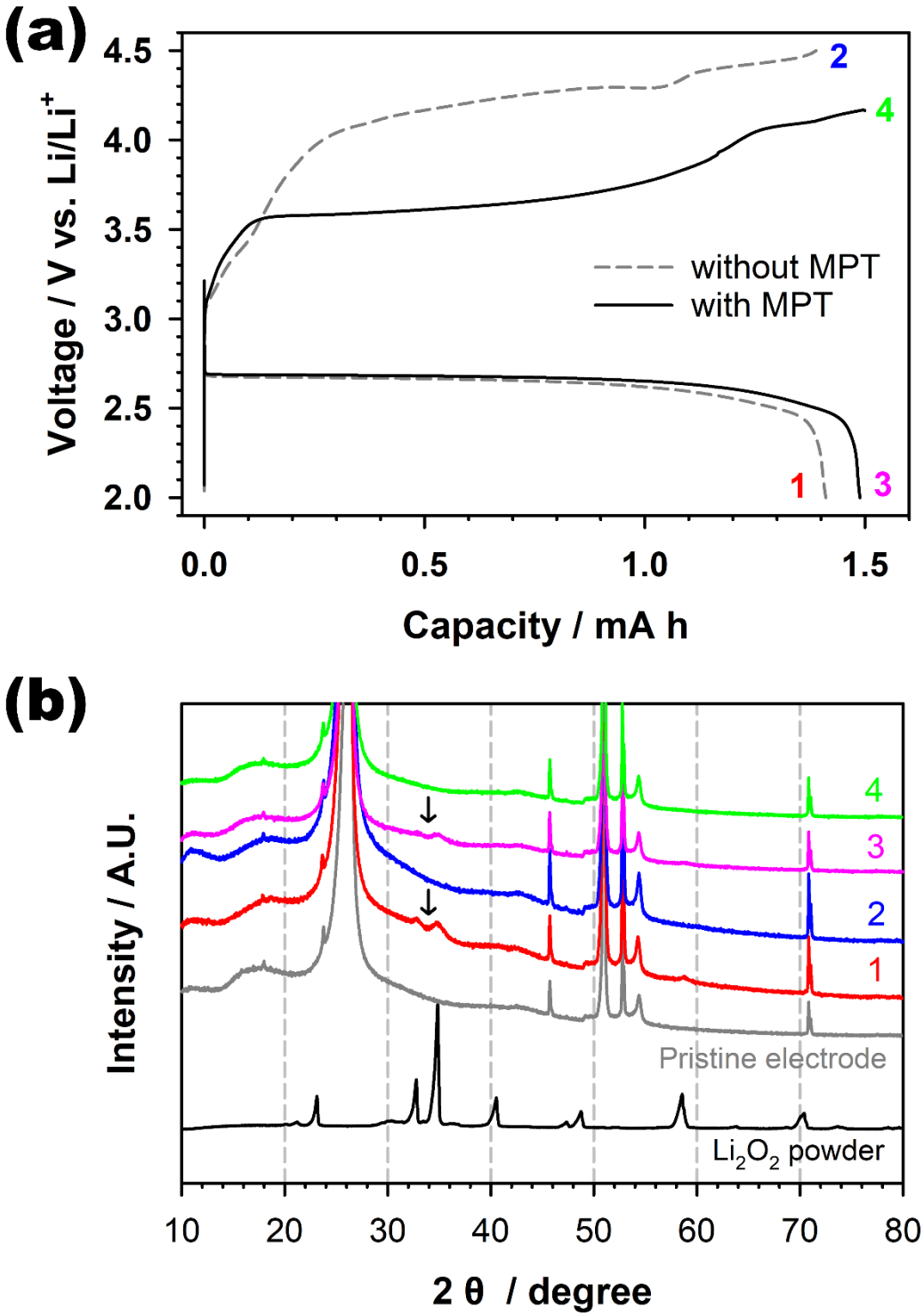

Figure 2.4 (a) The galvanostatic profile of the Li–O_2 cells with MPT–free and –containing electrolytes at a specific current of 300 mA g^{-1}_{KB} with a voltage range between 2.0 and 4.5 V *vs*. Li/Li^+. (b) The *ex situ* X–ray diffraction (XRD) spectra of the collected oxygen electrodes from the Li–O_2 cells with MPT–free and –containing electrolytes after cycle. The numbers in the figure 3.2b corresponds with the numbers in the figure 3.2a, indicating collected oxygen electrodes from the end of discharge or charge of the Li–O_2 cells with MPT–free and –containing electrolytes.

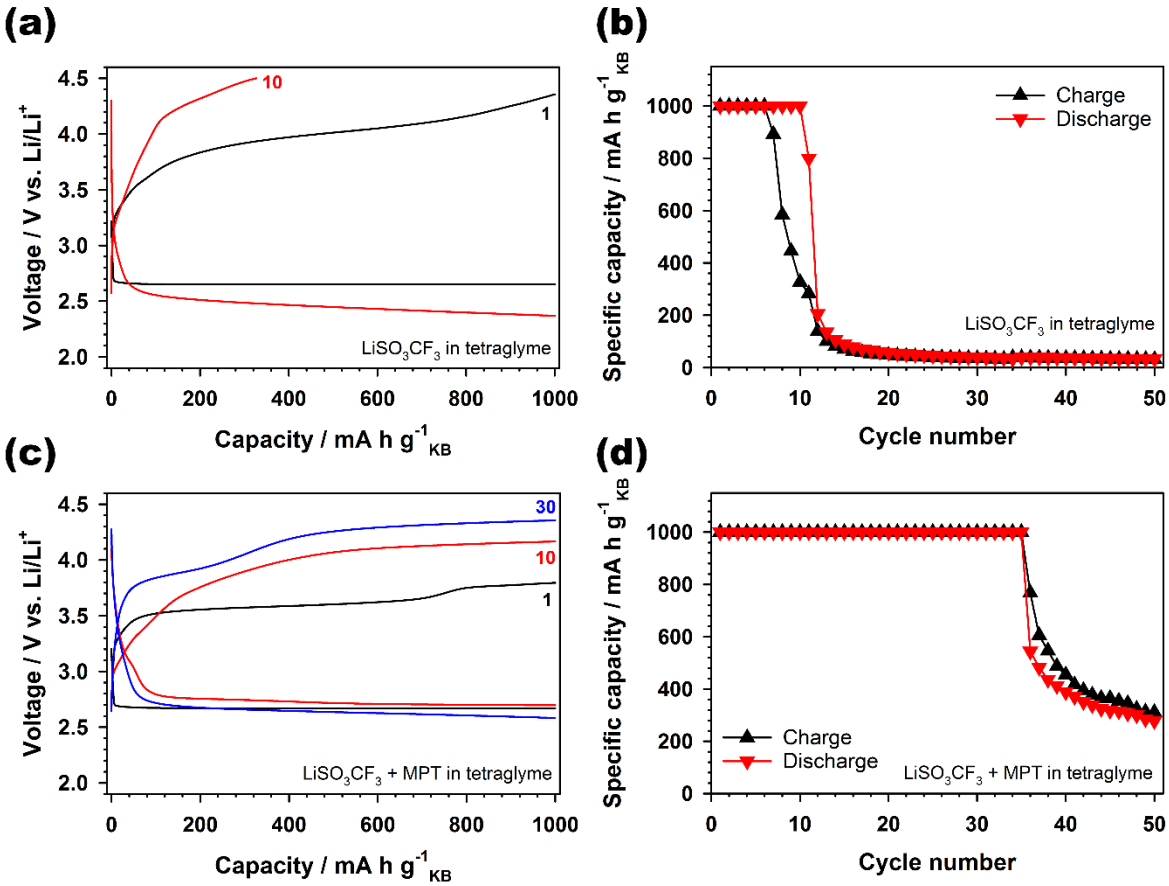

Figure 2.5 The voltage profiles and cycle performance of Li–O_2 batteries containing (a, b) MPT–free and (c, d) MPT with a constant capacity of 1000 mA h g^{-1}_{KB} and a specific current of 300 mA g^{-1}_{KB}.

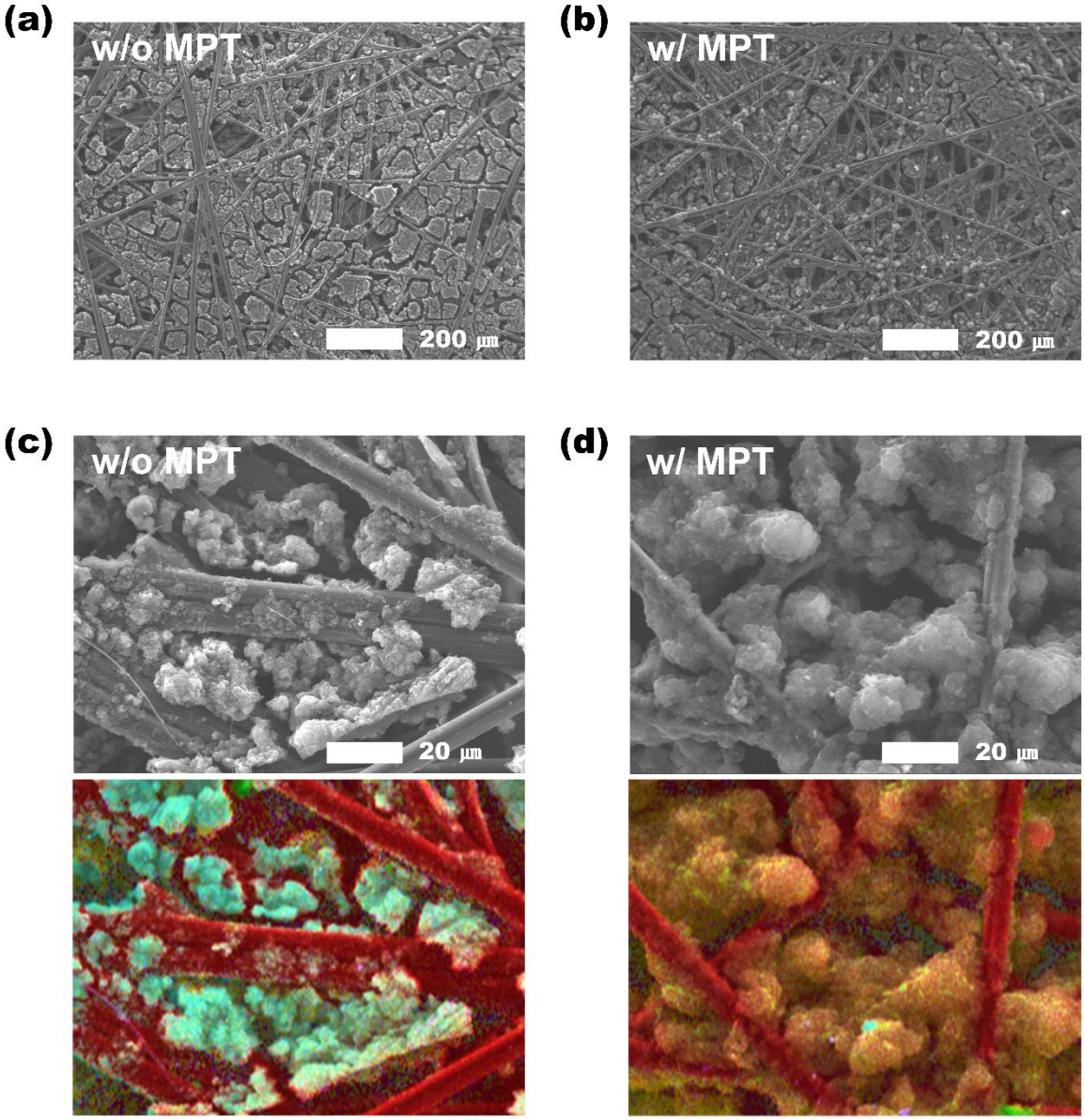

Figure 2.6 The *ex situ* scanning electron microscope (SEM) images of the collected oxygen electrode from the Li–O_2 cells with (a) MPT–free and (b) –containing electrolytes after 10 cycles. The *ex situ* scanning electron microscope (SEM) with higher magnification and its energy dispersive X–ray spectroscopy (EDS) mapping images of collected oxygen electrode from the Li–O_2 cells with (c) MPT–free and (d) –containing electrolytes after 10 cycles. (red: carbon, cyan: oxygen, green: fluorine)

Table 2.1 The energy–dispersive X–ray spectroscopy (EDS) results of the collected oxygen electrode from the Li–O_2 cells with MPT–free and –containing electrolytes after 10 cycles.

Elements (at %)	*C*	*O*	*F*	*S*	*Total*
MPT–free	73.23	25.09	1.54	0.14	100
MPT–containing	87.81	9.16	1.90	1.13	100

2.4 Summary

In this part, the suitability of MPT was examined as a redox mediator for Li–O_2 batteries by electrochemical, XRD, and SEM analyses, before the MPT use as a model redox mediator. The redox reaction of MPT in the tetraglyme electrolyte was fairly reversible up to 200 cycles in accompany with no change of redox peak, regardless of atmosphere. Moreover, the MPT radical decomposed effectively the discharge products, such as Li_2O_2, during cycling, resulting in the improved cycle performance of Li–O_2 batteries. However, MPT also showed the degrading performance of Li–O_2 batteries involving the increasing charging polarization over cycling, indicating the reducing the effective concentration of MPT, in other word, the losing in their electrochemical activity. These results suggests that the MPT possesses the limitation of enhancement for the electrochemical performance of Li–O_2 batteries, therefore, MPT as a model redox mediator is suitable for the analysis toward the failure mechanism of Li–O_2 batteries containing a redox mediator.

Above mentioned, the failure origin of redox mediator in the Li–O_2 batteries may be associated with the unexpected reaction between redox mediator and cell components. In part 3, the effect of electrolytes on the electrochemical performance of MPT for Li–O_2 batteries will be investigated by cyclic voltammetry and electron spin resonance (ESR). Furthermore, in part 4, the influence of Li metal anode on the stability of MPT for Li–O_2 batteries will be examined by combined analyses, such as electrochemical method, spectroscopy, and resonance analysis.

3. The appropriate electrolyte solvent for redox mediator in the Li–O_2 batteries

3.1 Introduction

The charging process of the Li–O_2 batteries with a redox mediator is consisted of two process; the one is electrochemical process and the other is catalytic process as shown in Figure 3.1. During the electrochemical process, a redox mediator in the electrolyte firstly oxidizes on the oxygen electrode and forms the redox mediator radical near to oxygen electrode. The electrochemical reversibility of the redox mediator, which indicates the reversible electron transfer, strongly influence on effectively oxidizing the Li_2O_2.[220] Moreover, the electrochemical reversibility and redox potential of redox mediator is significantly influenced by the nature of solvents.[221-225] The freely moving redox mediator radical in the electrolyte withdraws the electron from the Li_2O_2 on the oxygen electrode, and the Li_2O_2 converts to Li^+ and O_2 during catalytic process. In this situation, the redox mediator radical has to maintain their activity before encountering the discharge products, because the life time of the redox mediator radical, also strongly influence on the decomposition of discharge products. Although redox mediator own properties dominantly determines the ability of redox mediator toward decomposing Li_2O_2, the selectivity of redox mediator radical is affected by not only its own properties but also the nature of the solvent.[226]

Therefore, in this part, we investigated the correlation between the electrochemical reversibility and radical stability of redox mediator and the type of solvent for electrolyte using a cyclic voltammetry (CV) and electron spin resonance (ESR) analysis. The four solvents, such as tetraglyme, monoglyme, DMAc, and DMSO, which widely use as electrolyte for Li–O_2 batteries, was selected. Again, the model redox mediator is MPT.

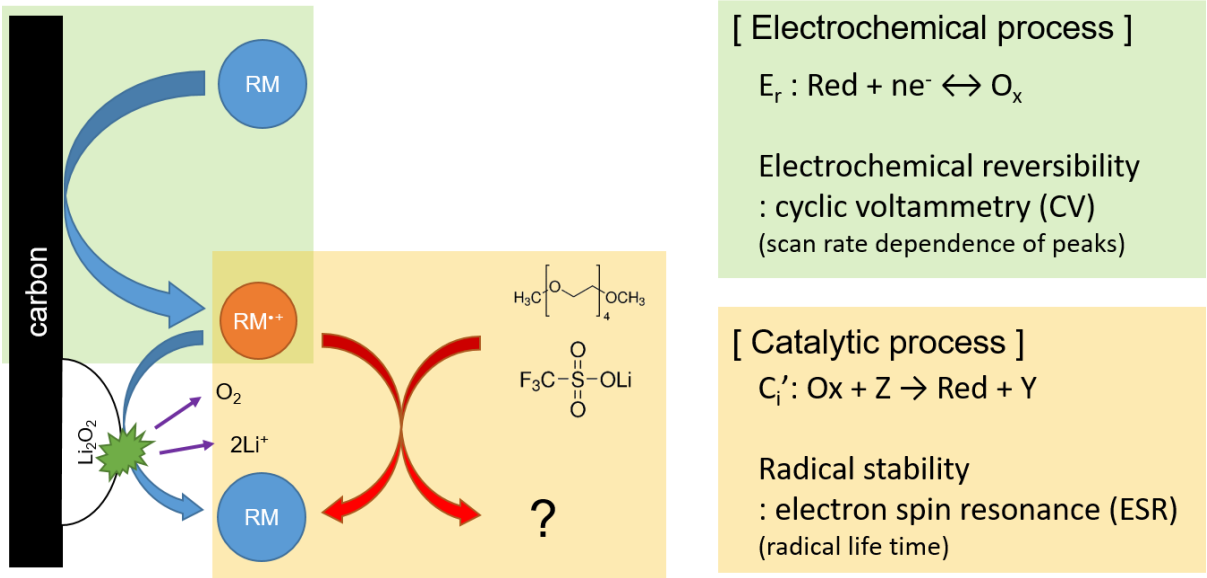

Figure 3.1 A schematic diagram of the charging process in the Li–O_2 batteries with redox mediator.

3.2 Experimental details

3.2.1 Materials

To minimize the side reaction by trace water, the water contents of all solvents, such as *N*,*N*–dimethylacetamide (DMAc, Alfa Aesar, 99.8%), dimethyl sulfoxide (DMSO, Alfa Aesar, 99.9%), 1,2–dimethoxyethane (monoglyme, Sigma–Aldrich, 99.9%), and tetraethylene glycol dimethyl ether (tetraglyme, Alfa Aesar, 99.69%), were controlled at less than 10 ppm via purifying with activated 4 Å molecular sieves (Alfa Aesar) before use. The value of water contents for the solvents was measured by Karl–Fischer titration (SP150, Metrohm). Moreover, Li and sodium salts, such as Lithium trifluoromethanesulfonate ($LiSO_3CF_3$, Sigma–Aldrich, 99.995%), were dehydrated at 150 °C for 24 h in a vacuum oven before use. The 10–methylphenothiazine (MPT, Alfa Aesar, 99.9%) was also dehydrated at 60 °C for 48 h in a vacuum oven before use. After completely drying, all salts was dissolved in the solvents at a 0.5 molarity, for example, 0.5 *M* Li SO_3CF_3 in DMAc, DMSO, monoglyme, or tetraglyme. MPT was also dissolved in the solvents at a 0.01 molarity. All chemicals were handled under a 99.9999 % Ar atmosphere.

3.2.2 Electrode preparation

The oxygen cathode were prepared by slurry casting onto a carbon paper (TGP–H–030, Toray) as a current collect. The slurry consisted of 90 wt % Ketjenblack (KB), 10 wt % poly(tetrafluoroethylene) (PTFE, Sigma–Aldrich), and the mixture solvents of isopropanol (IPA, 99.9 %, Alfa Aesar, 80 v/v %) and deionized water (20 v/v %). A KB of *ca.* 254 μg (0.4 ± 0.05 mg cm^{-2}) loaded on the electrode with a 9 mm diameter, and the electrode were dehydrated at 120 °C for 12 hrs in a vacuum oven.

The $LiFePO_4$ (LFP) electrodes as counter electrode for Li–O_2 batteries were prepared from a slurry made by dispersing 70 wt % LFP, 10 wt % carbon black (Super P), and 20 wt % poly(1,1–difluoroethylene) (polyvinylidene fluoride, PVdF) into the 1–Methylpyrrolidin–2–one (*N*–Methyl–2–pyrrolidone, NMP). The slurry was casted onto a 316 SUS foil of 12 mm as a current collector selected for avoiding Al corrosion by the electrolyte, and the electrodes were dehydrated at 120 °C for 12 hrs in a vacuum oven. The loading amounts of LFP were 6.2 ± 0.1 mg cm^{-2} (capacity: *ca.* 657.84 μA h cm^{-2}).

3.2.3 Electrochemical characterization

All voltammetry techniques were performed using a SP150 potentiostat (BioLogic Science Instruments) with the homemade three–electrode cells consisting of a glassy carbon rod (area = 0.03 cm^2, Alfa Aesar), 316 SUS mesh (area = 2.01 cm^2, 200 mesh), and Li metal foil (thickness = 700 μm, Honjo Metal) as the working, counter, and reference electrodes, respectively. The cyclic voltammetry

for the evaluating the electrochemical reversibility of redox mediator was conducted at a various scan rate in range of 1 ~ 50 mV s^{-1} in the voltage range of 2.8 ~ 4.2 V (*vs*. Li/Li^+) for minimizing the electrolyte decomposition.

All galvanostatic experiments were performed with two–electrode system using WBCS3000 galvanostat (WonATech). The oxygen cathode, Li metal anode (diameter = 11 mm), and glass fiber separator (Whatman® GF/C, Sigma–Aldrich, diameter = 12 mm) comprised a Swagelok cell for the Li–O_2 batteries. The various electrolyte including 0.5 *M* $LiSO_3CF_3$ + 10 *mM* MPT in DMAc, DMSO, monoglyme, and tetraglyme, was added to the Li–O_2 cell with an amount of 120 μL. The galvanostatic experiments of Li–O_2 batteries were performed at a current density of 0.12 mA $cm^{-2}_{geometric}$, a constant capacity of 0.2 mA h $cm^{-2}_{geometric}$ based on the area of oxygen electrode, and sealed cell chamber with a static pressure of 1 bar after purging with 99.999% O_2. The purging process was performed with a flow rate of 40 mL min^{-1} for 5 min and a pressure of 2 bar. Instead of continuous O_2 flowing, the Li–O_2 cell was purged with O_2 after every 33 cycles.

3.2.4 Characterization

The *in situ* electron spin resonance (ESR) analysis was conducted using homemade 3–electrode cell consisting of Au electrode, 316 SUS mesh, and Li metal as a working, counter, and reference electrode, respectively. The Au electrode possessed helix structure and rolled around other electrodes with polyethylene separator for insulation between electrodes. Therefore, the radical generated from the working electrode was detected clearly by ESR due to the signal amplifying effect of Au electrode. The 3–electrode cell was filled the 550 μl of MPT contained electrolytes, such as 0.5 *M* $LiSO_3CF_3$ in DMAc, DMSO, monoglyme, or tetraglyme with 10 *mM* MPT. The ESR spectra were obtained from a Bruker EMXmicro–9.5/2.7 continuous–wave (CW) X–band ESR spectrometer, equipped with a Bruker ER 4102ST resonator operating *ca*. 9.801 GHz combined with ER 4141 VT for measuring the temperature of cavity. The microwave power was set to 2 mW and sweeps were performed over a range of 15.0 mT with a center field of *ca*. 349.7 mT at *ca.* 293 K. The field modulation frequency was set to 100 kHz and the modulation amplitude was 0.1 mT. The first derivatives of CW ESR spectra were recorded continuously for 1 hour with an interval of 30 sec after the electrochemical oxidation of MPT applying a constant voltage of 3.8 V (*vs*. Li/Li^+) for 1 min by the potentiostat (1285A DC Potentiostat, Solartron).

3.3 Results and discussion

The electrochemical reversibility of MPT depending on the electrolyte, 0.5 *M* $LiSO_3CF_3$ in tetraglyme, monoglyme, DMAc, or DMSO, such as was evaluated by comparing the cyclic voltammograms of MPT at various scan rates with homemade 3–electrode cell. The 3–electrode cell was comprised of the glassy carbon rod, 316 SUS mesh, and Li metal as the working, counter, and reference electrodes, respectively. The redox peaks of MPT in tetraglyme– and monoglyme–based electrolyte was changed depending on the scan rate, indicating the irreversible reaction as shown in Figure 3.2a and b. Moreover, the polarization of redox reaction of MPT in monoglyme–based electrolyte slightly increased than that of MPT in tetrglyme. However, for DMAc and DMSO, the redox peaks of MPT remain the almost constant potential regardless of scan rate (Figure 3.2c and d), indicating the reversible reaction. The change of redox reaction of MPT depending on the solvent demonstrates that the DMAc– and DMSO–based electrolyte is more suitable for Li–O_2 batteries with redox mediator than glyme–based electrolytes due the increased reversibility of MPT in the solvents. However, the redox potential of MPT in both solvents shifted to higher potential (*vs*. Li/Li^+, oxidative potential) than that of MPT in glyme–based electrolytes, indicating that the energy efficiency of Li–O_2 batteries still remain low in spite of using redox mediator for reducing polarization. In addition, the operating on the higher potential (more than 4.0 V *vs*. Li/Li^+) for Li–O_2 batteries leads to the severe decomposition of cell components, such as electrolyte and oxygen electrode.[180, 219, 227] Therefore, DMAc and DMSO limit to use for Li–O_2 batteries with redox mediator due to up–shifting effect of redox potential of redox mediator in spite of their effect on the electrochemical reversibility of redox mediator. To use the solvents for Li–O_2 batteries with redox mediator, it is needed to the well–designed cell components, such as nano–porous gold electrode.[199]

The solvent effect on the chemical stability of redox mediator radical was investigated with comparing the life time of oxidized MPT (MPT radical, $MPT^{\bullet+}$) in the various electrolyte, such as 0.5 *M* $LiSO_3CF_3$ in tetraglyme, monoglyme, DMAc, or DMSO with 10 *mM* MPT. The life time of $MPT^{\bullet+}$ were measured by *in situ* electron spin resonance (ESR) analysis with homemade *in situ* electrochemical cell for 1 hr with an interval of 30 sec after the electrochemical oxidation for 1 min. The cell was consisted of gold, 316 SUS mesh, Li metal as working, counter, and reference electrode, respectively. Before the electrochemical oxidation of MPT, there was no ESR signal of all electrolytes, indicating that all electrolytes have no paramagnetic molecules. The ESR signal of $MPT^{\bullet+}$ in the all electrolytes after electrochemical oxidation of MPT exhibited with 6 absorption peak and g–factor value of *ca.* 2.005, which is consistent with the literature results for a single unpaired electron on the nitrogen atom of the MPT.[228-229] The ESR signal of $MPT^{\bullet+}$ in the all electrolytes maximized in 8 min after the termination of electrochemical oxidation of MPT, and decreased gradually over the time under the influence of the side reaction among $MPT^{\bullet+}$ itself or between $MPT^{\bullet+}$ and the components of electrolyte.[230] The area of

$MPT^{\bullet+}$ signal in tetraglyme–based electrolyte slowly decreased to 70.50 % of its initial peak area from 2 min to 30 min, as shown in Figure 3.3a. However, as shown in Figure 3.3b, the ESR signal area of $MPT^{\bullet+}$ in the monoglyme–based electrolyte significantly decreased to 34.62 % of its initial peak area from 2 min to 30 min. In addition, as shown in Figure 3.3c and d, the peak area of $MPT^{\bullet+}$ in the DMAc– and DMSO–based electrolyte rapidly diminished to 4.49 and 0.83 % of its initial peak area from 2 min to 30 min, respectively. The area change of $MPT^{\bullet+}$ signal over the time summarized in Figure 3.4. The rapid decrease of those peaks indicate that $MPT^{\bullet+}$ in those solvents hardly maintains their radical state and converts to other form. As a results, the tetraglyme as a solvent for Li–O_2 batteries helps the $MPT^{\bullet+}$ to maintain their radical state than other solvents. These results demonstrate that the properties of solvents strongly correlate with the electrochemical reversibility of redox mediator and chemical stability of redox mediator radicals. Interestingly, the relationship between the electrochemical stability of redox mediator and chemical stability of redox mediator radical is in inverse proportion. These results indicate that the two properties of redox mediator for the Li–O_2 batteries are difficult to satisfy simultaneously by selecting a specific solvent as an electrolyte for Li–O_2 batteries.

To demonstrate the correlation between the solvent and the electrochemical performance of Li–O_2 batteries with redox mediator, the galvanostatic experiments of Li–O_2 batteries with MPT and tetraglyme, monoglyme, DMAc, or DMSO were conducted with $LiFePO_4$ as a counter electrode for excluding the effect of Li metal anode. The Li–O_2 cells were performed with a constant capacity of 0.2 mA h cm^{-2} and the voltage range of 2.0 and 4.5 V (*vs*. Li/Li^+) at a current density of 0.12 mA cm^{-2}. The electrochemical performance of Li–O_2 cell with a tetraglyme–based electrolyte exhibited most stable cycling up to 34 cycles based on the capacity retention of 75 %, however, the polarization of Li–O_2 cell during charge increased steadily over the cycle, as shown in Figure 3.5a and 3.6. The electrochemical performance of Li–O_2 cells with a monoglyme–based electrolytes showed the faster fading after 26 cycles than that of tetraglyme, as shown in Figure 3.5b and 3.6. Furthermore, the Li–O_2 cells with DMAc– and DMSO– based electrolytes showed rapid fading and shorter cycle performance than that of monogylme as shown in Figure 3.5c and d and 3.6. The tendency of cycle performance of Li–O_2 batteries is consistent with that of chemical stability of MPT as shown in Figure 3.7, indicating that the chemical stability of redox mediator radical dominantly influence on the electrochemical performance of Li–O_2 batteries with a redox mediator than the electrochemical reversibility. As a result, the optimization of solvent for electrolyte is important for longer cycle performance of Li–O_2 batteries with redox mediator. The tetraglyme is most suitable solvent for MPT among the four electrolytes, and used as a main electrolyte solvent for analysis of Li metal effect on the stability of redox mediator in following part.

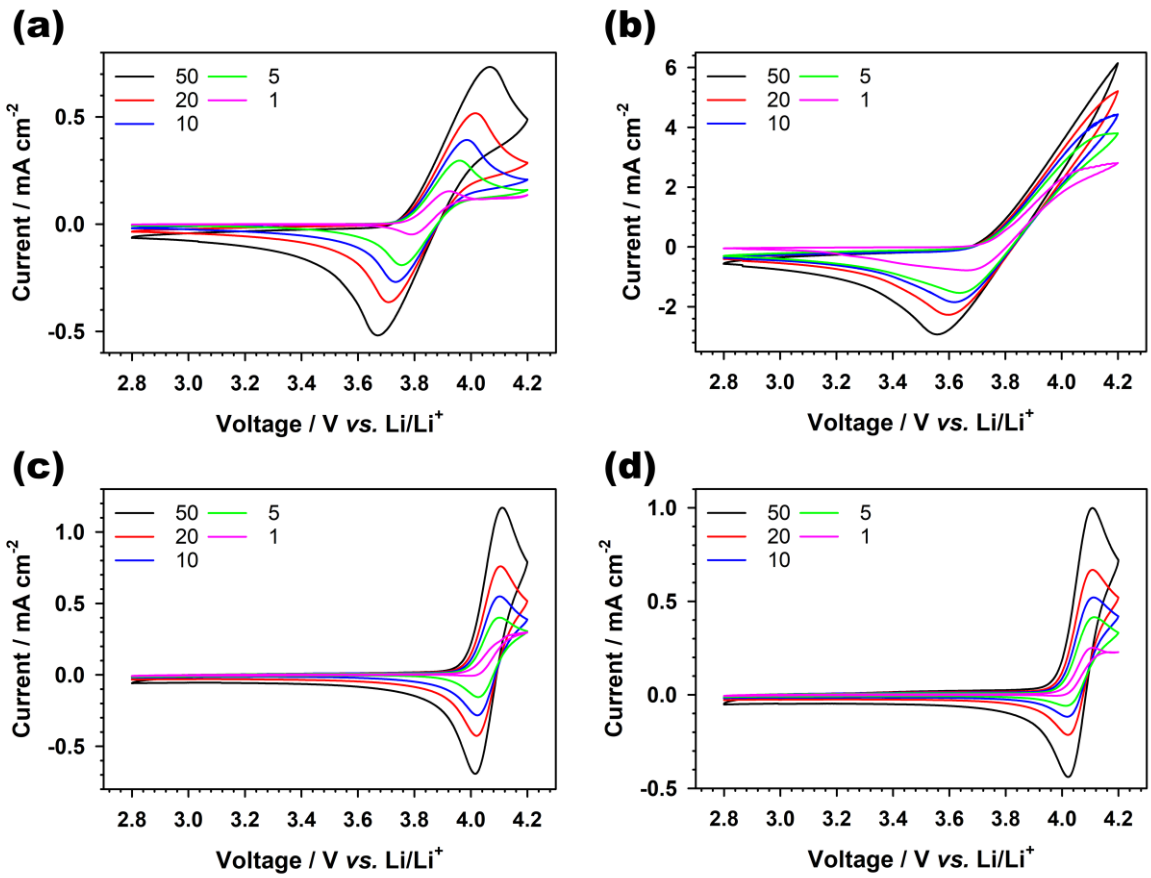

Figure 3.2 Cyclic voltammograms of 10 *mM* MPT with 0.5 *M* $LiSO_3CF_3$ in (a) tetraglyme, (b) monoglyme, (c) *N*,*N*–dimethylacetamide (DMAc), and (d) dimethyl sulfoxide (DMSO) at a various scan rate in range of 1 to 50 mV s^{-1} in the voltage range between 2.8 and 4.2 V *vs*. Li/Li^+ under a Ar atmosphere.

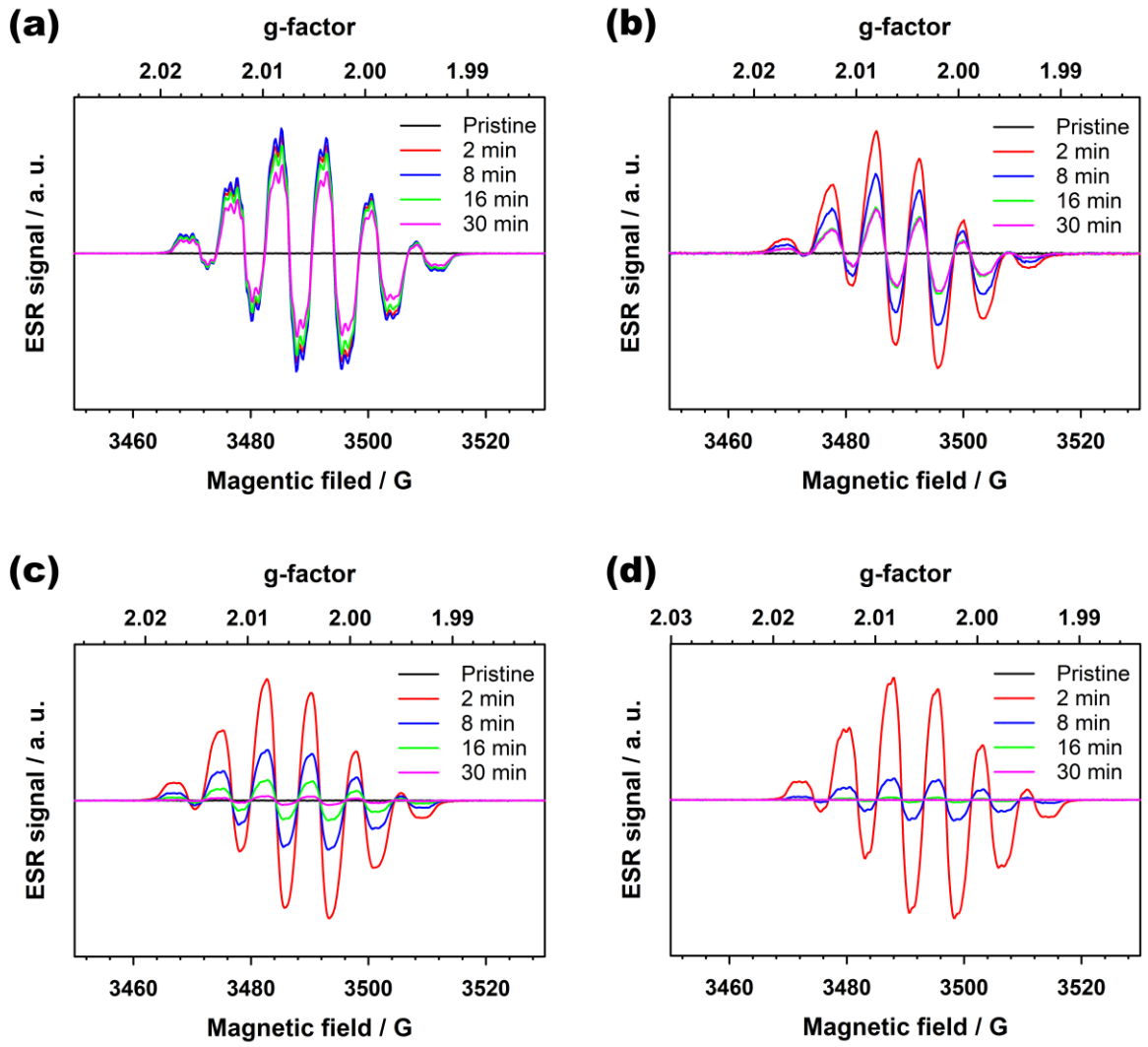

Figure 3.3 The *in situ* electron spin resonance (ESR) spectra of $MPT^{\bullet+}$ with 0.5 *M* $LiSO_3CF_3$ in (a) tetraglyme, (b) monoglyme, (c) *N*,*N*–dimethylacetamide (DMAc), and (d) dimethyl sulfoxide (DMSO). The time in the legend indicates the measuring time of ESR signal after the electrochemical oxidation of MPT for 1 min at 3.8 V *vs*. Li/Li^+. The all ESR spectra of $MPT^{\bullet+}$ exhibits the g–factor of *ca.* 2.005 in consistent with the literature.[228-229]

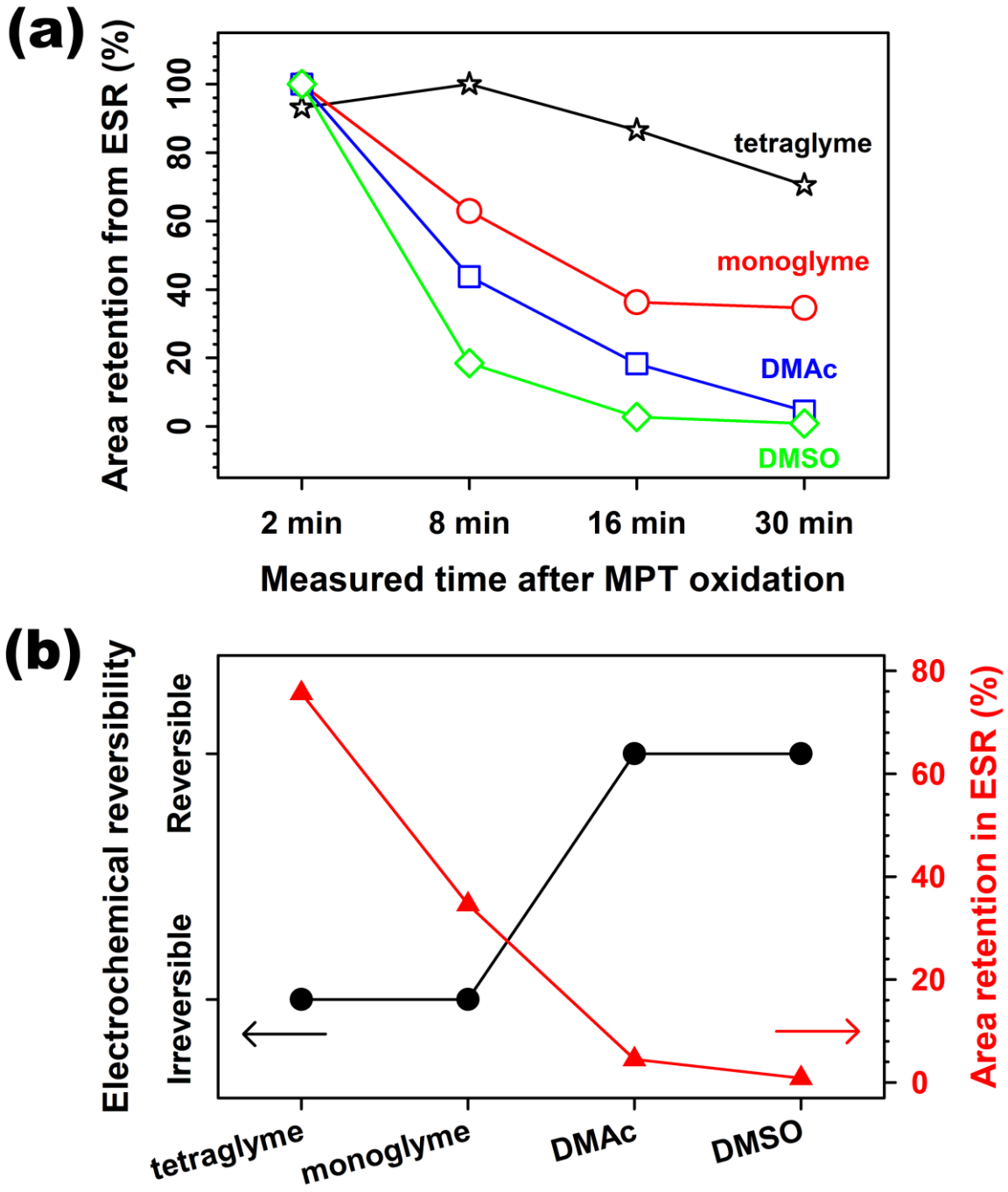

Figure 3.4 (a) The change of ESR signal area of $MPT^{\bullet+}$ over the time after electrochemical oxidation of MPT collected from Figure 2.3. (b) The electrochemical reversibility of MPT based on the cyclic voltammetry results and chemical stability of $MPT^{\bullet+}$ based on the ESR results in various electrolytes.

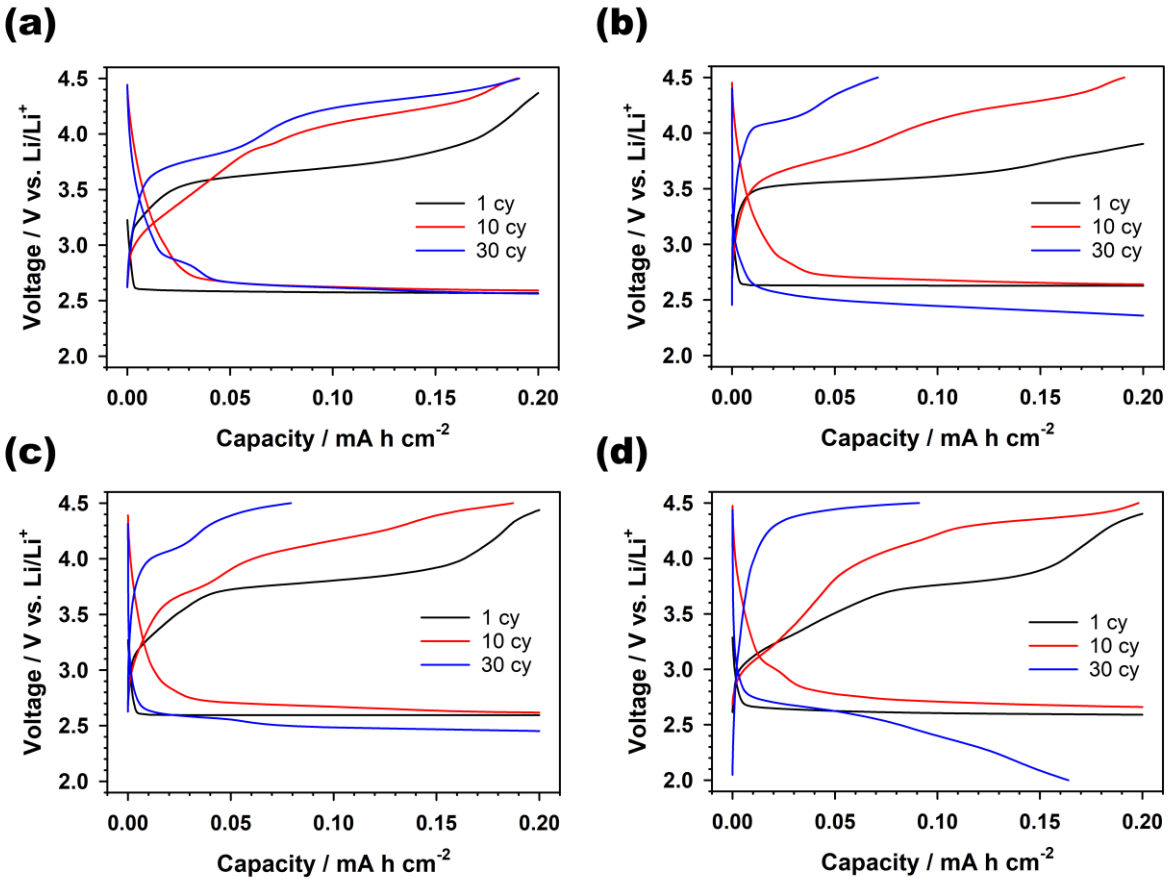

Figure 3.5 The voltage profiles of Li–O_2 cells with 0.5 *M* $LiSO_3CF_3$ and 10 *mM* MPT in a (a) tetraglyme, (b) monoglyme, (c) *N*,*N*–dimethylacetamide (DMAc), and (d) dimethyl sulfoxide (DMSO) at a constant current of 0.12 mA cm^{-2} with a constant capacity of 0.2 mA h cm^{-2} and the voltage range of 2.0 and 4.5 V *vs*. Li/Li^+. The Li–O_2 cells were performed with $LiFePO_4$ (LFP) as a counter electrode for avoiding the side effect of Li metal anode.

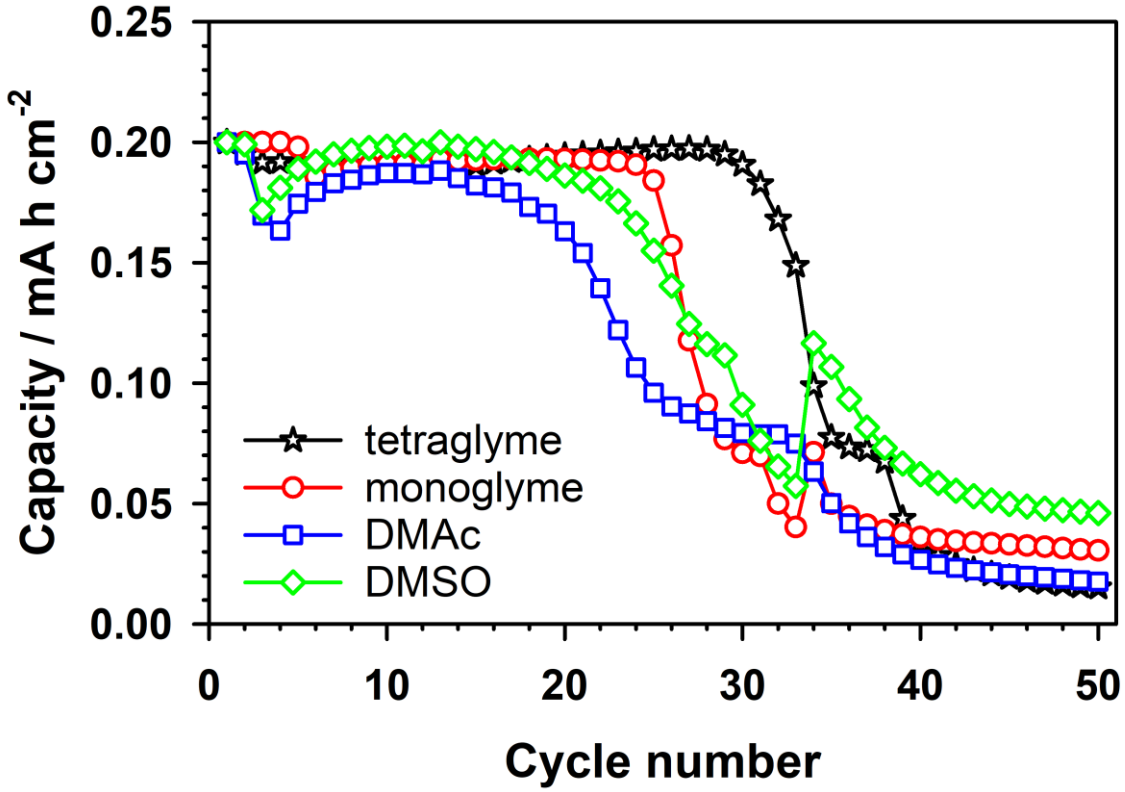

Figure 3.6 The cycle performance of Li–O_2 cells with 0.5 *M* $LiSO_3CF_3$ and 10 *mM* MPT in a (a) tetraglyme, (b) monoglyme, (c) *N*,*N*–dimethylacetamide (DMAc), and (d) dimethyl sulfoxide (DMSO).

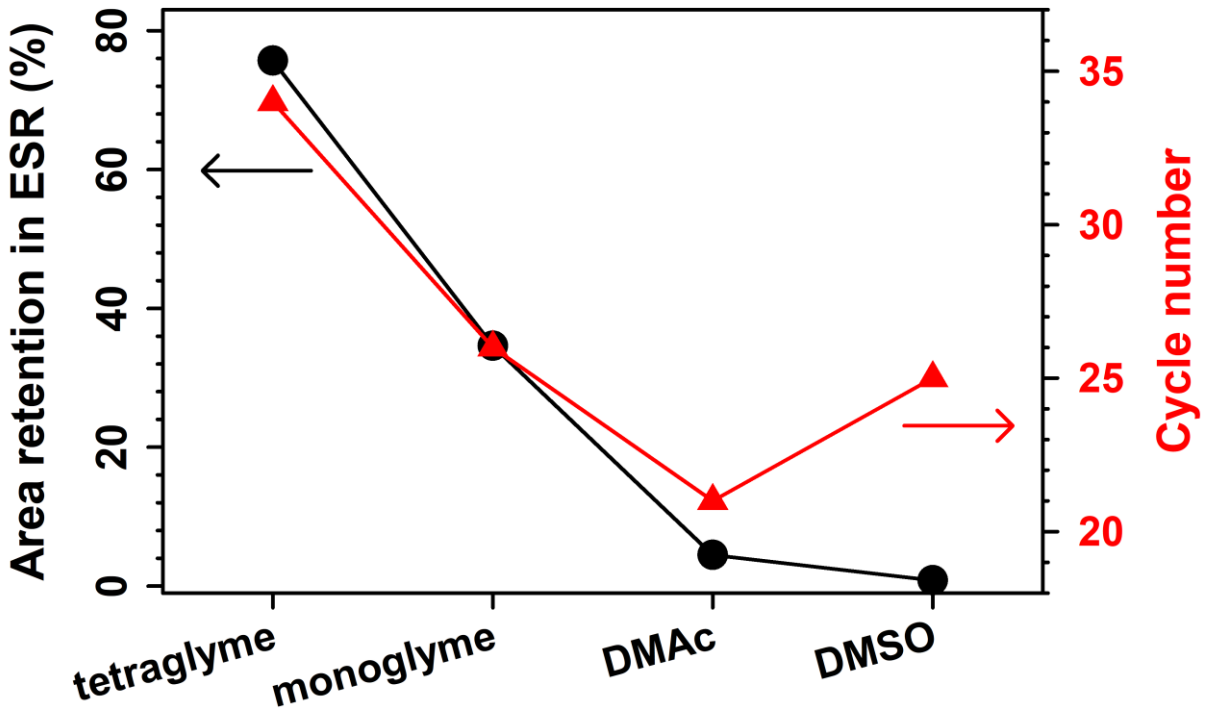

Figure 3.7 The chemical stability of $MPT^{\bullet+}$ collected from the ESR result of Figure 2.3 and cycle performance of Li–O_2 cells with various electrolytes collected from the Figure 2.6. The cycle performance of Li–O_2 cells was determined by the last cycle maintaining over the capacity retention of 75 %.

3.4 Summary

In this part, we investigated the relationship between the electrochemical performance of redox mediator and solvent. We selected four solvents, such as tetraglyme, monoglyme, DMAc, and DMSO, which widely use as electrolyte for Li–O_2 batteries and focused on the redox mediator for oxygen evolution reaction (OER). We evaluated the electrochemical reversibility of redox mediator via the cyclic voltammetry (CV) analysis and the chemical stability of redox mediator via the electron spin resonance (ESR) analysis. The model redox mediator is MPT.

The redox peak position of MPT in a tetraglyme–based electrolyte changed over the change of scan rate, indicating that the electrochemical reaction of MPT in a tetraglyme is irreversible. The redox peak position of MPT in a monoglyme–based electrolyte also increased with increasing scan rate, indicating that the electrochemical reaction of MPT in a monoglyme also is irreversible. In contrast, the redox peak position of MPT in the DMAc– and DMSO–based electrolyte maintain regardless of scan rate, indicating that the electrochemical reaction of MPT in those solvents is reversible. Therefore, the redox mediator is most reversible in DMAc– and DMSO solvents with MPT. However, the redox potential of MPT in the DMAc– and DMSO–based electrolyte shifted to higher potential than the theoretical redox potential of MPT, as a result, using these solvent for Li–O_2 batteries with MPT has no benefit for the improving energy efficiency.

The ESR peak area of $MPT^{\bullet+}$ in a tetraglyme–based electrolyte remain 70.50 % from the maximum peak area, indicating that the tetraglyme suppresses the side reaction among $MPT^{\bullet+}$ itself or between $MPT^{\bullet+}$ and electrolyte. In contrast, the ESR peak area of $MPT^{\bullet+}$ in monoglyme–, DMAc–, and DMSO–based electrolyte rapidly decreased to 34.62, 4.49, and 0.83 % from the maximum peak area, indicating that the those solvent hardly suppress the side reaction of $MPT^{\bullet+}$. Therefore, a tetraglyme is most suitable for the $MPT^{\bullet+}$ in the Li–O_2 batteries. Interestingly, the relationship between the electrochemical reversibility of MPT and the chemical stability of $MPT^{\bullet+}$ with the type of solvent is inverse proportion. Therefore, a use of specific solvent can't enhance both properties of redox mediator, and the analysis for the performance determining issue between them are needed.

To investigate the performance determining issue, the Li–O_2 cells with the four solvent as an electrolyte were examined with LFP counter electrode for excluding the effect of Li metal anode. The cycle performance of Li–O_2 batteries with a tetraglyme operated up to 34 cycles based on the capacity retention of 75 %. The cycle performance of Li–O_2 batteries with a monoglyme, DMAc, and DMSO performed up to 26 cycles, 21 cycles, and 25 cycles, respectively. These results demonstrated that the cycle performance of Li–O_2 batteries with MPT is strongly correlated with the chemical stability of $MPT^{\bullet+}$. Therefore, when the solvent improves the chemical stability of redox mediator radical, the effect of solvent clearly exhibited in the enhanced cycle performance Li–O_2 batteries with redox mediator. In other words, the increasing polarization of redox mediator in the Li–O_2 batteries over the increasing

cycle number correlates with the consumption of effective $MPT^{\bullet+}$, which is able to decompose the discharge products.

As a result, the most suitable solvent for MPT is tetraglyme. Therefore, a tetraglyme used as main electrolyte solvent in following part.

4. The stability of redox mediator with lithium metal anode for Li–O_2 batteries

4.1 Introduction

In the prior part, it is demonstrated the dependence of electrochemical performance of redox mediator on the electrolyte solvents. Despite using appropriate solvent can ensure the extended cyclability of Li–O_2 batteries, the Li–O_2 batteries are still suffered from the shortage of performance. To find the way for improving electrochemical performance of Li–O_2 batteries containing a redox mediator, Li metal anode is considered as a candidate to exacerbate the catalytic activity of redox mediator. Kim, Zhou, and Janek's group have been suggested that the failure of the Li–O_2 batteries is associated with the Li metal anode.[210, 213-214] They elucidates that the increasing polarization is arose from the reduced concentration of redox mediator radicals near the cathode by shuttle phenomenon, and preventing shuttling could be improved the performance of Li–O_2 batteries via Li metal protection. However, we disagrees this explanation based on shuttle effect, which is insufficient to clarify the failure mechanism of Li–O_2 cells containing redox mediators. The elucidation toward the loss of redox mediator as mentioned by a few research groups is more reliable than that based on shuttling.[211, 214] However, the precise failure mechanism associated with redox mediators in Li–O_2 cells remains unclear.

In this part, the failure mechanism is associated with the irreversible decomposition of redox mediator on the Li metal anode for the first time. This unexpected reaction leads to the both passivating Li metal anode and exhausting the redox mediators, resulting in the degradation of Li–O_2 batteries. Interestingly, despite the protective layer mainly consisting of lithium oxide formed by dissolved oxygen in the electrolyte covers the Li metal anode, the redox mediators in Li–O_2 batteries still decompose on the Li metal ignoring the protective layer. It demonstrates that this undesirable reaction is occurred by the redox mediator radicals diffused from the cathode. The redox mediator radicals spontaneously removes the protective layer consisting of lithium oxide, as a result, the exposed Li metal degrades due to the reductive decomposition of residual redox mediator. This failure process can be also delayed the protection of Li metal anode using $LiNO_3$ as a Li salt, which is simpler method than the previous suggestions.

4.2 Experimental details

4.2.1 Materials

To minimize the side reaction by trace water, the water contents of all solvents, such as *N*,*N*–dimethylacetamide (DMAc, Alfa Aesar, 99.8%) and tetraethylene glycol dimethyl ether (tetraglyme, Alfa Aesar, 99.69%), were controlled at less than 10 ppm via purifying with activated 4 Å molecular sieves (Alfa Aesar) before use. The value of water contents for the solvents was measured by Karl–Fischer titration (SP150, Metrohm). Moreover, Li and sodium salts, such as lithium nitrate ($LiNO_3$, Alfa Aesar, 99%), Lithium trifluoromethanesulfonate ($LiSO_3CF_3$, Sigma–Aldrich, 99.995%), and sodium nitrite ($NaNO_2$, Sigma–Aldrich, 99.999%), were dehydrated at 150 °C for 24 h in a vacuum oven before use. The 10–methylphenothiazine (MPT, Alfa Aesar, 99.9%) was also dehydrated at 60 °C for 48 h in a vacuum oven before use. After completely drying, all salts was dissolved in the solvents at a 1 molarity, for example, 1 *M* $LiNO_3$ in DMAc, 1 *M* $LiNO_3$ in tetraglyme, and 1 *M* $LiSO_3CF_3$ in tetraglyme. MPT was also dissolved in the solvents at a 0.05 for the majority of experiments or 0.2 molarity for only linear sweep voltammetry. All chemicals were handled under a 99.9999 % Ar atmosphere.

4.2.2 Electrode preparation

The oxygen cathode were prepared by slurry casting onto a carbon paper (TGP–H–030, Toray) as a current collect. The slurry consisted of 90 wt % Ketjenblack (KB), 10 wt % poly(tetrafluoroethylene) (PTFE, Sigma–Aldrich), and the mixture solvents of isopropanol (IPA, 99.9 %, Alfa Aesar, 80 v/v %) and deionized water (20 v/v %). A KB of *ca.* 254 μg (0.4 ± 0.05 mg cm^{-2}) loaded on the electrode with a 9 mm diameter, and the electrode were dehydrated at 120 °C for 12 hrs in a vacuum oven.

The $LiFePO_4$ (LFP) electrodes as reference electrode for three–electrode cells were prepared from a slurry made by dispersing 60 wt % LFP, 20 wt % carbon black (Super P), and 20 wt % poly(1,1–difluoroethylene) (polyvinylidene fluoride, PVdF) into the 1–Methylpyrrolidin–2–one (*N*–Methyl–2–pyrrolidone, NMP). The slurry was casted onto a 316 SUS foil of 9 mm diameter as a current collector selected for avoiding Al corrosion by the electrolyte, and the electrodes were dehydrated at 120 °C for 12 hrs in a vacuum oven. The loading amounts of LFP were 1.5 ± 0.1 mg cm^{-2}.

4.2.3 Electrochemical characterization

All voltammetry techniques were performed using a SP150 potentiostat (BioLogic Science Instruments) with the homemade three–electrode cells consisting of a glassy carbon rod (area = 0.03 cm^2, Alfa Aesar), 316 SUS mesh (area = 2.01 cm^2, 200 mesh), and Li metal foil (thickness = 700 μm, Honjo Metal) or partially discharged lithium iron phosphate (Li_xFePO_4, x < 1, LFP) as the working,

counter, and reference electrodes, respectively. The cyclic voltammetry for the evaluating the electrochemical reversibility of redox mediator was conducted at a scan rate of 50 mV s^{-1} in the voltage range of 2.0 ~ 4.5 V (*vs*. Li/Li^+). In case of examining the electrolyte containing a $LiSO_3CF_3$ and MPT, The LFP was used as a reference electrode, whereas the Li metal was used as a reference electrode for the examining the electrolyte containing a $LiNO_3$ and MPT. The linear sweep voltammetry for investigating the reductive electrochemical window of tetraglyme electrolyte containing 1 *M* $LiSO_3CF_3$ and 0.2 *M* MPT or MPT–free was performed in the voltage range from open circuit voltage (OCV) to 0 V (*vs*. Li/Li^+) at a scan rate of 10 mV s^{-1}.

All galvanostatic experiments were performed with two–electrode system using WBCS3000 galvanostat (WonATech). The galvanostatic voltage profiles of Li symmetric cells were collected with performing at a current density of 88 μA cm^{-2} and a constant capacity of 44 μA h cm^{-2} using a 2032 coin cell for Ar dissolved electrolytes and a Swagelok cell for O_2 dissolved electrolytes. The galvanostatic experments of the Li symmetric cells containing the oxidized MPT (MPT radical, $MPT^{\bullet+}$) was performed using a homemade five–electrode cell consisting of two Li electrodes for symmetric cell experiment, a glassy carbon rod as a working, 316 SUS mesh as a counter, and $Li_{0.5}FePO_4$ as a reference electrodes. The plating/stripping of Li in the Li symmetric cell in the five–electrode cell was conducted at a current density of 88 μA cm^{-2} and a constant capacity of 44 μA h cm^{-2} over 50 cycles. After Li symmetric cell was terminated up to 50 cycles, MPT was oxidized to $MPT^{\bullet+}$ by applying a constant voltage at 3.7 V (*vs*. Li/Li^+) for 72 h using the three–electrode cell in the five–electrode cell. After $MPT^{\bullet+}$ formation, the ended Li symmetric cells was resumed under same condition as before termination.

The oxygen cathode, Li metal anode (diameter = 11 mm), and glass fiber separator (Whatman® GF/C, Sigma–Aldrich, diameter = 12 mm) comprised the Swagelok cell for the Li–O_2 batteries. The various electrolyte, such as tetraglyme electrolyte containing 1 *M* $LiSO_3CF_3$ or 1 *M* $LiNO_3$ + 50 *mM* MPT and DMAc containing 1 *M* $LiNO_3$ + 50 *mM* MPT, was added to the Li–O_2 cell with an amount of 120 μL. The galvanostatic experiments of Li–O_2 batteries were performed at a current density of 300 mA g^{-1}_{KB}, a constant capacity of 1000 mA h g^{-1}_{KB} based on the weight of KB on the oxygen electrode, and sealed cell chamber with a static pressure of 1 bar after purging with 99.999% O_2. The purging process was performed with a flow rate of 40 mL min^{-1} for 5 min and a pressure of 2 bar. Instead of continuous O_2 flowing, the Li–O_2 cell was purged with O_2 after every 33 cycles.

4.2.4 Characterization

The *ex situ* ^1H nuclear magnetic resonance (NMR) analysis of collected 1 mL electrolyte from the homemade three–electrode cell after every three cycles of cyclic voltammetry over a month interval was performed in an Ar–filled glove box using ^1H NMR (ASCEND 400, Bruker, 400 MHz, solvent:

Acetone–d_6) with the internal reference of tetramethylsilane (TMS). The chemical components of Li metal surface immersing in tetraglyme electrolyte containing 1.0 *M* $LiSO_3CF_3$ under Ar and O_2 atmospheres for 2 days was analyzed using the *ex situ* X–ray photoelectron spectroscopy (XPS, Sigma probe, Thermo Fisher Scientific, Al K_α) analysis. The XPS of Li metal surface was conducted after 420 seconds etching with minimizing exposure to air. The chemical components of Li metal surface after the cycling of Li symmetric cell with in tetraglyme electrolyte containing 1.0 *M* $LiSO_3CF_3$ and 50 *mM* MPT under Ar and O_2 atmospheres were examined by the time–of–flight secondary ion mass spectrometry (TOF–SIMS) analyses using a TOF.SIMS 5 system (ION–TOF GmbH, Germany) equipped with a Bi^+ primary ion beam source. The pulsed 30–keV Bi^+ beam bombarded the surface of 45° at an incident to the surface normal within a raster size of 100 μm × 100 μm with a constant pulsed current of 0.40 pA. A 2–keV Cs^+ primary ion beam with a Cameca IMS 4FE7 instrument was used for dynamic SIMS depth profiles. Depth profiles measured by negative secondary ions were obtained within a raster size of 250 μm × 250 μm with the primary beam current of 160 nA and at a sputtering rate of 0.8227 nm s^{-1}. The *in situ* electron spin resonance (ESR) analysis was conducted using homemade 3–electrode cell consisting of Au electrode, 316 SUS mesh, and Li metal as a working, counter, and reference electrode, respectively. The Au electrode possessed helix structure and rolled around other electrodes with polyethylene separator for insulation between electrodes. Therefore, the radical generated from the working electrode was detected clearly by ESR due to the signal amplifying effect of Au electrode. The 3–electrode cell was filled the 550 μl of MPT contained electrolytes, such as tetraglyme electrolyte containing 1.0 *M* $LiSO_3CF_3$, 50 *mM* MPT or MPT–free and 50 *mM* $NaNO_2$. The ESR spectra were obtained from a Bruker EMXmicro–9.5/2.7 continuous–wave (CW) X–band ESR spectrometer, equipped with a Bruker ER 4102ST resonator operating *ca*. 9.801 GHz combined with ER 4141 VT for measuring the temperature of cavity. The microwave power was set to 2 mW and sweeps were performed over a range of 15.0 mT with a center field of *ca*. 349.7 mT at *ca.* 293 K. The field modulation frequency was set to 100 kHz and the modulation amplitude was 0.1 mT. The first derivatives of CW ESR spectra were recorded continuously for 1 hour with an interval of 30 sec after the electrochemical oxidation of MPT applying a constant voltage of 3.8 V (*vs*. Li/Li^+) for 1 min by the potentiostat (1285A DC Potentiostat, Solartron).

4.3 Result and Discussion

4.3.1 Failure mechanism for Li–O_2 cells containing a redox mediator

The electrochemical performance of Li symmetric cells with MPT–free and MPT under Ar and O_2 atmospheres was evaluated for investigating the failure mechanism of Li–O_2 cells with a redox mediator. Figures 4.1a and b show the galvanostatic profiles of the Li/Li cells with MPT–free, under Ar and O_2, respectively. These figures demonstrates that the Li metal stripping/plating was remained reversibly over 300 cycles with only a small polarization of *ca.* 20 mV. However, as shown in Figures 4.1c and d, the behaviors of Li symmetric cell with MPT could be observed the distinction depending on atmospheres. Whereas the Li symmetric cells containing a MPT showed stable cycle performance under O_2 over 300 cycles with a small polarization, by contrast, the polarization of the Li symmetric cells with containing a MPT significantly increased to a few hundreds of mV after tens of cycles, i.e., it was ten times higher than the polarization under O_2. In addition, whereas there is no fluctuation of voltage profile for Li symmetric cells containing a MPT under O_2 (Figure 4.1e), the instability of profiles under Ar could be observed, as shown in Figure 4.1f. This indicates that there is inhomogeneous degradation of Li metal surface under Ar, correlating with thick passivation impeding the uniform Li plating/stripping. On the contrary, an O_2 atmosphere positively influences on the Li metal surface. Aurbach et al. and other researchers demonstrated that the O_2 in the electrolyte help the formation of protective layers containing lithium oxides on Li metal.[97, 231-232] The O 1s and Li 1s XPS spectra of the Li metals stored in the electrolyte with O_2 showed that Li–O peak associated with lithium oxide was mainly observed under O_2, whereas Li–O–C peak associated with lithium alkyl carbonates was mainly observed under Ar as shown in Figure 4.2.[232-235] This reveals that the Li metal surface covered with oxygen derived protective layer in the linear ethereal electrolyte exposed to O_2. This layer retards the side reaction between MPT and Li metal, leading to improved cycle performance with low polarization of the Li symmetric cells.

To verify the MPT decomposition under Ar, linear sweep voltammetry and cyclic voltammetry of MPT were conducted under an Ar–atmosphere using a three–electrode cell with 1.0 *M* $LiSO_3CF_3$ in tetraglyme. An new reduction peak for the electrolyte containing 200 *mM* MPT was observed at *ca.* 1.3 V (*vs*. Li/Li^+) as shown in Figure 4.3a, but there is no additional peak for the MPT–free pristine electrolyte, indicating that the reductive decomposition of MPT occurs near to *ca.* 1.3 V (*vs*. Li/Li^+). This implies that MPT in contact with Li metal will be decomposed owing to the low redox potential of Li metal (0 V *vs*. Li/Li^+) than 1.3 V (*vs*. Li/Li^+). The cyclic voltammograms of MPT with Li metal was also clarified the irreversible decomposition of MPT, as shown in Figure 4.3b. To evaluate the influence of Li metal toward MPT, a piece of Li metal were immersed into the electrolyte for 12 and 30 days before performing controlled cyclic voltammetry of MPT. Before the immersing, the MPT maintained their redox reaction, however, the intensity of reduction peak of MPT gradually reduced

over stirring, and almost disappeared after 30 days in accompanying with the appearance of a new broad oxidation peak at near 3.2–3.7 V (*vs*. Li/Li^+). The *ex situ* ^1H NMR of MPT directly demonstrated that the new peak is attributed to the oxidation of decomposed MPT species (Figure 4.3c). The NMR spectrum of MPT in the pristine electrolyte consisted of three sets of peaks: 6.98–6.93 ppm (4H, multiplet), 7.24–7.19 ppm (2H, triplet), and 7.16–7.12 ppm (2H, doublet), which corresponded to protons in the aromatic ring.[233] However, after exposure to Li metal, the intensity of these peaks related with MPT decreased, and new ^1H peaks appeared at 6.70–6.50 ppm, 7.12–7.02 ppm, and 7.44–7.30 ppm, indicating to the decomposition products of MPT. These new ^1H peaks remain in range of the aromatic region between 6.0 and 8.0 ppm, which is identical to peak–splitting pattern of MPT but with small chemical shift. This implies that the aromatic ring in MPT maintain their structure after the side reaction, however, the sulfur element connecting between two benzene rings reacts with the Li metal. Gilman et al. described that the sulfur in heterocyclic dibenzo–derivatives is easily dissociated by Li metal owing to their weaker bond energy than other bonds, resulting in the converting into Li adducts.[236]

The change of Li metal surface were analyzed after the Li plating/stripping of Li symmetric cell over 50 cycles to clarify the origin of Li metal failure. As shown Figure 4.4a and b, The surface of Li metal performing with MPT–containing electrolyte was covered with thick grayish brown passivation, whereas the Li metal performing with MPT–free electrolyte still maintained metallic and shiny surface. This pictures indicate that the severe side reactions occur during Li plating and stripping over 50 cycles with MPT–containing electrolyte, as a results, the unexpected products passivate on the surface of Li metal and deteriorate the electrochemical performance of Li metal. The chemical species constituted the passivation on Li metal were analyzed by *ex situ* TOF–SIMS. The ion counts of S^- and LiS^- species for with MPT were approximately 100 times higher than for MPT–free on the basis of C^- species as shown in Figure 4.4c and d. Because sulfur elements only make up MPT and Li salt anion, this results clearly demonstrates that sulfur element in the MPT reacts with Li metal and their decomposition products accumulates on the Li metal surface during cycling. The decomposition of $LiSO_3CF_3$ as a Li salt contributes the observation of a trace sulfur–containing species for with MPT–free.

Prior results under Ar atmosphere demonstrates the undesirable reaction between MPT and Li metal anode leads the failure of Li metal. On the other hand, the electrochemical operation of Li metal anode containing MPT under O_2 atmosphere maintain the stable state due to oxygen derived protective layer. In point of view based on the two conclusion, the hypothesis, which is supported by the fact that undesirable reaction significantly influences the failure of $Li–O_2$ batteries with MPT, may be illogical. The difference among the conflicting results raises questions why does the $Li–O_2$ batteries containing a redox mediator still degrades. To account for the reason of the failure, the difference among the results must be considered: whether redox mediator radicals forms or not, is a key to explaining the failure. The influence of degradation oxidized MPT (MPT radical, $MPT^{\bullet+}$) toward the deterioration of $Li–O_2$ cells containing O_2 atmosphere during cycling was further investigated via performing the

electrochemical performance of a Li symmetric cell with the electrolyte dissolved MPT and O_2, as shown in Figure 4.5. A homemade five–electrode cell was introduced for this analysis; the cell consists of two independent sub–cells, such as a two–electrode sub–cell and a three–electrode sub–cell (Figure 4.5a). The two–electrode sub–cell consists of two Li electrodes for Li plating/stripping. The three electrode sub–cell for the electrochemical oxidation of MPT is composed of a glassy carbon rod, a 316 SUS mesh, and $Li_{0.5}FePO_4$ as working, counter, and reference electrodes, respectively. The Li symmetric cell was initially conducted at a current density of 88 μA cm^{-2} and with a capacity of 44 μA h cm^{-2} up to 50 cycles. It coincides the voltage profile of cell as shown in Figure 4.5b with the prior results as shown in Figure 4.1d: the cycle performance of the symmetric cell maintains stably with a constant polarization of *ca.* 14 mV. This result clarify again that Li symmetric cell shows stable performance during cycling when the electrolyte containing with MPT and O_2 but $MPT^{\bullet+}$–free was adopted. After Li symmetric cell performed up to 50 cycles, it disconnect the symmetric cell from the galvanostat to excluding the influence of other external circuit to the closed circuit for MPT oxidation. Afterward, MPT oxidizes to $MPT^{\bullet+}$ with a constant voltage of 3.7 V (*vs*. Li/Li^+) for 72 h by the three–electrode sub–cell. When the MPT oxidation ended, the 3–electrode cell isolated from potentiostatic devices. Subsequently, the galvanostatic Li plating/stripping of the terminated Li symmetric cell were then restarted. After the exposure of Li metal to $MPT^{\bullet+}$, the Li symmetric cell instantly shows a significantly large polarization of *ca.* 100 mV and unstable voltage profiles. This degraded electrochemical behavior was analogous with that of the Li symmetric cell with MPT under Ar as shown in Figure 4.1c. This result indicates that the lithium oxides based protective layer on the Li metal surface had been damaged after exposure to $MPT^{\bullet+}$. In other words, when $MPT^{\bullet+}$ formed on the glassy carbon electrode by the electrochemical oxidation of MPT, the radicals diffused to the Li metal anode due to low concentration of $MPT^{\bullet+}$ near to the Li metal anode. The diffused $MPT^{\bullet+}$ was reduced to MPT on the surface of Li metal anode, simultaneously, the lithium oxide constituting the protective layers on the Li metal decomposes into Li^+ and O_2.[203] The catalytic reaction mechanism of redox mediators for the decomposition of Li_2O_2 formed in the oxygen cathode is identical to this undesirable reaction. The unprotected site of Li metal anode, which be able to expose to the MPT dissolved in the electrolytes, increases due to $MPT^{\bullet+}$, resulting in the continuous and severe side reaction between MPT and exposed Li metal surface. As a result, the thick passivation on Li metal anode arise from this unexpected reaction due to MPT radicals. The result was the rapidly increased polarization of the Li symmetric cell after 50 cycles. This mechanism is summarized as shown in Figure 4.6.

The conflicting results, which occur the performance degradation of Li–O_2 cells containing a redox mediator in spite of the protection of Li metal anode by O_2 dissolved in the electrolyte, is clearly elucidated by this considering of redox mediator radical in the failure mechanism. Moreover, this elucidation also demonstrates that not solely the depletion of MPT but also the degradation of Li metal anode owing to the accumulation of thick passivation arising from the undesirable reaction between

MPT and Li metal anode deteriorates the Li–O_2 cells containing redox mediators.

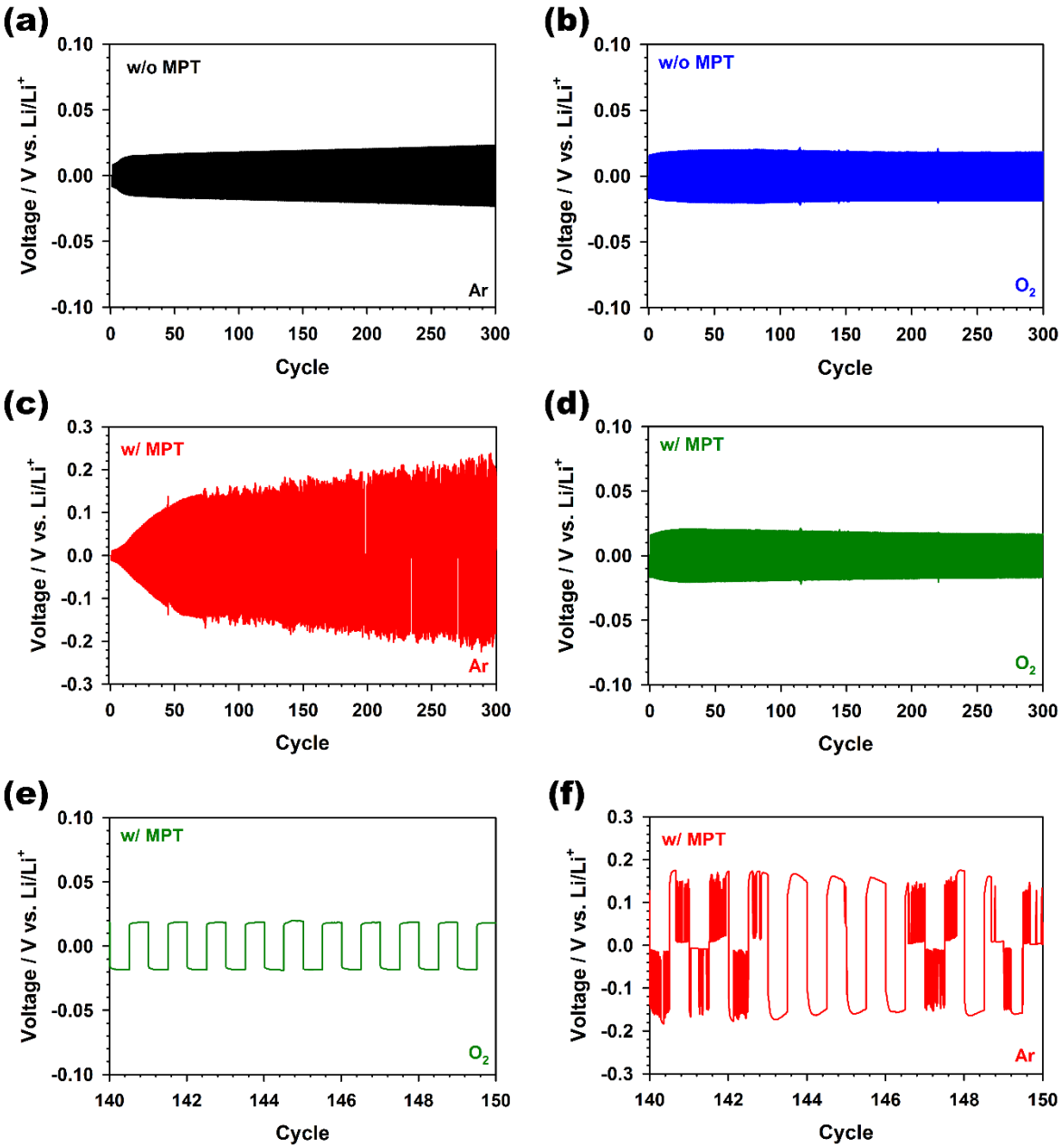

Figure 4.1 Galvanostatic stripping and plating profiles of Li symmetric cell containing 10–methylphenothiazine (MPT) under (a) Ar and (b) O_2, and containing MPT–free under (c) Ar and (d) O_2. Enlarged profiles of the Li symmetric cell containing MPT under (e) O_2 and (f) Ar in the chosen cycles between 140 and 150 cycles. Current density: discharge/charge with a current density of ± 88 μA cm^{-2} for 30 min in each step.

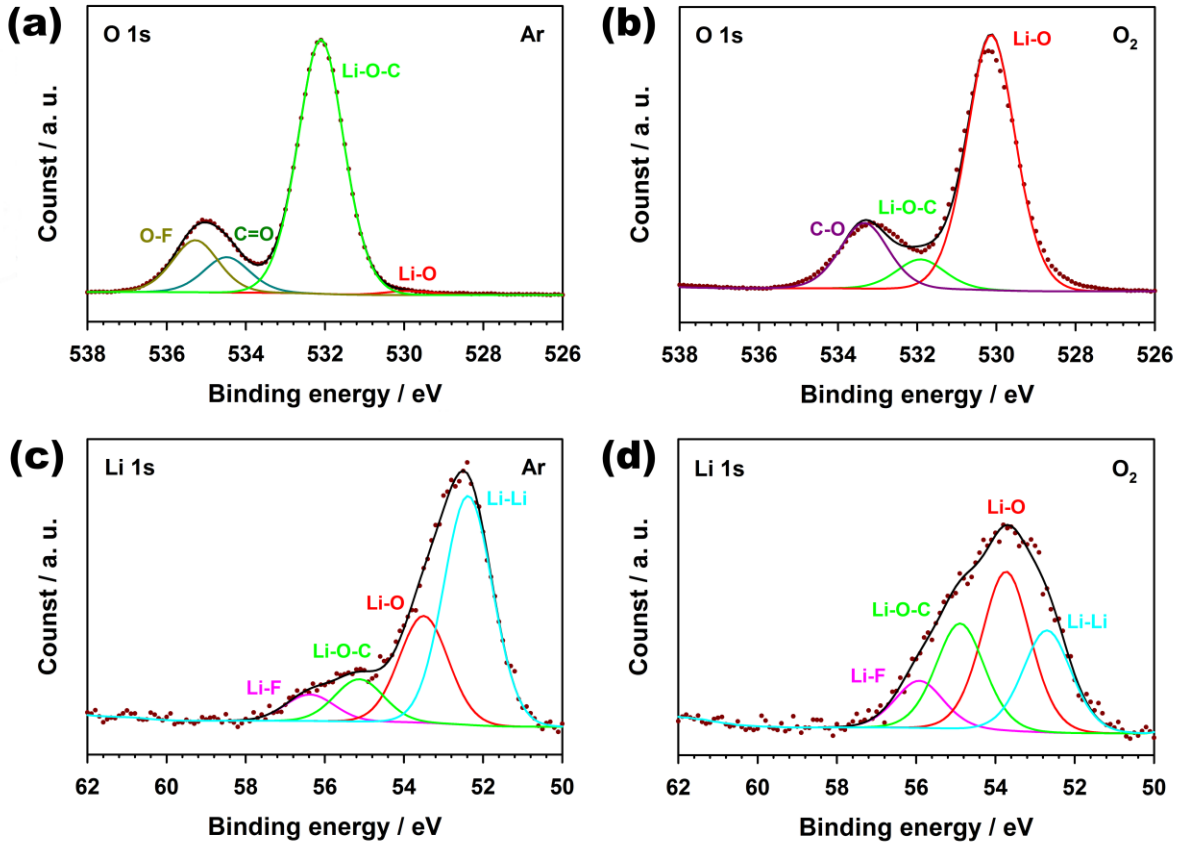

Figure 4.2 O 1s and Li 1s XPS spectra of the Li metal surfaces immersed for 2 days in tetraglyme electrolyte containing 1 *M* $LiSO_3CF_3$ + 50 *mM* MPT dissolved (a, c) Ar or (b, d) O_2, respectively.

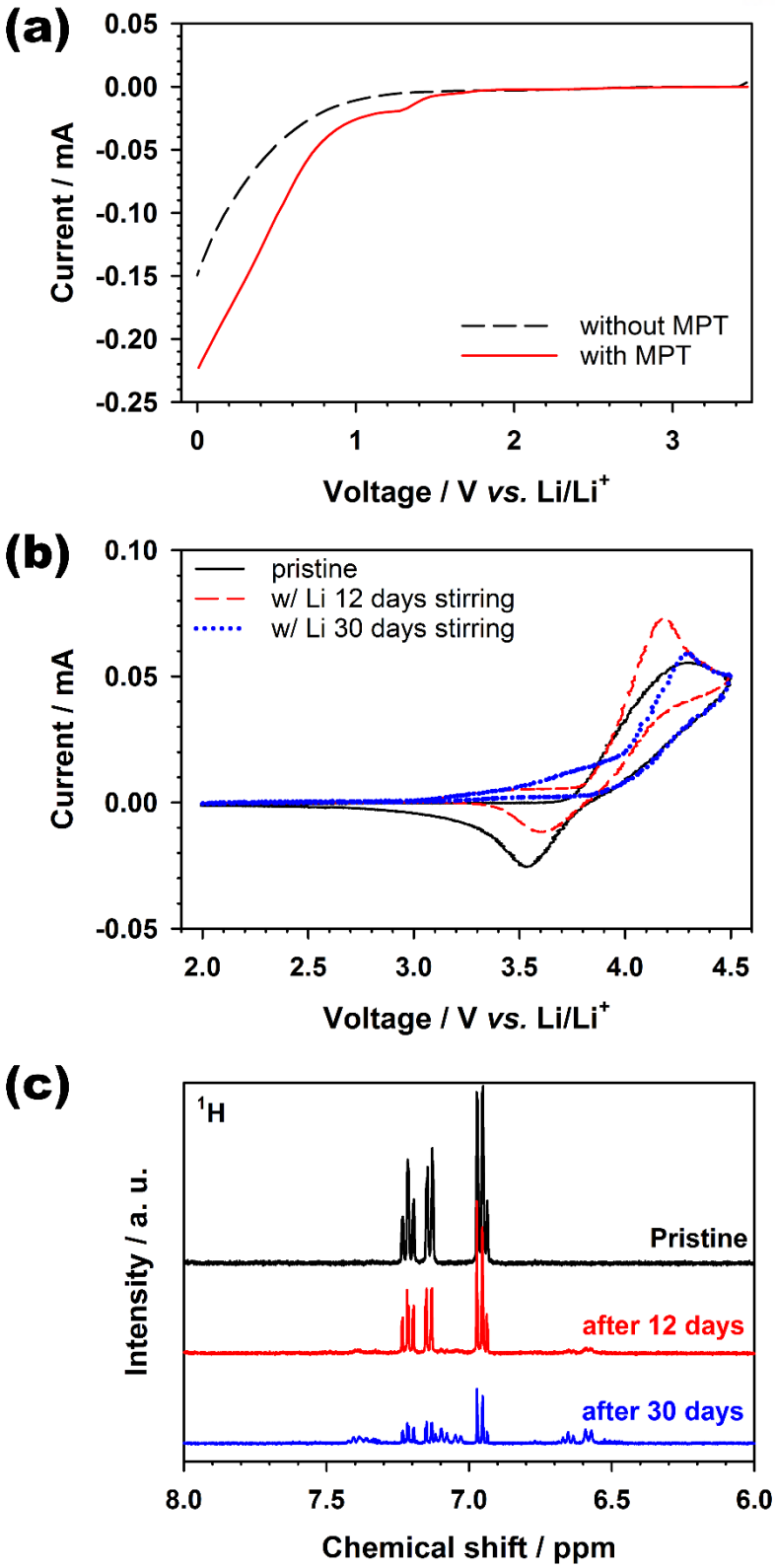

Figure 4.3 (a) Linear sweep voltammograms of tetraglyme electrolyte containing 1 *M* $LiSO_3CF_3$ + 200 *mM* MPT or MPT–free at a scan rate of 10 mV s^{-1}. (b) Cyclic voltammograms of MPT in the electrolyte before and after stirring with Li metal for 12 and 30 days at a scan rate of 10 mV s^{-1}. (c) ^1H NMR spectra of the collected electrolyte before and after stirring with Li metal for 12 and 30 days.

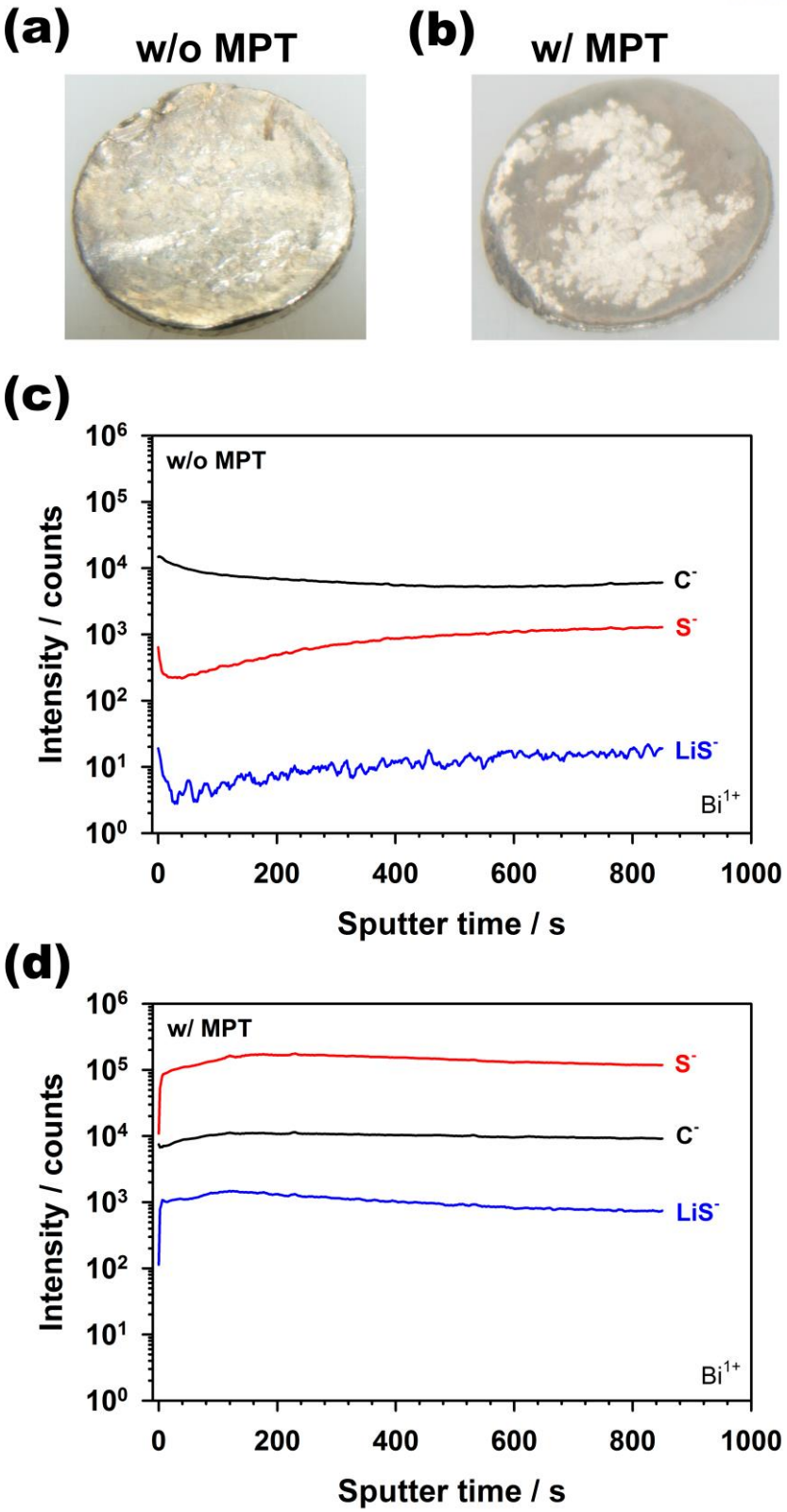

Figure 4.4 The optical images and dynamic secondary ion mass spectrometry (SIMS) depth profiles of the collected Li metals after performing the galvanostatic Li plating and stripping of the Li symmetric cell containing (a, c) MPT and (b, d) MPT–free over 50 cycles. Current density: discharge/charge with a current density of ± 88 μA cm^{-2} for 30 min in each step.

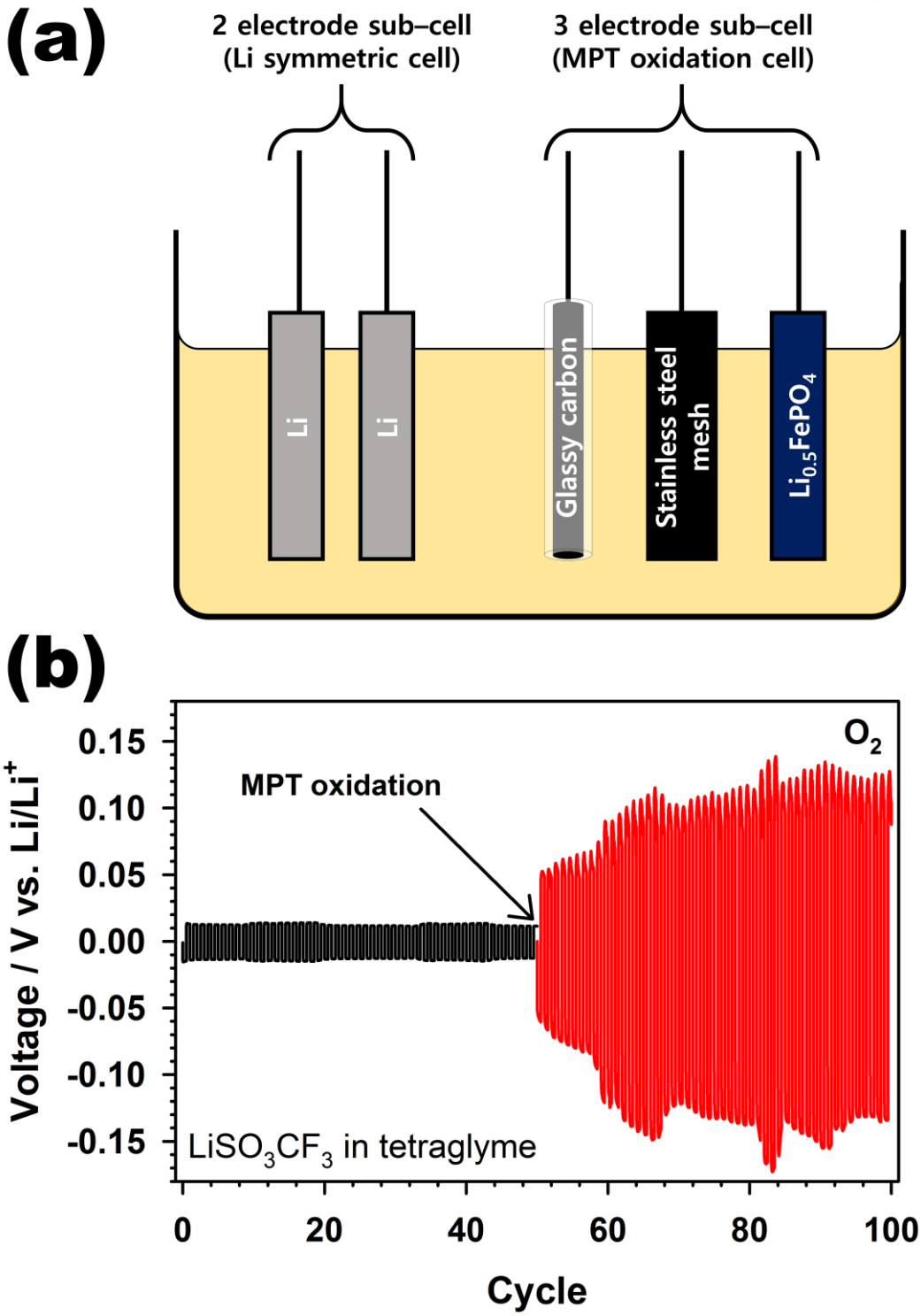

Figure 4.5 (a) A schematic diagram of the homemade five–electrode cell consisting of a two–electrode sub–cell for examining the electrochemical performance of Li and a 3–electrode sub–cell for the electrochemical oxidation of MPT. (b) Galvanostatic voltage profiles of the Li symmetric cell with tetraglyme electrolyte containing 1 *M* $LiSO_3CF_3$ + 50 *mM* MPT using the five–electrode cell. The MPT was oxidized to $MPT^{\bullet+}$ after 50 cycles at a constant voltage of 3.8 V (*vs.* Li/Li^+). Current density: discharge/charge with a current density of ± 88 μA cm^{-2} for 30 min in each step.

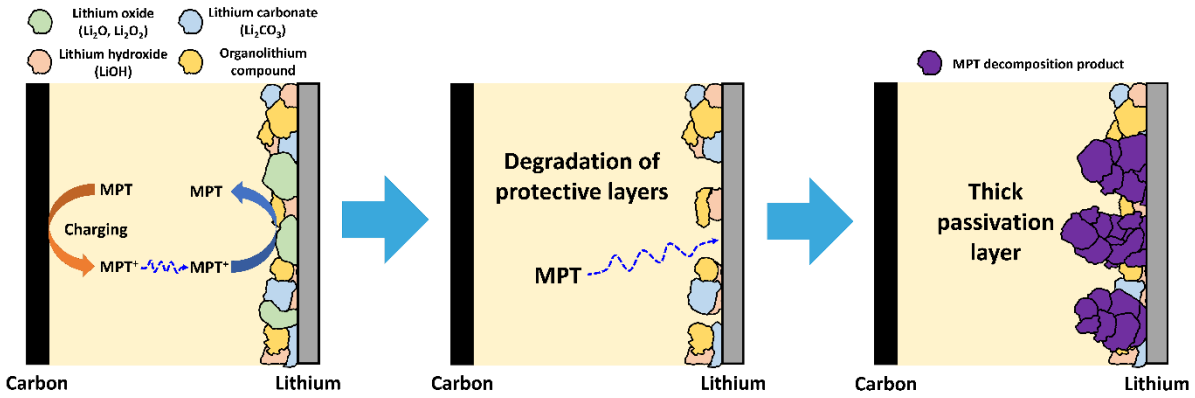

Figure 4.6 Schematic diagram for the failure mechanism of the Li–O_2 batteries containing MPT.

4.3.2 Redox mediator protection

The Li–O_2 cells with various electrolytes containing MPT was examined to evaluation their electrochemical performance as shown in Figure 4.7. The Li–O_2 cells using DMAc electrolyte containing $LiNO_3$ and MPT showed the stable cycle performance without capacity fading up to 120 cycles, whereas the electrochemical performance of Li–O_2 cells using tetraglyme electrolyte with $LiNO_3$ and MPT. The difference between the performance of Li–O_2 cells using DMAc and that using tetraglyme–based electrolyte is influenced by the solvent effect on the reversibility of Li_2O_2. In the tetraglyme, the Li_2O_2 converts to irreversible Li_2CO_3 occasionally during cycling, whereas DMAc arise the reversible formation of Li_2O_2.[180] This Li_2CO_3 leads to the obstruction of ORR and OER on the oxygen cathode and electrolyte depletion, resulting in the degradation of the Li–O_2 cells, which is analogous to the surface morphologies as shown in Figure 1.4.

Furthermore, the salt anion also significantly influences to the electrochemical performance of the Li–O_2 cells. The Li–O_2 cell using tetraglyme electrolyte containing $LiNO_3$ and MPT exhibited improved cyclability than that of Li–O_2 cell containing $LiSO_3CF_3$. This improvement of electrochemical performance is associated with the extension for the electrochemical activity of MPT by the salt anion. The Li–O_2 cell using $LiSO_3CF_3$ showed sharply increasing charging potential as cycle number increase, on the other hand, the Li–O_2 cell containing $LiNO_3$ showed the gradually increasing potential with cycle number. This comparison suggests that the electrochemical activity of MPT remained longer with $LiNO_3$ than with $LiSO_3CF_3$.

The origin of the extended MPT activity was investigated by comparison between the cyclic voltammograms of MPT using electrolytes containing $LiSO_3CF_3$, $LiNO_3$, and $LiSO_3CF_3$ + $NaNO_2$ at various scan rates. The working, counter, and reference electrodes were glassy carbon rod, 316 SUS mesh, and Li metal, respectively. The MPT with $LiSO_3CF_3$ shows the redox peaks to be irrelevant to the scan rate as shown in Figure 4.8a. Contrastively, the reduction peak of MPT with $LiNO_3$ disappeared at a slow scan rate of 50 mV s^{-1}, whereas the all redox peaks of MPT were exhibited at a fast scan rate of 300 mV s^{-1} as shown in Figure 4.8b. The change of MPT redox peaks depending on scan rate indicates that $MPT^{\bullet+}$ formed after the oxidation of MPT converted slowly to nonreactive form via an unexpected route before the electrochemical reduction. In other words, $MPT^{\bullet+}$, which formed electrochemically from MPT during an anodic scan, changed slowly to other form via chemical reaction, resulting in the disappearing of MPT reduction peak in the cyclic voltammogram at the slow scan rate. However, because this chemical reaction has slow kinetics, the $MPT^{\bullet+}$ was reduced to MPT electrochemically before $MPT^{\bullet+}$ was totally converted to inactive form through the chemical reaction. Therefore, the reduction peak on the cathodic scan was observed at the fast scan rate. The following chemical equation shows the proposed $MPT^{\bullet+}$ consumption process:

$$NO_3^- + 2Li \rightarrow Li_2O + NO_2^- \qquad (1)$$

$$NO_2^- + MPT^{\bullet+} \rightarrow NO_2 + MPT \quad (2)$$

The $LiNO_3$ dissolved in ethereal electrolyte has been suggested as an effective Li salt or additive for building a protective SEI layer on the Li metal anode in the Li–S and Li–O_2 electrochemical system. The protection mechanism of NO_3^- has been proposed that the formation of Li_2O or LiN_xO_y as a main component for the protective layer on Li metal are carried out by the reaction between NO_3^- and Li, leading to forming by–product, such as soluble NO_2^- as shown in the equation 1.[95, 173, 237] Furthermore, Aurbach's group introduced that this NO_2^- has the oxidation potential of *ca.* 3.6 V (*vs*. Li/Li^+), as a result of the oxidation, forming to gaseous NO_2.[238] This oxidation of NO_2^- is surmised to be associated with the disappearing of MPT reduction peak. Because the redox potential of MPT (*ca.* 3.8 V *vs*. Li/Li^+) is slightly higher than that of NO_2^-, the electron of NO_2^- can transfers spontaneously to the $MPT^{\bullet+}$, resulting in the forming NO_2 and MPT. The self–discharge reaction between $MPT^{\bullet+}$ and NO_2^- was investigated by performing cyclic voltammograms of MPT using tetraglyme electrolyte dissolving $LiSO_3CF_3$ and 50 *mM* $NaNO_2$. A $NaNO_2$ dissociates itself into Na^+ and NO_2^- in the electrolyte. After the addition of $NaNO_2$ to the electrolyte, the reduction peak of $MPT^{\bullet+}$ was not observed without the association of the scan rate as shown in Figure 4.8c. This disappearance is analogous to that of tetraglyme electrolyte dissolving $LiNO_3$ at the slow scan rate as shown in Figure 4.8b. Furthermore, despite the electrochemical reaction of $MPT^{\bullet+}$ does not exists, the redox reaction of MPT with the electrolyte containing $NaNO_2$ showed high reversibility over 200 cycles without the intensity change of the oxidation peaks for MPT, as shown in Figure 4.8d. This results suggests that the $MPT^{\bullet+}$ reversibly returns to the original form of MPT with no side reaction when self–discharge reaction between $MPT^{\bullet+}$ and NO_2^- undergo. This chemical reaction between $MPT^{\bullet+}$ and NO_2^- was also demonstrated by the electron spin resonance (ESR) analysis of $MPT^{\bullet+}$ change as shown in Figure 4.9. All ESR signal of $MPT^{\bullet+}$ showed the g–factor value of *ca.* 2.005, which is consistent with the literature results for a single unpaired electron on the nitrogen atom of the MPT.[228] As shown in Figure 4.9a, the pristine tetraglyme electrolyte containing $LiSO_3CF_3$ and 50 *mM* MPT showed no ESR signal, indicating that no radical state molecules in the electrolyte. However, the strong signal of $MPT^{\bullet+}$ exhibited after the electrochemical oxidation at a constant voltage of 3.8 V (*vs.* Li/Li^+). Moreover, the intensity of this signal just decreased slightly after 25 min in consistent with the chapter 2 results. In contrast, the signal of $MPT^{\bullet+}$ with NO_2^- significantly decreased in a few minutes and completely disappeared after 25 min as shown in Figure 4.9b, suggesting that $MPT^{\bullet+}$ readily react with NO_2^- following the equation 2 rather than the side reaction. In addition, the no ESR signal of NO_2^- and NO_2 exhibited before and after electrochemical oxidation as shown in Figure 4.9c. This results indicates that despite the NO_2 molecule possesses a paramagnetic property, the ESR signal of NO_2 is undetectable due to the gaseous phase of the molecule in room temperature. As a result, All ESR signal were no correlation with the ESR signal

of NO_2. Therefore, the results of the cyclic voltammograms and the ESR supports our conjecture that MPT in the Li–O_2 cells with $LiNO_3$ was not decomposed on the Li metal, because NO_2^- obtained from $LiNO_3$ in the electrolyte scavenged the $MPT^{\bullet+}$ that diffused into the Li metal. This implies that the better cycle performance of Li–O_2 cells with $LiNO_3$ is attributed to the increased lifetime of MPT.

Furthermore, the effect of $LiNO_3$ against the decomposing lithium oxide protective layer on the Li metal anode by $MPT^{\bullet+}$ was also demonstrated by examining the electrochemical performance of Li symmetric cell using tetraglym electrolyte containing $LiNO_3$, $MPT^{\bullet+}$, and O_2 as shown in Figure 4.10. This analysis also used the homemade five–electrode cell as shown in Figure 4.5a. After the MPT oxidation using the three–electrode sub–cell, the resumed galvanostatic experiment of Li symmetric cell remarkable maintains the stable voltage profile over 50 cycles, in contrast to the profile with the electrolyte containing $LiSO_3CF_3$. The small increase of polarization existed but it is negligible. This protection effect suppressed the formation of thick passivation layer on the Li metal anode and the exhaustion of MPT, leading to the enhanced electrochemical performance of the Li–O_2 cells using $LiNO_3$ as a Li salt.

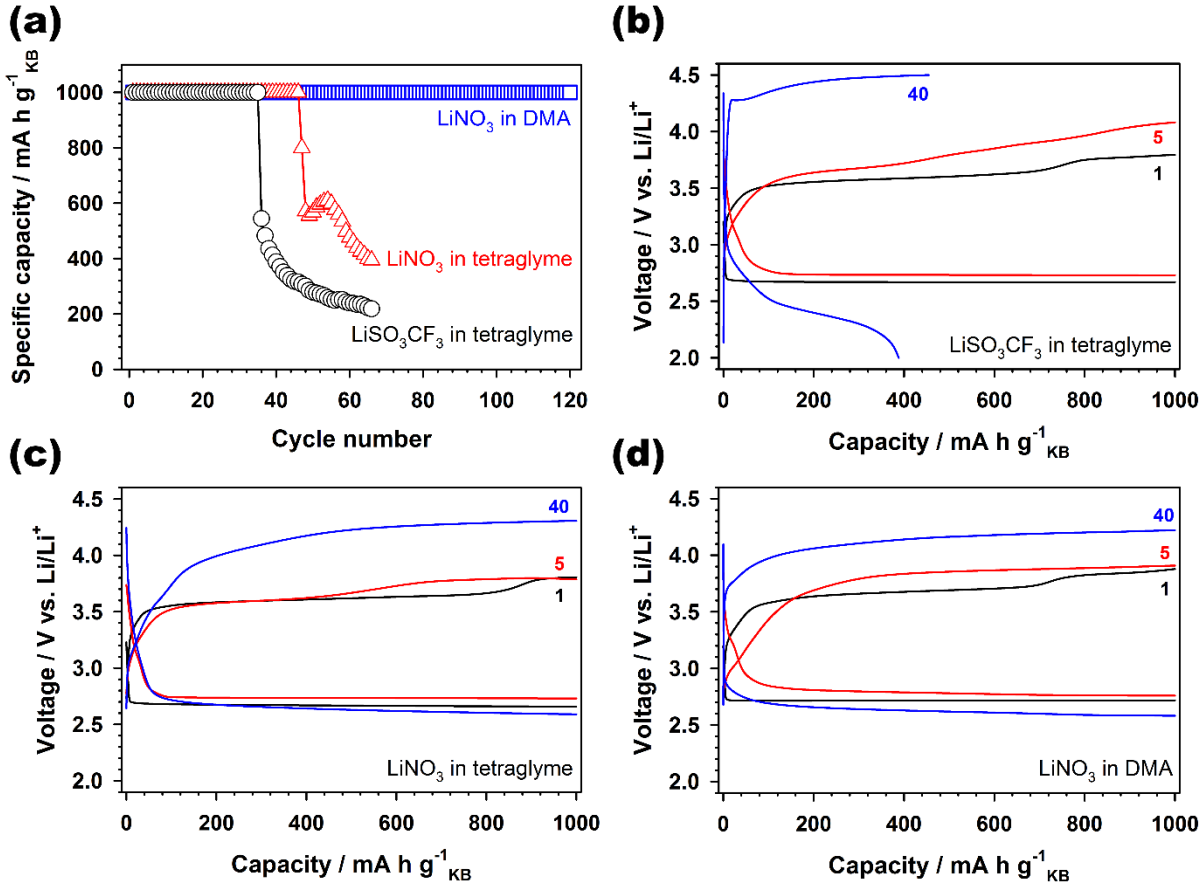

Figure 4.7 (a) Cycle performance of Li–O_2 batteries with various electrolytes, such as tetraglyme electrolyte containing 1 *M* $LiSO_3CF_3$ + 50 *mM* MPT, 1 *M* $LiNO_3$ + 50 *mM* MPT, and DMAc electrolyte containing 1 *M* $LiNO_3$ + 50 *mM* MPT with a constant capacity of 1000 mA h g^{-1}_{KB} and a specific current of 300 mA g^{-1}_{KB}. The corresponding voltage profiles of Li–O_2 batteries with tetraglyme electrolyte containing (b)1 *M* $LiSO_3CF_3$ + 50 *mM* MPT, (c) 1 *M* $LiNO_3$ + 50 *mM* MPT, and (d) DMAc electrolyte containing 1 *M* $LiNO_3$ + 50 *mM* MPT, respectively.

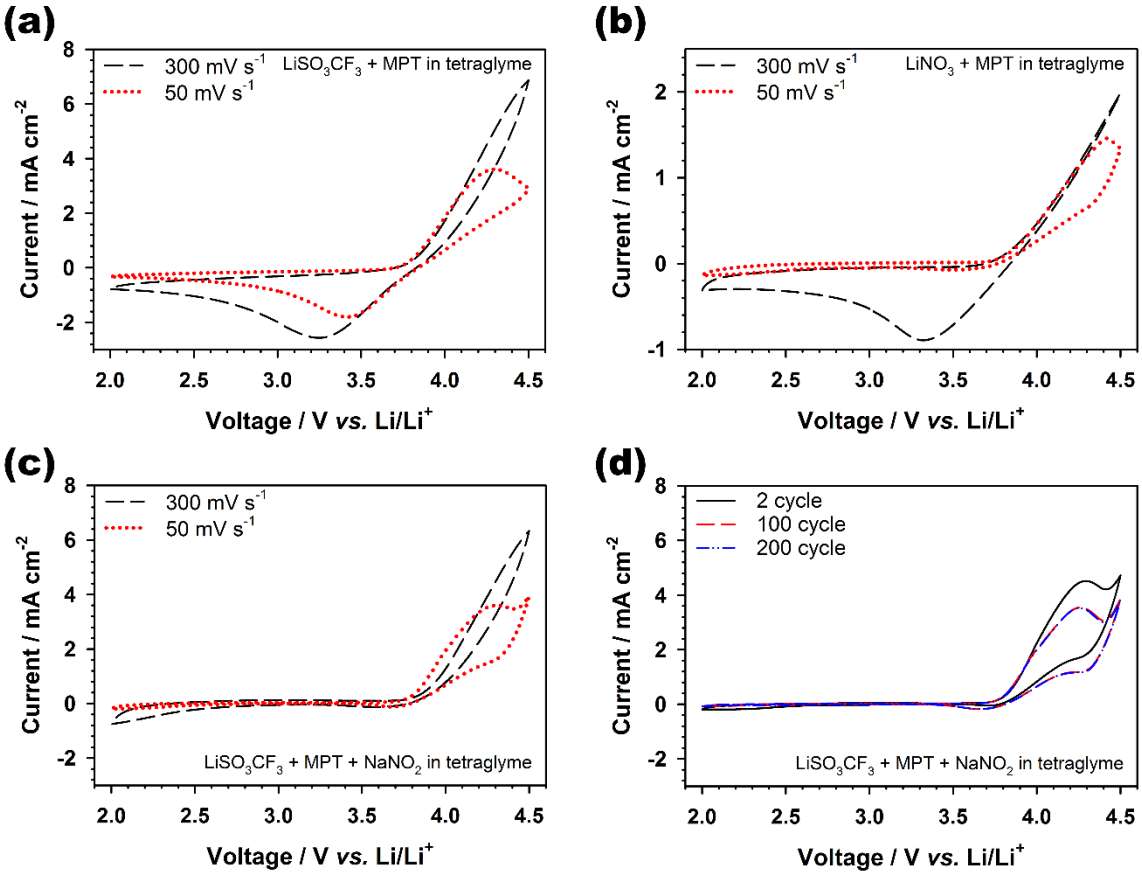

Figure 4.8 Cyclic voltammograms of (a) tetaglyme electrolyte containing 1 *M* $LiSO_3CF_3$ + 50 *mM* MPT, (b) 1 *M* $LiNO_3$ + 50 *mM* MPT, and (c) 1 *M* $LiSO_3CF_3$ + 50 *mM* MPT + 50 *mM* $NaNO_2$ at scan rates of 300 and 50 mV s^{-1}. (d) Cyclic voltammograms of tetraglyme electrolyte containing 1.0 M $LiSO_3CF_3$ + 50 *mM* $NaNO_2$ at scan rate: 50 mV s^{-1} up to 200 cycles.

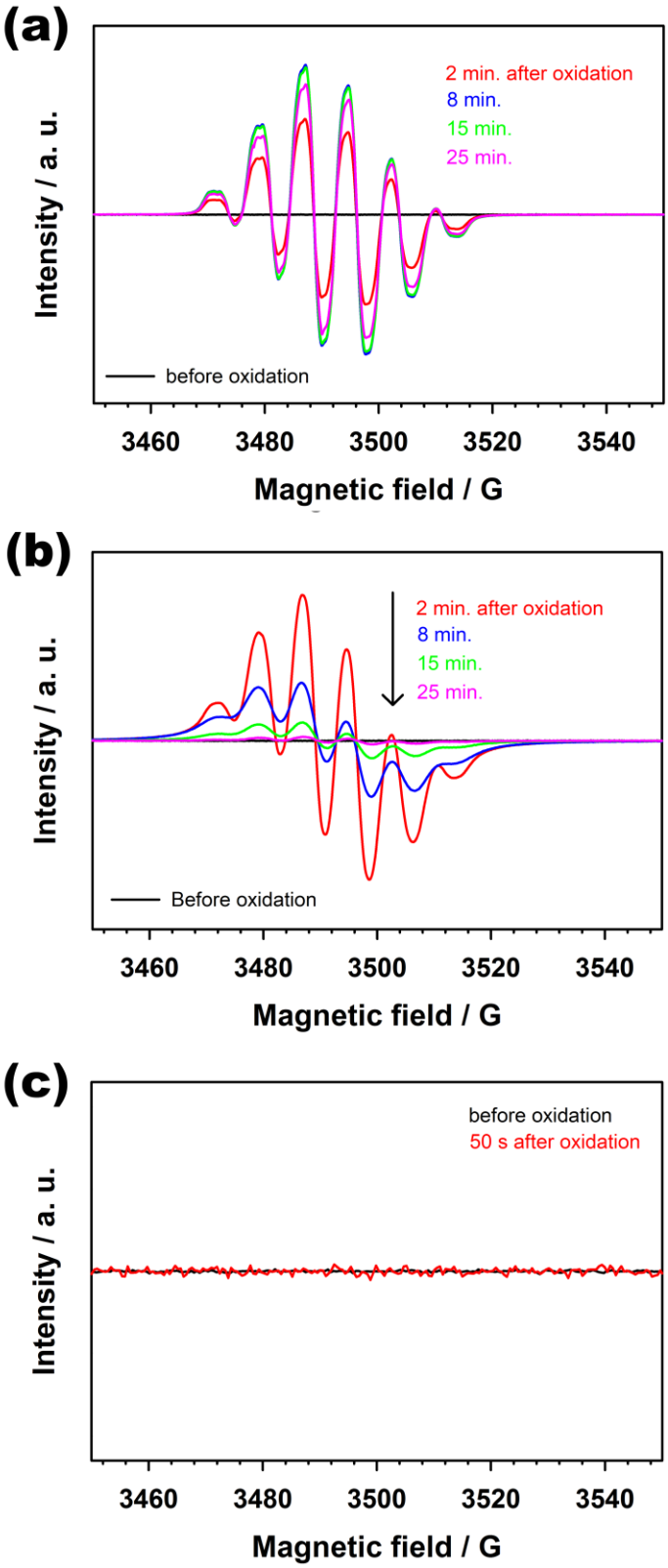

Figure 4.9 The electron spin resonance (ESR) spectra of tetraglyme electrolyte containing (a) 1 *M* $LiSO_3CF_3$ + 50 *mM* MPT, (b) 1 *M* $LiSO_3CF_3$ + 50 *mM* MPT + 50 *mM* $NaNO_2$, and (c) 1 *M* $LiSO_3CF_3$ + 50 *mM* $NaNO_2$ before and after electrochemical oxidation at a constant voltage of 3.8 V (*vs*. Li/Li^+) for 1 min.

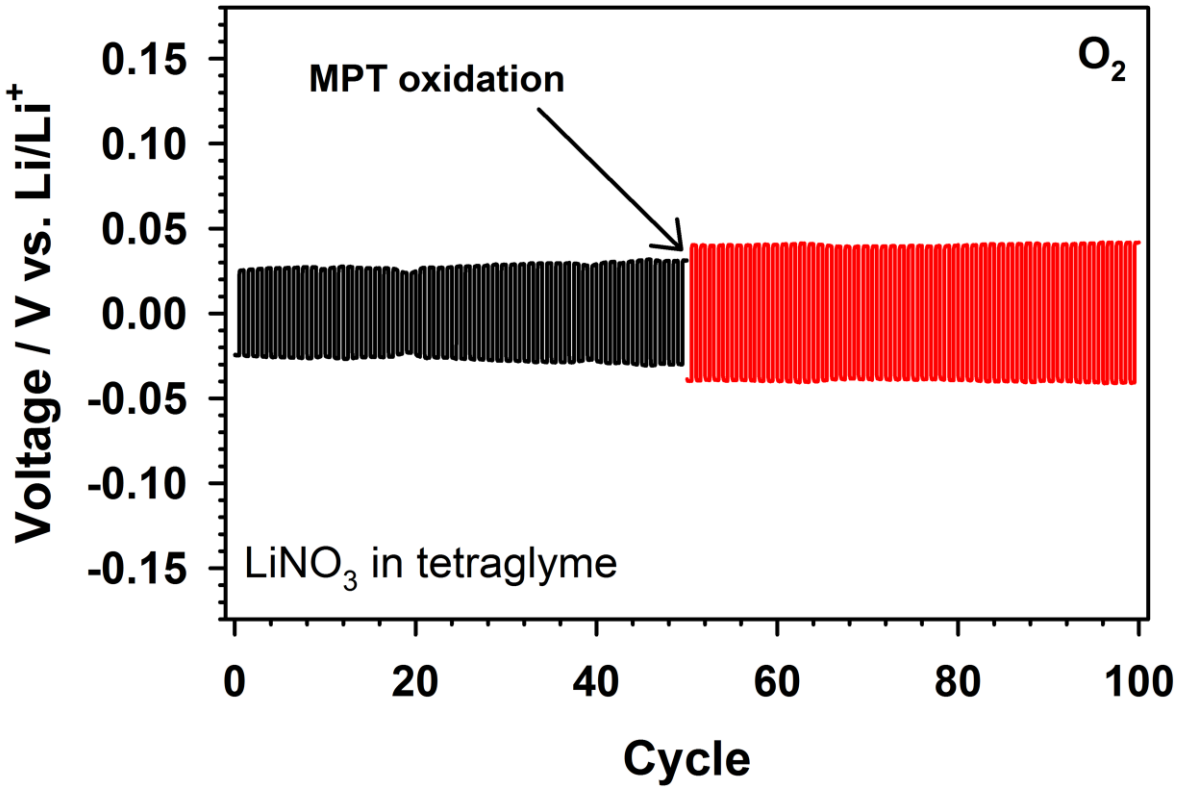

Figure 4.10 Voltage profiles of the Li symmetric cell with tetraglyme electrolyte containing 1 *M* $LiNO_3$ + 50 *mM* MPT in the homemade five–electrode cell, where MPT was oxidized after 50 cycles. Current density: discharge/charge with a current density of ± 88 μA cm^{-2} for 30 min in each step.

4.4 Summary

MPT as a model redox mediator was examined for a case study that exploring the origin of increasing polarization for the Li–O_2 batteries containing redox mediators. In this chapter, the association between redox mediator and Li metal anode was clarified by various combined analyses, such as electrochemical method, spectroscopy, and magnetic resonance. First of all, the effect of a redox mediator on the Li metal anode was demonstrated via the galvanostatic Li symmetric cell containing MPT. The undesirable reaction between MPT and Li metal anode was observed on performing the galvanostatic Li symmetric cell experiments under Ar, leading to the severe depletion of MPT and passivation of Li metal, as a result, the rapid failure of Li symmetric cell. However, in contrast to that under Ar, the galvanostatic experiment of Li symmetric cell under O_2 showed the stable cycle performance with small polarization due to the formation of protective layer on the Li metal anode consisting of lithium oxide derived by O_2 dissolved in the electrolyte. This results indicates that unexpected reaction between redox mediator and Li metal anode is alleviated in the Li–O_2 cells containing redox mediator because of the operating under O_2 atmosphere. In this context, the deterioration of Li–O_2 cells seems to be irrelevant to the undesirable reaction between MPT and Li metal.

However, the correlation between the failure of Li–O_2 cells and the undesirable reaction was clearly elucidated the considering of $MPT^{\bullet+}$, which forms during charging on the oxygen cathode in Li–O_2 cells. Despite the protective layer on Li metal anode forms under the O_2 atmosphere, $MPT^{\bullet+}$ formed on the oxygen cathode and diffusing to Li metal anode decomposes spontaneously the lithium oxide consisting of protective layer on the Li metal anode. This reaction occurs naturally owing to the difference of redox potential between MPT and lithium oxide in consistent with the reaction mechanism of redox mediator in Li–O_2 cells. As a result, the formation of thick passivation on the Li metal anode and the exhaustion of MPT causes the failure of Li–O_2 symmetric cell.

This proposed failure mechanism for Li–O_2 batteries containing a redox mediator was further verified by the introduction of $LiNO_3$ as a Li salt for Li–O_2 batteries leading to the improved electrochemical performance. As widely known, a $LiNO_3$ reacts with Li metal anode resulting in the protective layer on Li metal anode consisting of lithium oxide. There was demonstrated that this layer possesses the function of resistance against the $MPT^{\bullet+}$. Moreover, The NO_2^- obtained from the protective reaction between NO_3^- and Li metal captured the $MPT^{\bullet+}$ which diffused from oxygen cathode to Li metal. This anion reduces the probability of contact between $MPT^{\bullet+}$ and the protective lithium oxide layer. As a result, these protective effects of NO_3^- ensure the prolonged electrochemical activity of MPT, thereby enhancing the electrochemical performance of the Li–O_2 cells containing MPT.

Therefore, the failure mechanism for Li–O_2 cells containing a redox mediator can be attributed to the irreversible reductive decomposition of the redox mediators on the Li metal anode, which both exhausts the redox mediators and deteriorates the Li metal anode.

5. Conclusion

Redox mediator for Li–O_2 batteries have the potential to solve the limitation of Li–O_2 batteries, such as low energy efficiency, low cycle performance, and limited discharge capacity. However, the Li–O_2 batteries is still confronted with deficient performance to satisfy the practical use. In spite of various research on Li–O_2 batteries containing redox mediator for years, the understanding of operating and failure mechanism of redox mediator in the Li–O_2 batteries still remains the initial stage. Here, this dissertation showed the failure mechanism of Li–O_2 batteries containing redox mediator. A MPT used as a model redox mediator for analysis.

The electrochemical reversibility and radical stability of redox mediator with selected electrolytes, such as tetraglyme, monoglyme, DMAc, and DMSO, was examined by CV and ESR, respectively. The MPT in DMAc and DMSO exhibited higher electrochemical reversibility than other solvent, whereas the $MPT^{\bullet+}$ in tetraglyme exhibited highest radical stability. Moreover, the cycle performance of Li metal–free Li–O_2 batteries is high in the tetraglyme–based electrolyte, which indicating that the stability of $MPT^{\bullet+}$ strongly influence on the performance of Li–O_2 batteries. Therefore, the optimization of solvent for enhanced life time of redox mediator radical is important for Li–O_2 batteries. In case of MPT, tetralogyme solvent is most suitable for Li–O_2 batteries.

The correlation between the stability of redox mediator and the Li metal anode was demonstrated using the various analysis. Oxygen in the cells protects the Li metal anode toward MPT, whereas Li metal with pristine surface rapidly react with MPT. However, the $MPT^{\bullet+}$ corrode the protective passivation on the Li metal anode, as a result, it is accelerated the side reaction between a redox mediator and a Li metal anode. To improve the limitation of redox mediator stability, a $LiNO_3$ was introduced as a Li salt and the protection agent for Li metal anode. Therefore, the protection of Li metal act a key role for enhanced performance of Li–O_2 batteries.

This proposed failure mechanism for Li–O_2 batteries with redox mediators can provide new avenues for developing redox mediators. Furthermore, to contribute the making a better planet to creature living in earth, these works are expected to help achieving the practical commercialization of Li–O_2 batteries

References

1. Bruce, P. G.; Freunberger, S. A.; Hardwick, L. J.; Tarascon, J. M., Li–O_2 and Li–S batteries with high energy storage. *Nat. Mater.* **2011,** *11*, 19.

2. Andre, D.; Kim, S. J.; Lamp, P.; Lux, S. F.; Maglia, F.; Paschos, O.; Stiaszny, B., Future generations of cathode materials: an automotive industry perspective. *J. Mater. Chem. A* **2015,** *3* (13), 6709-6732.

3. Placke, T.; Kloepsch, R.; Dühnen, S.; Winter, M., Lithium ion, lithium metal, and alternative rechargeable battery technologies: the odyssey for high energy density. *J. Solid State Electrochem.* **2017,** *21* (7), 1939-1964.

4. Nagura, T.; Tozawa, K., Lithium ion rechargeable battery. *Prog. Batteries Sol. Cells.* **1990,** *9*, 209.

5. Ozawa, K., Lithium–ion rechargeable batteries with $LiCoO_2$ and carbon electrodes: the $LiCoO_2$/C system. *Solid State Ion.* **1994,** *69* (3), 212-221.

6. Yoshio, M.; Noguchi, H.; Itoh, J. i.; Okada, M.; Mouri, T., Preparation and properties of $LiCo_yMn_xNi_{1-x-y}O_2$ as a cathode for lithium ion batteries. *J. Power Sources* **2000,** *90* (2), 176-181.

7. Tsutomu, O.; Yoshinari, M., Layered Lithium Insertion Material of $LiCo_{1/3}Ni_{1/3}Mn_{1/3}O_2$ for Lithium-Ion Batteries. *Chem. Lett.* **2001,** *30* (7), 642-643.

8. Choi, J. W.; Aurbach, D., Promise and reality of post–lithium–ion batteries with high energy densities. *Nat. Rev. Mater.* **2016,** *1*, 16013.

9. Rossen, E.; Jones, C. D. W.; Dahn, J. R., Structure and electrochemistry of $Li_xMn_yNi_{1-y}O_2$. *Solid State Ion.* **1992,** *57* (3), 311-318.

10. Chen, C. H.; Liu, J.; Stoll, M. E.; Henriksen, G.; Vissers, D. R.; Amine, K., Aluminum–doped lithium nickel cobalt oxide electrodes for high–power lithium–ion batteries. *J. Power Sources* **2004,** *128* (2), 278-285.

11. Leifer, N.; Srur–Lavi, O.; Matlahov, I.; Markovsky, B.; Aurbach, D.; Goobes, G., $LiNi_{0.8}Co_{0.15}Al_{0.05}O_2$ Cathode Material: New Insights via ^{7}Li and ^{27}Al Magic–Angle Spinning NMR Spectroscopy. *Chem. Mater.* **2016,** *28* (21), 7594-7604.

12. Schipper, F.; Erickson, E. M.; Erk, C.; Shin, J. Y.; Chesneau, F. F.; Aurbach, D., Review—Recent Advances and Remaining Challenges for Lithium Ion Battery Cathodes: I. Nickel–Rich, $LiNi_xCo_yMn_zO_2$. *J. Electrochem. Soc.* **2017,** *164* (1), A6220-A6228.

13. Pouillerie, C.; Croguennec, L.; Biensan, P.; Willmann, P.; Delmas, C., Synthesis and Characterization of New $LiNi_{1-y}Mg_yO_2$ Positive Electrode Materials for Lithium–Ion Batteries. *J. Electrochem. Soc.* **2000,** *147* (6), 2061-2069.

14. Lin, F.; Markus, I. M.; Nordlund, D.; Weng, T. C.; Asta, M. D.; Xin, H. L.; Doeff, M. M., Surface reconstruction and chemical evolution of stoichiometric layered cathode materials for lithium–ion batteries. *Nat. Commun.* **2014,** *5*, 3529.

15. Jung, S. K.; Gwon, H.; Hong, J.; Park, K. Y.; Seo, D. H.; Kim, H.; Hyun, J.; Yang, W.; Kang, K., Understanding the Degradation Mechanisms of $LiNi_{0.5}Co_{0.2}Mn_{0.3}O_2$ Cathode Material in Lithium Ion Batteries. *Adv. Energy Mater.* **2014,** *4* (1).

16. Zheng, H.; Sun, Q.; Liu, G.; Song, X.; Battaglia, V. S., Correlation between dissolution behavior and electrochemical cycling performance for $LiNi_{1/3}Co_{1/3}Mn_{1/3}O_2$–based cells. *J. Power Sources* **2012,** *207*, 134-140.

17. Myung, S. T.; Amine, K.; Sun, Y. K., Surface modification of cathode materials from nano– to microscale for rechargeable lithium–ion batteries. *J. Mater. Chem.* **2010,** *20* (34), 7074-7095.

18. Choi, A.; Lim, J.; Kim, H. J.; Jung, S. C.; Lim, H. W.; Kim, H.; Kwon, M. S.; Han, Y. K.; Oh, S. M.; Lee, K. T., Site–Selective In Situ Electrochemical Doping for Mn–Rich Layered Oxide Cathode Materials in Lithium–Ion Batteries. *Adv. Energy Mater.* **2017**, 10.1002/aenm.201702514.

19. Pan, C.; Lee, Y. J.; Ammundsen, B.; Grey, C. P., ^{6}Li MAS NMR Studies of the Local Structure and Electrochemical Properties of Cr–doped Lithium Manganese and Lithium Cobalt Oxide Cathode Materials for Lithium–Ion Batteries. *Chem. Mater.* **2002,** *14* (5), 2289-2299.

20. Kam, K. C.; Doeff, M. M., Aliovalent titanium substitution in layered mixed Li Ni–Mn–Co oxides for lithium battery applications. *J. Mater. Chem.* **2011,** *21* (27), 9991-9993.

21. Wang, C. C.; Manthiram, A., Influence of cationic substitutions on the first charge and reversible capacities of lithium–rich layered oxide cathodes. *J. Mater. Chem. A* **2013,** *1* (35), 10209-10217.

22. Knight, J. C.; Nandakumar, P.; Kan, W. H.; Manthiram, A., Effect of Ru substitution on the first charge–discharge cycle of lithium–rich layered oxides. *J. Mater. Chem. A* **2015,** *3* (5), 2006-2011.

23. Lee, E.; Park, J. S.; Wu, T.; Sun, C. J.; Kim, H.; Stair, P. C.; Lu, J.; Zhou, D.; Johnson, C. S., Role of Cr^{3+}/Cr^{6+} redox in chromium–substituted $Li_2MnO_3 \cdot LiNi_{1/2}Mn_{1/2}O_2$ layered composite cathodes: electrochemistry and voltage fade. *J. Mater. Chem. A* **2015,** *3* (18), 9915-9924.

24. Abdel–Ghany, A. E.; Hashem, A. M.; Elzahany, E. A.; Abuzeid, H. A.; Indris, S.; Nikolowski, K.; Ehrenberg, H.; Zaghib, K.; Mauger, A.; Julien, C. M., Structural properties and application in lithium cells of $Li(Ni_{0.5}Co_{0.5})_{1-y}Fe_yO_2$ ($0 \le y \le 0.25$) prepared by sol–gel route: Doping optimization. *J. Power Sources* **2016,** *320*, 168-179.

25. Cho, J.; Kim, T. J.; Kim, Y. J.; Park, B., High-Performance ZrO_2–Coated $LiNiO_2$ Cathode Material. *Electrochemical and Solid-State Letters* **2001,** *4* (10), A159-A161.

26. Omanda, H.; Brousse, T.; Marhic, C.; Schleich, D. M., Improvement of the Thermal Stability of $LiNi_{0.8}Co_{0.2}O_2$ Cathode by a SiO_x Protective Coating. *J. Electrochem. Soc.* **2004,** *151* (6), A922-A929.

27. Myung, S. T.; Izumi, K.; Komaba, S.; Yashiro, H.; Bang, H. J.; Sun, Y. K.; Kumagai, N., Functionality of Oxide Coating for $Li[Li_{0.05}Ni_{0.4}Co_{0.15}Mn_{0.4}]O_2$ as Positive Electrode Materials for Lithium–Ion Secondary Batteries. *J. Phys. Chem. C* **2007,** *111* (10), 4061-4067.

28. Cho, Y.; Lee, Y. S.; Park, S. A.; Lee, Y.; Cho, J., $LiNi_{0.8}Co_{0.15}Al_{0.05}O_2$ cathode materials prepared by TiO_2 nanoparticle coatings on $Ni_{0.8}Co_{0.15}Al_{0.05}(OH)_2$ precursors. *Electrochim. Acta* **2010,** *56* (1), 333-

339.

29. Yoon, W. S.; Nam, K. W.; Jang, D.; Chung, K. Y.; Hanson, J.; Chen, J. M.; Yang, X. Q., Structural study of the coating effect on the thermal stability of charged MgO–coated $LiNi_{0.8}Co_{0.2}O_2$ cathodes investigated by in situ XRD. *J. Power Sources* **2012,** *217*, 128-134.

30. Sim, S.; Oh, P.; Park, S.; Cho, J., Critical Thickness of SiO_2 Coating Layer on Core@Shell Bulk@Nanowire Si Anode Materials for Li–Ion Batteries. *Adv. Mater.* **2013,** *25* (32), 4498-4503.

31. Lee, H. J.; Park, Y. J., Interface characterization of MgF_2–coated $LiCoO_2$ thin films. *Solid State Ion.* **2013,** *230*, 86-91.

32. Cho, Y.; Lee, S.; Lee, Y.; Hong, T.; Cho, J., Spinel–Layered Core–Shell Cathode Materials for Li–Ion Batteries. *Adv. Energy Mater.* **2011,** *1* (5), 821-828.

33. Sun, Y. K.; Chen, Z.; Noh, H. J.; Lee, D. J.; Jung, H. G.; Ren, Y.; Wang, S.; Yoon, C. S.; Myung, S. T.; Amine, K., Nanostructured high-energy cathode materials for advanced lithium batteries. *Nat. Mater.* **2012,** *11*, 942.

34. Rossouw, M. H.; Liles, D. C.; Thackeray, M. M., Synthesis and Structural Characterization of a Novel Layered Lithium Manganese Oxide, $Li_{0.36}Mn_{0.91}O_2$, and Its Lithiated Derivative, $Li_{1.09}Mn_{0.91}O_2$. *J. Solid State Chem.* **1993,** *104* (2), 464-466.

35. Lu, Z.; MacNeil, D. D.; Dahn, J. R., Layered Cathode Materials $Li[Ni_xLi_{(1/3-2x/3)}Mn_{(2/3-x/3)}]O_2$ for Lithium–Ion Batteries. *Electrochemical and Solid-State Letters* **2001,** *4* (11), A191-A194.

36. Johnson, C. S.; Kim, J. S.; Lefief, C.; Li, N.; Vaughey, J. T.; Thackeray, M. M., The significance of the Li_2MnO_3 component in 'composite' $xLi_2MnO_3\cdot(1-x)LiMn_{0.5}Ni_{0.5}O_2$ electrodes. *Electrochem. Commun.* **2004,** *6* (10), 1085-1091.

37. Kim, J. S.; Johnson, C. S.; Vaughey, J. T.; Thackeray, M. M.; Hackney, S. A.; Yoon, W.; Grey, C. P., Electrochemical and Structural Properties of $xLi_2M'O_3\cdot(1-x)LiMn_{0.5}Ni_{0.5}O_2$ Electrodes for Lithium Batteries (M' = Ti, Mn, Zr; $0 \leq x \leqslant 0.3$). *Chem. Mater.* **2004,** *16* (10), 1996-2006.

38. Johnson, C. S.; Li, N.; Vaughey, J. T.; Hackney, S. A.; Thackeray, M. M., Lithium–manganese oxide electrodes with layered–spinel composite structures $xLi_2MnO_3\cdot(1-x)Li_{1+y}Mn_{2-y}O_4$ ($0<x<1$, $0\leqslant y\leqslant 0.33$) for lithium batteries. *Electrochem. Commun.* **2005,** *7* (5), 528-536.

39. Jarvis, K. A.; Deng, Z.; Allard, L. F.; Manthiram, A.; Ferreira, P. J., Atomic Structure of a Lithium–Rich Layered Oxide Material for Lithium–Ion Batteries: Evidence of a Solid Solution. *Chem. Mater.* **2011,** *23* (16), 3614-3621.

40. Erickson, E. M.; Schipper, F.; Penki, T. R.; Shin, J. Y.; Erk, C.; Chesneau, F. F.; Markovsky, B.; Aurbach, D., Review—Recent Advances and Remaining Challenges for Lithium Ion Battery Cathodes: II. Lithium-Rich, $xLi_2MnO_3\cdot(1-x)LiNi_aCo_bMn_cO_2$. *J. Electrochem. Soc.* **2017,** *164* (1), A6341-A6348.

41. Choi, N. S.; Yeon, J. T.; Lee, Y. W.; Han, J. G.; Lee, K. T.; Kim, S. S., Degradation of spinel lithium manganese oxides by low oxidation durability of $LiPF_6$–based electrolyte at 60 °C. *Solid State Ion.* **2012,** *219*, 41-48.

42. Armstrong, A. R.; Dupre, N.; Paterson, A. J.; Grey, C. P.; Bruce, P. G., Combined Neutron Diffraction, NMR, and Electrochemical Investigation of the Layered–to–Spinel Transformation in $LiMnO_2$. *Chem. Mater.* **2004,** *16* (16), 3106-3118.

43. Croy, J. R.; Gallagher, K. G.; Balasubramanian, M.; Long, B. R.; Thackeray, M. M., Quantifying Hysteresis and Voltage Fade in $xLi_2MnO_3 \cdot (1-x)LiMn_{0.5}Ni_{0.5}O_2$ Electrodes as a Function of Li_2MnO_3 Content. *J. Electrochem. Soc.* **2014,** *161* (3), A318-A325.

44. Choi, N. S.; Han, J. G.; Ha, S. Y.; Park, I.; Back, C., Recent advances in the electrolytes for interfacial stability of high–voltage cathodes in lithium–ion batteries. *RSC Adv.* **2015,** *5* (4), 2732-2748.

45. Masaru, A.; Futoshi, M.; Miwa, S.; Hiroshi, Y.; Genki, K.; Atsushi, I.; Takashi, S.; Masaharu, H.; Yasuhiko, O.; Yuichi, S., Activation of a Li–rich Solid–Solution Layered $Li[Ni_{0.18}Li_{0.20}Co_{0.03}Mn_{0.58}]O_2$ Cathode and Retention of High Capacities via an Electrochemical Pretreatment with a Low Discharge Voltage Limit. *Chem. Lett.* **2012,** *41* (4), 418-419.

46. Nayak, P. K.; Grinblat, J.; Levi, E.; Markovsky, B.; Aurbach, D., Effect of cycling conditions on the electrochemical performance of high capacity Li and Mn–rich cathodes for Li–ion batteries. *J. Power Sources* **2016,** *318*, 9-17.

47. Erickson, E.; Schipper, F.; Tian, R.; Shin, J. Y.; Erk, C.; Chesneau, F. F.; Lampert, J. K.; Markovsky, B.; Aurbach, D., Enhanced capacity and lower mean charge voltage of Li–rich cathodes for lithium ion batteries resulting from low–temperature electrochemical activation. *RSC Adv.* **2017,** *7* (12), 7116-7121.

48. Lu, Y. C.; Gallant, B. M.; Kwabi, D. G.; Harding, J. R.; Mitchell, R. R.; Whittingham, M. S.; Shao-Horn, Y., Lithium–oxygen batteries: bridging mechanistic understanding and battery performance. *Energy Environ. Sci.* **2013,** *6* (3), 750-768.

49. Nelson, P. A.; Steunenberg, R. K.; Chilenskas, A. A.; Gay, E. C.; Battles, J. E.; Hornstra, F.; Miller, W. E.; Roche, M. F.; Shimotake, H. *Development of lithium/metal sulfide batteries at Argonne National Laboratory: summary report for 1977*; ANL-78-20; ; Argonne National Lab., Ill. (USA): 1978; p 34.

50. Seefurth, R. N.; Sharma, R. A., Investigation of Lithium Utilization from A Lithium–Silicon Electrode. *J. Electrochem. Soc.* **1977,** *124* (8), 1207-1214.

51. Chan, C. K.; Peng, H.; Liu, G.; McIlwrath, K.; Zhang, X. F.; Huggins, R. A.; Cui, Y., High–performance lithium battery anodes using silicon nanowires. *Nat. Nanotechnol.* **2008,** *3*, 31-35.

52. Magasinski, A.; Dixon, P.; Hertzberg, B.; Kvit, A.; Ayala, J.; Yushin, G., High–performance lithium–ion anodes using a hierarchical bottom–up approach. *Nat. Mater.* **2010,** *9*, 353-358.

53. Wilson, A. M.; Dahn, J. R., Lithium Insertion in Carbons Containing Nanodispersed Silicon. *J. Electrochem. Soc.* **1995,** *142* (2), 326-332.

54. Park, M. H.; Kim, M. G.; Joo, J.; Kim, K.; Kim, J.; Ahn, S.; Cui, Y.; Cho, J., Silicon Nanotube Battery Anodes. *Nano Lett.* **2009,** *9* (11), 3844-3847.

55. Yu, Y.; Gu, L.; Zhu, C.; Tsukimoto, S.; van Aken, P. A.; Maier, J., Reversible Storage of Lithium in Silver–Coated Three–Dimensional Macroporous Silicon. *Adv. Mater.* **2010,** *22* (20), 2247-2250.

56. Hwang, T. H.; Lee, Y. M.; Kong, B. S.; Seo, J. S.; Choi, J. W., Electrospun Core–Shell Fibers for Robust Silicon Nanoparticle–Based Lithium Ion Battery Anodes. *Nano Lett.* **2012,** *12* (2), 802-807.

57. Jung, D. S.; Hwang, T. H.; Park, S. B.; Choi, J. W., Spray Drying Method for Large–Scale and High–Performance Silicon Negative Electrodes in Li–Ion Batteries. *Nano Lett.* **2013,** *13* (5), 2092-2097.

58. Son, I. H.; Hwan Park, J.; Kwon, S.; Park, S.; Rümmeli, M. H.; Bachmatiuk, A.; Song, H. J.; Ku, J.; Choi, J. W.; Choi, J. m.; Doo, S. G.; Chang, H., Silicon carbide–free graphene growth on silicon for lithium–ion battery with high volumetric energy density. *Nat. Commun.* **2015,** *6*, 7393.

59. Kovalenko, I.; Zdyrko, B.; Magasinski, A.; Hertzberg, B.; Milicev, Z.; Burtovyy, R.; Luzinov, I.; Yushin, G., A Major Constituent of Brown Algae for Use in High–Capacity Li–Ion Batteries. *Science* **2011,** *334* (6052), 75-79.

60. Liu, G.; Xun, S.; Vukmirovic, N.; Song, X.; Olalde–Velasco, P.; Zheng, H.; Battaglia, V. S.; Wang, L.; Yang, W., Polymers with Tailored Electronic Structure for High Capacity Lithium Battery Electrodes. *Adv. Mater.* **2011,** *23* (40), 4679-4683.

61. Koo, B.; Kim, H.; Cho, Y.; Lee, K. T.; Choi, N. S.; Cho, J., A Highly Cross–Linked Polymeric Binder for High–Performance Silicon Negative Electrodes in Lithium Ion Batteries. *Angew. Chem. Int. Ed.* **2012,** *51* (35), 8762-8767.

62. Wang, C.; Wu, H.; Chen, Z.; McDowell, M. T.; Cui, Y.; Bao, Z., Self–healing chemistry enables the stable operation of silicon microparticle anodes for high–energy lithium–ion batteries. *Nat. Chem.* **2013,** *5*, 1042-1048.

63. Wu, H.; Yu, G.; Pan, L.; Liu, N.; McDowell, M. T.; Bao, Z.; Cui, Y., Stable Li–ion battery anodes by in–situ polymerization of conducting hydrogel to conformally coat silicon nanoparticles. *Nat. Commun.* **2013,** *4*, 1943.

64. Jeong, Y. K.; Kwon, T. w.; Lee, I.; Kim, T. S.; Coskun, A.; Choi, J. W., Hyperbranched β–Cyclodextrin Polymer as an Effective Multidimensional Binder for Silicon Anodes in Lithium Rechargeable Batteries. *Nano Lett.* **2014,** *14* (2), 864-870.

65. Chen, Z.; Wang, C.; Lopez, J.; Lu, Z.; Cui, Y.; Bao, Z., High–Areal–Capacity Silicon Electrodes with Low–Cost Silicon Particles Based on Spatial Control of Self–Healing Binder. *Adv. Energy Mater.* **2015,** *5* (8), 1401826.

66. Jeong, Y. K.; Kwon, T. w.; Lee, I.; Kim, T. S.; Coskun, A.; Choi, J. W., Millipede–inspired structural design principle for high performance polysaccharide binders in silicon anodes. *Energy Environ. Sci.* **2015,** *8* (4), 1224-1230.

67. Etacheri, V.; Geiger, U.; Gofer, Y.; Roberts, G. A.; Stefan, I. C.; Fasching, R.; Aurbach, D., Exceptional Electrochemical Performance of Si–Nanowires in 1,3–Dioxolane Solutions: A Surface Chemical Investigation. *Langmuir* **2012,** *28* (14), 6175-6184.

68. Markevich, E.; Fridman, K.; Sharabi, R.; Elazari, R.; Salitra, G.; Gottlieb, H. E.; Gershinsky, G.; Garsuch, A.; Semrau, G.; Schmidt, M. A.; Aurbach, D., Amorphous Columnar Silicon Anodes for

Advanced High Voltage Lithium Ion Full Cells: Dominant Factors Governing Cycling Performance. *J. Electrochem. Soc.* **2013,** *160* (10), A1824-A1833.

69. Markevich, E.; Salitra, G.; Rosenman, A.; Talyosef, Y.; Aurbach, D.; Garsuch, A., High performance of thick amorphous columnar monolithic film silicon anodes in ionic liquid electrolytes at elevated temperature. *RSC Adv.* **2014,** *4* (89), 48572-48575.

70. Doh, C. H.; Park, C. W.; Shin, H. M.; Kim, D. H.; Chung, Y. D.; Moon, S. I.; Jin, B. S.; Kim, H. S.; Veluchamy, A., A new SiO/C anode composition for lithium–ion battery. *J. Power Sources* **2008,** *179* (1), 367-370.

71. Park, E.; Yoo, H.; Lee, J.; Park, M. S.; Kim, Y. J.; Kim, H., Dual–Size Silicon Nanocrystal–Embedded SiO_x Nanocomposite as a High–Capacity Lithium Storage Material. *ACS Nano* **2015,** *9* (7), 7690-7696.

72. Liu, N.; Hu, L.; McDowell, M. T.; Jackson, A.; Cui, Y., Prelithiated Silicon Nanowires as an Anode for Lithium Ion Batteries. *ACS Nano* **2011,** *5* (8), 6487-6493.

73. Zhao, J.; Lu, Z.; Liu, N.; Lee, H. W.; McDowell, M. T.; Cui, Y., Dry–air–stable lithium silicide–lithium oxide core–shell nanoparticles as high–capacity prelithiation reagents. *Nat. Commun.* **2014,** *5*, 5088.

74. Kim, H. J.; Choi, S.; Lee, S. J.; Seo, M. W.; Lee, J. G.; Deniz, E.; Lee, Y. J.; Kim, E. K.; Choi, J. W., Controlled Prelithiation of Silicon Monoxide for High Performance Lithium–Ion Rechargeable Full Cells. *Nano Lett.* **2016,** *16* (1), 282-288.

75. Whittingham, M. S., Electrical Energy Storage and Intercalation Chemistry. *Science* **1976,** *192* (4244), 1126-1127.

76. Brandt, K.; Laman, F. C., Reproducibility and reliability of rechargeable lithium/molybdenum disulfide batteries. *J. Power Sources* **1989,** *25* (4), 265-276.

77. Fouchard, D.; Taylor, J. B., The molicel® rechargeable lithium system: Multicell aspects. *J. Power Sources* **1987,** *21* (3), 195-205.

78. Aurbach, D.; Zinigrad, E.; Cohen, Y.; Teller, H., A short review of failure mechanisms of lithium metal and lithiated graphite anodes in liquid electrolyte solutions. *Solid State Ion.* **2002,** *148* (3), 405-416.

79. Lin, D.; Liu, Y.; Cui, Y., Reviving the lithium metal anode for high–energy batteries. *Nat. Nanotechnol.* **2017,** *12* (3), 194-206.

80. Xu, W.; Wang, J.; Ding, F.; Chen, X.; Nasybulin, E.; Zhang, Y.; Zhang, J. G., Lithium metal anodes for rechargeable batteries. *Energy Environ. Sci.* **2014,** *7* (2), 513-537.

81. Koo, D.; Ha, S.; Kim, D. M.; Lee, K. T., Recent approaches to improving lithium metal electrodes. *Curr. Opin. Electrochem.* **2017,** *6* (1), 70-76.

82. Aurbach, D.; Daroux, M. L.; Faguy, P. W.; Yeager, E., Identification of Surface Films Formed on Lithium in Propylene Carbonate Solutions. *J. Electrochem. Soc.* **1987,** *134* (7), 1611-1620.

83. Aurbach, D.; Ein–Ely, Y.; Zaban, A., The Surface Chemistry of Lithium Electrodes in Alkyl Carbonate Solutions. *J. Electrochem. Soc.* **1994,** *141* (1), L1-L3.

84. Peled, E., The Electrochemical Behavior of Alkali and Alkaline Earth Metals in Nonaqueous Battery Systems—The Solid Electrolyte Interphase Model. *J. Electrochem. Soc.* **1979,** *126* (12), 2047-2051.

85. Peled, E.; Golodnitsky, D.; Ardel, G., Advanced Model for Solid Electrolyte Interphase Electrodes in Liquid and Polymer Electrolytes. *J. Electrochem. Soc.* **1997,** *144* (8), L208-L210.

86. Abraham, K. M.; Foos, J. S.; Goldman, J. L., Long Cycle–Life Secondary Lithium Cells Utilizing Tetrahydrofuran. *J. Electrochem. Soc.* **1984,** *131* (9), 2197-2199.

87. Abraham, K. M.; Goldman, J. L.; Natwig, D. L., Characterization of Ether Electrolytes for Rechargeable Lithium Cells. *J. Electrochem. Soc.* **1982,** *129* (11), 2404-2409.

88. Foos, J. S.; Stolki, T. J., A New Ether Solvent for Lithium Cells. *J. Electrochem. Soc.* **1988,** *135* (11), 2769-2771.

89. Gofer, Y.; Ben–Zion, M.; Aurbach, D., Solutions of $LiAsF_6$ in 1,3–dioxolane for secondary lithium batteries. *J. Power Sources* **1992,** *39* (2), 163-178.

90. Koch, V. R.; Goldman, J. L.; Mattos, C. J.; Mulvaney, M., Specular Lithium Deposits from Lithium Hexafluoroarsenate/Diethyl Ether Electrolytes. *J. Electrochem. Soc.* **1982,** *129* (1), 1-4.

91. Koch, V. R.; Young, J. H., The Stability of the Secondary Lithium Electrode in Tetrahydrofuran–Based Electrolytes. *J. Electrochem. Soc.* **1978,** *125* (9), 1371-1377.

92. Koch, V. R.; Young, J. H., 2–Methyltetrahydrofuran—Lithium Hexafluoroarsenate: A Superior Electrolyte for the Secondary Lithium Electrode. *Science* **1979,** *204* (4392), 499-501.

93. Yoshimatsu, I.; Hirai, T.; Yamaki, J. i., Lithium Electrode Morphology during Cycling in Lithium Cells. *J. Electrochem. Soc.* **1988,** *135* (10), 2422-2427.

94. Miao, R.; Yang, J.; Xu, Z.; Wang, J.; Nuli, Y.; Sun, L., A new ether–based electrolyte for dendrite–free lithium–metal based rechargeable batteries. *Sci. Rep.* **2016,** *6*, 21771.

95. Aurbach, D.; Pollak, E.; Elazari, R.; Salitra, G.; Kelley, C. S.; Affinito, J., On the Surface Chemical Aspects of Very High Energy Density, Rechargeable Li–Sulfur Batteries. *J. Electrochem. Soc.* **2009,** *156* (8), A694-A702.

96. Li, W.; Yao, H.; Yan, K.; Zheng, G.; Liang, Z.; Chiang, Y. M.; Cui, Y., The synergetic effect of lithium polysulfide and lithium nitrate to prevent lithium dendrite growth. *Nat. Commun.* **2015,** *6*, 7436.

97. Malik, Y.; Aurbach, D.; Dan, P.; Meitav, A., The electrochemical behaviour of 2–methyltetrahydrofuran solutions. *J. Electroanal. Chem.* **1990,** *282* (1), 73-105.

98. Besenhard, J. O.; Wagner, M. W.; Winter, M.; Jannakoudakis, A. D.; Jannakoudakis, P. D.; Theodoridou, E., Inorganic film–forming electrolyte additives improving the cycling behaviour of metallic lithium electrodes and the self–discharge of carbon—lithium electrodes. *J. Power Sources* **1993,** *44* (1), 413-420.

99. Osaka, T.; Momma, T.; Matsumoto, Y.; Uchida, Y., Surface Characterization of Electrodeposited

Lithium Anode with Enhanced Cycleability Obtained by CO_2 Addition. *J. Electrochem. Soc.* **1997,** *144* (5), 1709-1713.

100. Koch, S. L.; Morgan, B. J.; Passerini, S.; Teobaldi, G., Density functional theory screening of gas–treatment strategies for stabilization of high energy–density lithium metal anodes. *J. Power Sources* **2015,** *296*, 150-161.

101. Miao, R.; Yang, J.; Feng, X.; Jia, H.; Wang, J.; Nuli, Y., Novel dual–salts electrolyte solution for dendrite–free lithium–metal based rechargeable batteries with high cycle reversibility. *J. Power Sources* **2014,** *271*, 291-297.

102. Lu, Y.; Tu, Z.; Shu, J.; Archer, L. A., Stable lithium electrodeposition in salt–reinforced electrolytes. *J. Power Sources* **2015,** *279*, 413-418.

103. Guo, J.; Wen, Z.; Wu, M.; Jin, J.; Liu, Y., Vinylene carbonate–$LiNO_3$: A hybrid additive in carbonic ester electrolytes for SEI modification on Li metal anode. *Electrochem. Commun.* **2015,** *51*, 59-63.

104. Morita, M.; Aoki, S.; Matsuda, Y., ac imepedance behaviour of lithium electrode in organic electrolyte solutions containing additives. *Electrochim. Acta* **1992,** *37* (1), 119-123.

105. Takehara, Z. i., Future prospects of the lithium metal anode. *J. Power Sources* **1997,** *68* (1), 82-86.

106. Kanamura, K.; Shiraishi, S.; Takehara, Z. i., Electrochemical deposition of lithium metal in nonaqueous electrolyte containing $(C_2H_5)_4NF(HF)_4$ additive. *J. Fluorine Chem.* **1998,** *87* (2), 235-243.

107. Mori, M.; Naruoka, Y.; Naoi, K.; Fauteux, D., Modification of the Lithium Metal Surface by Nonionic Polyether Surfactants: Quartz Crystal Microbalance Studies. *J. Electrochem. Soc.* **1998,** *145* (7), 2340-2348.

108. Shiraishi, S.; Kanamura, K.; Takehara, Z. i., Surface Condition Changes in Lithium Metal Deposited in Nonaqueous Electrolyte Containing HF by Dissolution–Deposition Cycles. *J. Electrochem. Soc.* **1999,** *146* (5), 1633-1639.

109. Mogi, R.; Inaba, M.; Jeong, S. K.; Iriyama, Y.; Abe, T.; Ogumi, Z., Effects of Some Organic Additives on Lithium Deposition in Propylene Carbonate. *J. Electrochem. Soc.* **2002,** *149* (12), A1578-A1583.

110. Ota, H.; Shima, K.; Ue, M.; Yamaki, J. i., Effect of vinylene carbonate as additive to electrolyte for lithium metal anode. *Electrochim. Acta* **2004,** *49* (4), 565-572.

111. Lu, Y.; Tu, Z.; Archer, L. A., Stable lithium electrodeposition in liquid and nanoporous solid electrolytes. *Nat. Mater.* **2014,** *13*, 961-969.

112. Zhang, Y.; Qian, J.; Xu, W.; Russell, S. M.; Chen, X.; Nasybulin, E.; Bhattacharya, P.; Engelhard, M. H.; Mei, D.; Cao, R.; Ding, F.; Cresce, A. V.; Xu, K.; Zhang, J. G., Dendrite–Free Lithium Deposition with Self–Aligned Nanorod Structure. *Nano Lett.* **2014,** *14* (12), 6889-6896.

113. Ding, F.; Xu, W.; Graff, G. L.; Zhang, J.; Sushko, M. L.; Chen, X.; Shao, Y.; Engelhard, M. H.; Nie, Z.; Xiao, J.; Liu, X.; Sushko, P. V.; Liu, J.; Zhang, J. G., Dendrite–Free Lithium Deposition via Self–Healing Electrostatic Shield Mechanism. *J. Am. Chem. Soc.* **2013,** *135* (11), 4450-4456.

114. Suo, L.; Hu, Y. S.; Li, H.; Armand, M.; Chen, L., A new class of Solvent–in–Salt electrolyte for high–energy rechargeable metallic lithium batteries. *Nat. Commun.* **2013,** *4*, 1481.

115. Qian, J.; Henderson, W. A.; Xu, W.; Bhattacharya, P.; Engelhard, M.; Borodin, O.; Zhang, J. G., High rate and stable cycling of lithium metal anode. *Nat. Commun.* **2015,** *6*, 6362.

116. Belov, D. G.; Yarmolenko, O. V.; Peng, A.; Efimov, O. N., Lithium surface protection by polyacetylene in situ polymerization. *Synth. Met.* **2006,** *156* (9), 745-751.

117. Marchioni, F.; Star, K.; Menke, E.; Buffeteau, T.; Servant, L.; Dunn, B.; Wudl, F., Protection of Lithium Metal Surfaces Using Chlorosilanes. *Langmuir* **2007,** *23* (23), 11597-11602.

118. Thompson, R. S.; Schroeder, D. J.; López, C. M.; Neuhold, S.; Vaughey, J. T., Stabilization of lithium metal anodes using silane–based coatings. *Electrochem. Commun.* **2011,** *13* (12), 1369-1372.

119. Umeda, G. A.; Menke, E.; Richard, M.; Stamm, K. L.; Wudl, F.; Dunn, B., Protection of lithium metal surfaces using tetraethoxysilane. *J. Mater. Chem.* **2011,** *21* (5), 1593-1599.

120. Wu, M.; Wen, Z.; Liu, Y.; Wang, X.; Huang, L., Electrochemical behaviors of a Li_3N modified Li metal electrode in secondary lithium batteries. *J. Power Sources* **2011,** *196* (19), 8091-8097.

121. Zhang, Y. J.; Wang, W.; Tang, H.; Bai, W. Q.; Ge, X.; Wang, X. L.; Gu, C. D.; Tu, J. P., An ex–situ nitridation route to synthesize Li_3N–modified Li anodes for lithium secondary batteries. *J. Power Sources* **2015,** *277*, 304-311.

122. Li, N. W.; Yin, Y. X.; Yang, C. P.; Guo, Y. G., An Artificial Solid Electrolyte Interphase Layer for Stable Lithium Metal Anodes. *Adv. Mater.* **2016,** *28* (9), 1853-1858.

123. Liu, J. Q.; Zhuang, Q. C.; Shi, Y. L.; Yan, X.; Zhao, X.; Chen, X., Tertiary butyl hydroquinone as a novel additive for SEI film formation in lithium–ion batteries. *RSC Adv.* **2016,** *6* (49), 42885-42891.

124. Choi, N. S.; Lee, Y. M.; Cho, K. Y.; Ko, D. H.; Park, J. K., Protective layer with oligo(ethylene glycol) borate anion receptor for lithium metal electrode stabilization. *Electrochem. Commun.* **2004,** *6* (12), 1238-1242.

125. Choi, N. S.; Lee, Y. M.; Seol, W.; Lee, J. A.; Park, J. K., Protective coating of lithium metal electrode for interfacial enhancement with gel polymer electrolyte. *Solid State Ion.* **2004,** *172* (1), 19-24.

126. Kozen, A. C.; Lin, C. F.; Pearse, A. J.; Schroeder, M. A.; Han, X.; Hu, L.; Lee, S. B.; Rubloff, G. W.; Noked, M., Next–Generation Lithium Metal Anode Engineering via Atomic Layer Deposition. *ACS Nano* **2015,** *9* (6), 5884-5892.

127. Liu, Y.; Lin, D.; Yuen, P. Y.; Liu, K.; Xie, J.; Dauskardt, R. H.; Cui, Y., An Artificial Solid Electrolyte Interphase with High Li–Ion Conductivity, Mechanical Strength, and Flexibility for Stable Lithium Metal Anodes. *Adv. Mater.* **2017,** *29* (10), 1605531.

128. Yan, K.; Lee, H. W.; Gao, T.; Zheng, G.; Yao, H.; Wang, H.; Lu, Z.; Zhou, Y.; Liang, Z.; Liu, Z.; Chu, S.; Cui, Y., Ultrathin Two–Dimensional Atomic Crystals as Stable Interfacial Layer for Improvement of Lithium Metal Anode. *Nano Lett.* **2014,** *14* (10), 6016-6022.

129. Zhang, Y. j.; Xia, X. h.; Wang, D. h.; Wang, X. i.; Gu, C. d.; Tu, J. p., Integrated reduced graphene oxide multilayer/Li composite anode for rechargeable lithium metal batteries. *RSC Adv.* **2016,** *6* (14), 11657-11664.

130. Zheng, G.; Lee, S. W.; Liang, Z.; Lee, H. W.; Yan, K.; Yao, H.; Wang, H.; Li, W.; Chu, S.; Cui, Y., Interconnected hollow carbon nanospheres for stable lithium metal anodes. *Nat. Nanotechnol.* **2014,** *9*, 618.

131. Liu, K.; Pei, A.; Lee, H. R.; Kong, B.; Liu, N.; Lin, D.; Liu, Y.; Liu, C.; Hsu, P. c.; Bao, Z.; Cui, Y., Lithium Metal Anodes with an Adaptive "Solid–Liquid" Interfacial Protective Layer. *J. Am. Chem. Soc.* **2017,** *139* (13), 4815-4820.

132. Zhu, B.; Jin, Y.; Hu, X.; Zheng, Q.; Zhang, S.; Wang, Q.; Zhu, J., Poly(dimethylsiloxane) Thin Film as a Stable Interfacial Layer for High–Performance Lithium–Metal Battery Anodes. *Adv. Mater.* **2017,** *29* (2), 1603755.

133. Lu, Y.; Tikekar, M.; Mohanty, R.; Hendrickson, K.; Ma, L.; Archer, L. A., Stable Cycling of Lithium Metal Batteries Using High Transference Number Electrolytes. *Adv. Energy Mater.* **2015,** *5* (9), 1402073.

134. Cheng, X. B.; Hou, T. Z.; Zhang, R.; Peng, H. J.; Zhao, C. Z.; Huang, J. Q.; Zhang, Q., Dendrite–Free Lithium Deposition Induced by Uniformly Distributed Lithium–Ions for Efficient Lithium Metal Batteries. *Adv. Mater.* **2016**, 28 (15), 2888-2895.

135. Lin, D.; Liu, Y.; Liang, Z.; Lee, H. W.; Sun, J.; Wang, H.; Yan, K.; Xie, J.; Cui, Y., Layered reduced graphene oxide with nanoscale interlayer gaps as a stable host for lithium metal anodes. *Nat. Nanotechnol.* **2016,** *11*, 626-632.

136. Liu, Y.; Lin, D.; Liang, Z.; Zhao, J.; Yan, K.; Cui, Y., Lithium–coated polymeric matrix as a minimum volume–change and dendrite–free lithium metal anode. *Nat. Commun.* **2016,** *7*, 10992.

137. Yan, K.; Lu, Z.; Lee, H. W.; Xiong, F.; Hsu, P. C.; Li, Y.; Zhao, J.; Chu, S.; Cui, Y., Selective deposition and stable encapsulation of lithium through heterogeneous seeded growth. *Nat. Energy* **2016,** *1*, 16010.

138. Ryou, M. H.; Lee, Y. M.; Lee, Y.; Winter, M.; Bieker, P., Mechanical Surface Modification of Lithium Metal: Towards Improved Li Metal Anode Performance by Directed Li Plating. *Adv. Funct. Mater.* **2015,** *25* (6), 834-841.

139. Chung, K. i.; Kim, W. S.; Choi, Y. K., Lithium phosphorous oxynitride as a passive layer for anodes in lithium secondary batteries. *J. Electroanal. Chem.* **2004,** *566* (2), 263-267.

140. Lee, H.; Lee, D. J.; Kim, Y. J.; Park, J. K.; Kim, H. T., A simple composite protective layer coating that enhances the cycling stability of lithium metal batteries. *J. Power Sources* **2015,** *284*, 103-108.

141. Sudo, R.; Nakata, Y.; Ishiguro, K.; Matsui, M.; Hirano, A.; Takeda, Y.; Yamamoto, O.; Imanishi, N., Interface behavior between garnet–type lithium–conducting solid electrolyte and lithium metal. *Solid State Ion.* **2014,** *262*, 151-154.

142. Tu, Z.; Kambe, Y.; Lu, Y.; Archer, L. A., Nanoporous Polymer–Ceramic Composite Electrolytes for Lithium Metal Batteries. *Adv. Energy Mater.* **2014,** *4* (2), 1300654.

143. Zhang, J.; Bai, Y.; Sun, X. G.; Li, Y.; Guo, B.; Chen, J.; Veith, G. M.; Hensley, D. K.; Paranthaman, M. P.; Goodenough, J. B.; Dai, S., Superior Conductive Solid–like Electrolytes: Nanoconfining Liquids within the Hollow Structures. *Nano Lett.* **2015,** *15* (5), 3398-3402.

144. Danuta, H.; Juliusz, U. Electric dry cells and storage batteries. US3043896A, 1962.

145. Bhaskara, R. M. L. Organic electrolyte cells. US3413154A, 1968.

146. Abraham, K. M.; Rauh, R. D.; Brummer, S. B., A low temperature Na–S battery incorporating A soluble S cathode. *Electrochim. Acta* **1978,** *23* (6), 501-507.

147. Ji, X.; Nazar, L. F., Advances in Li–S batteries. *J. Mater. Chem.* **2010,** *20* (44), 9821-9826.

148. Ji, X.; Lee, K. T.; Nazar, L. F., A highly ordered nanostructured carbon–sulphur cathode for lithium–sulphur batteries. *Nat. Mater.* **2009,** *8*, 500-506.

149. Elazari, R.; Salitra, G.; Garsuch, A.; Panchenko, A.; Aurbach, D., Sulfur–Impregnated Activated Carbon Fiber Cloth as a Binder–Free Cathode for Rechargeable Li–S Batteries. *Adv. Mater.* **2011,** *23* (47), 5641-5644.

150. Schuster, J.; He, G.; Mandlmeier, B.; Yim, T.; Lee, K. T.; Bein, T.; Nazar, L. F., Spherical Ordered Mesoporous Carbon Nanoparticles with High Porosity for Lithium–Sulfur Batteries. *Angew. Chem. Int. Ed.* **2012,** *51* (15), 3591-3595.

151. Song, J.; Xu, T.; Gordin, M. L.; Zhu, P.; Lv, D.; Jiang, Y. B.; Chen, Y.; Duan, Y.; Wang, D., Nitrogen–Doped Mesoporous Carbon Promoted Chemical Adsorption of Sulfur and Fabrication of High–Areal–Capacity Sulfur Cathode with Exceptional Cycling Stability for Lithium–Sulfur Batteries. *Adv. Funct. Mater.* **2014,** *24* (9), 1243-1250.

152. Zhang, S. S., A new finding on the role of $LiNO_3$ in lithium–sulfur battery. *J. Power Sources* **2016,** *322*, 99-105.

153. Markevich, E.; Salitra, G.; Rosenman, A.; Talyosef, Y.; Chesneau, F.; Aurbach, D., The effect of a solid electrolyte interphase on the mechanism of operation of lithium–sulfur batteries. *J. Mater. Chem. A* **2015,** *3* (39), 19873-19883.

154. Markevich, E.; Salitra, G.; Rosenman, A.; Talyosef, Y.; Chesneau, F.; Aurbach, D., Fluoroethylene carbonate as an important component in organic carbonate electrolyte solutions for lithium sulfur batteries. *Electrochem. Commun.* **2015,** *60*, 42-46.

155. Xin, S.; Gu, L.; Zhao, N. H.; Yin, Y. X.; Zhou, L. J.; Guo, Y. G.; Wan, L. J., Smaller Sulfur Molecules Promise Better Lithium–Sulfur Batteries. *J. Am. Chem. Soc.* **2012,** *134* (45), 18510-18513.

156. Chung, W. J.; Griebel, J. J.; Kim, E. T.; Yoon, H.; Simmonds, A. G.; Ji, H. J.; Dirlam, P. T.; Glass, R. S.; Wie, J. J.; Nguyen, N. A.; Guralnick, B. W.; Park, J.; Somogyi, Á.; Theato, P.; Mackay, M. E.; Sung, Y. E.; Char, K.; Pyun, J., The use of elemental sulfur as an alternative feedstock for polymeric materials. *Nat. Chem.* **2013,** *5*, 518-524.

157. Kim, J. S.; Hwang, T. H.; Kim, B. G.; Min, J.; Choi, J. W., A Lithium–Sulfur Battery with a High Areal Energy Density. *Adv. Funct. Mater.* **2014,** *24* (34), 5359-5367.

158. Girishkumar, G.; McCloskey, B.; Luntz, A. C.; Swanson, S.; Wilcke, W., Lithium–Air Battery: Promise and Challenges. *J. Phys. Chem. Lett.* **2010,** *1* (14), 2193-2203.

159. Lu, J.; Li, L.; Park, J. B.; Sun, Y. K.; Wu, F.; Amine, K., Aprotic and Aqueous Li–O_2 Batteries. *Chem. Rev.* **2014,** *114* (11), 5611-5640.

160. Feng, N.; He, P.; Zhou, H., Critical Challenges in Rechargeable Aprotic Li–O_2 Batteries. *Adv. Energy Mater.* **2016,** *6* (9), 1502303.

161. Johnson, L.; Li, C.; Liu, Z.; Chen, Y.; Freunberger, S. A.; Ashok, P. C.; Praveen, B. B.; Dholakia, K.; Tarascon, J. M.; Bruce, P. G., The role of LiO_2 solubility in O_2 reduction in aprotic solvents and its consequences for Li–O_2 batteries. *Nat. Chem.* **2014,** *6* (12), 1091-1099.

162. Aurbach, D.; McCloskey, B. D.; Nazar, L. F.; Bruce, P. G., Advances in understanding mechanisms underpinning lithium–air batteries. *Nat. Energy* **2016,** *1*, 16128.

163. Laoire, C. O.; Mukerjee, S.; Abraham, K. M.; Plichta, E. J.; Hendrickson, M. A., Influence of Nonaqueous Solvents on the Electrochemistry of Oxygen in the Rechargeable Lithium–Air Battery. *J. Phys. Chem. C* **2010,** *114* (19), 9178-9186.

164. Burke, C. M.; Pande, V.; Khetan, A.; Viswanathan, V.; McCloskey, B. D., Enhancing electrochemical intermediate solvation through electrolyte anion selection to increase nonaqueous Li–O_2 battery capacity. *Proc. Natl. Acad. Sci. U.S.A.* **2015,** *112* (30), 9293-9298.

165. Meini, S.; Piana, M.; Tsiouvaras, N.; Garsuch, A.; Gasteiger, H. A., The Effect of Water on the Discharge Capacity of a Non–Catalyzed Carbon Cathode for Li–O_2 Batteries. *Electrochemical and Solid-State Letters* **2012,** *15* (4), A45-A48.

166. Aetukuri, N. B.; McCloskey, B. D.; García, J. M.; Krupp, L. E.; Viswanathan, V.; Luntz, A. C., Solvating additives drive solution–mediated electrochemistry and enhance toroid growth in non–aqueous Li–O_2 batteries. *Nat. Chem.* **2014,** *7*, 50-56.

167. Ogasawara, T.; Débart, A.; Holzapfel, M.; Novák, P.; Bruce, P. G., Rechargeable Li_2O_2 Electrode for Lithium Batteries. *J. Am. Chem. Soc.* **2006,** *128* (4), 1390-1393.

168. Freunberger, S. A.; Chen, Y.; Peng, Z.; Griffin, J. M.; Hardwick, L. J.; Bardé, F.; Novák, P.; Bruce, P. G., Reactions in the Rechargeable Lithium–O_2 Battery with Alkyl Carbonate Electrolytes. *J. Am. Chem. Soc.* **2011,** *133* (20), 8040-8047.

169. Jung, H. G.; Hassoun, J.; Park, J. B.; Sun, Y. K.; Scrosati, B., An improved high–performance lithium–air battery. *Nat. Chem.* **2012,** *4* (7), 579-585.

170. Laoire, C.; Mukerjee, S.; Plichta, E. J.; Hendrickson, M. A.; Abraham, K. M., Rechargeable Lithium/TEGDME–$LiPF_6$/O_2 Battery. *J. Electrochem. Soc.* **2011,** *158* (3), A302-A308.

171. Chen, Y.; Freunberger, S. A.; Peng, Z.; Bardé, F.; Bruce, P. G., Li–O_2 Battery with a Dimethylformamide Electrolyte. *J. Am. Chem. Soc.* **2012,** *134* (18), 7952-7957.

172. Bryantsev, V. S.; Uddin, J.; Giordani, V.; Walker, W.; Addison, D.; Chase, G. V., The Identification of Stable Solvents for Nonaqueous Rechargeable Li–Air Batteries. *J. Electrochem. Soc.* **2013,** *160* (1), A160-A171.

173. Walker, W.; Giordani, V.; Uddin, J.; Bryantsev, V. S.; Chase, G. V.; Addison, D., A Rechargeable Li–O_2 Battery Using a Lithium Nitrate/*N,N*–Dimethylacetamide Electrolyte. *J. Am. Chem. Soc.* **2013,** *135* (6), 2076-2079.

174. Peng, Z.; Freunberger, S. A.; Chen, Y.; Bruce, P. G., A Reversible and Higher–Rate Li–O_2 Battery. *Science* **2012,** *337* (6094), 563-566.

175. Trahan, M. J.; Mukerjee, S.; Plichta, E. J.; Hendrickson, M. A.; Abraham, K. M., Studies of Li–Air Cells Utilizing Dimethyl Sulfoxide–Based Electrolyte. *J. Electrochem. Soc.* **2013,** *160* (2), A259-A267.

176. Bardé, F.; Chen, Y.; Johnson, L.; Schaltin, S.; Fransaer, J.; Bruce, P. G., Sulfone–Based Electrolytes for Nonaqueous Li–O_2 Batteries. *J. Phys. Chem. C* **2014,** *118* (33), 18892-18898.

177. Bryantsev, V. S.; Faglioni, F., Predicting Autoxidation Stability of Ether– and Amide–Based Electrolyte Solvents for Li–Air Batteries. *J. Phys. Chem. A* **2012,** *116* (26), 7128-7138.

178. Freunberger, S. A.; Chen, Y.; Drewett, N. E.; Hardwick, L. J.; Bardé, F.; Bruce, P. G., The Lithium–Oxygen Battery with Ether–Based Electrolytes. *Angew. Chem. Int. Ed.* **2011,** *50* (37), 8609-8613.

179. Khetan, A.; Luntz, A.; Viswanathan, V., Trade–Offs in Capacity and Rechargeability in Nonaqueous Li–O_2 Batteries: Solution-Driven Growth versus Nucleophilic Stability. *J. Phys. Chem. Lett.* **2015,** *6* (7), 1254-1259.

180. Kim, D. W.; Ahn, S. M.; Kang, J.; Suk, J.; Kim, H. K.; Kang, Y., In situ real–time and quantitative investigation on the stability of non–aqueous lithium oxygen battery electrolytes. *J. Mater. Chem. A* **2016,** *4* (17), 6332-6341.

181. Kwabi, D. G.; Batcho, T. P.; Amanchukwu, C. V.; Ortiz–Vitoriano, N.; Hammond, P.; Thompson, C. V.; Shao–Horn, Y., Chemical Instability of Dimethyl Sulfoxide in Lithium–Air Batteries. *J. Phys. Chem. Lett.* **2014,** *5* (16), 2850-2856.

182. McCloskey, B. D.; Valery, A.; Luntz, A. C.; Gowda, S. R.; Wallraff, G. M.; Garcia, J. M.; Mori, T.; Krupp, L. E., Combining Accurate O_2 and Li_2O_2 Assays to Separate Discharge and Charge Stability Limitations in Nonaqueous Li–O_2 Batteries. *J. Phys. Chem. Lett.* **2013,** *4* (17), 2989-2993.

183. Ryan, K. R.; Trahey, L.; Ingram, B. J.; Burrell, A. K., Limited Stability of Ether–Based Solvents in Lithium–Oxygen Batteries. *J. Phys. Chem. C* **2012,** *116* (37), 19724-19728.

184. Sharon, D.; Afri, M.; Noked, M.; Garsuch, A.; Frimer, A. A.; Aurbach, D., Oxidation of Dimethyl Sulfoxide Solutions by Electrochemical Reduction of Oxygen. *J. Phys. Chem. Lett.* **2013,** *4* (18), 3115-3119.

185. Sharon, D.; Hirsberg, D.; Afri, M.; Garsuch, A.; Frimer, A. A.; Aurbach, D., Reactivity of Amide Based Solutions in Lithium–Oxygen Cells. *J. Phys. Chem. C* **2014,** *118* (28), 15207-15213.

186. Jeong, Y. S.; Park, J. B.; Jung, H. G.; Kim, J.; Luo, X.; Lu, J.; Curtiss, L.; Amine, K.; Sun, Y. K.; Scrosati, B.; Lee, Y. J., Study on the Catalytic Activity of Noble Metal Nanoparticles on Reduced Graphene Oxide for Oxygen Evolution Reactions in Lithium–Air Batteries. *Nano Lett.* **2015,** *15* (7), 4261-4268.

187. Lu, Y. C.; Xu, Z.; Gasteiger, H. A.; Chen, S.; Hamad–Schifferli, K.; Shao–Horn, Y., Platinum–Gold Nanoparticles: A Highly Active Bifunctional Electrocatalyst for Rechargeable Lithium–Air Batteries. *J. Am. Chem. Soc.* **2010,** *132* (35), 12170-12171.

188. Choi, R.; Jung, J.; Kim, G.; Song, K.; Kim, Y. I.; Jung, S. C.; Han, Y. K.; Song, H.; Kang, Y. M., Ultra–low overpotential and high rate capability in Li–O_2 batteries through surface atom arrangement of PdCu nanocatalysts. *Energy Environ. Sci.* **2014,** *7* (4), 1362-1368.

189. Lee, J. H.; Black, R.; Popov, G.; Pomerantseva, E.; Nan, F.; Botton, G. A.; Nazar, L. F., The role of vacancies and defects in $Na_{0.44}MnO_2$ nanowire catalysts for lithium–oxygen batteries. *Energy Environ. Sci.* **2012,** *5* (11), 9558-9565.

190. Maiyalagan, T.; Chemelewski, K. R.; Manthiram, A., Role of the Morphology and Surface Planes on the Catalytic Activity of Spinel $LiMn_{1.5}Ni_{0.5}O_4$ for Oxygen Evolution Reaction. *ACS Catal.* **2014,** *4* (2), 421-425.

191. Oh, S. H.; Black, R.; Pomerantseva, E.; Lee, J. H.; Nazar, L. F., Synthesis of a metallic mesoporous pyrochlore as a catalyst for lithium–O_2 batteries. *Nat. Chem.* **2012,** *4* (12), 1004-1010.

192. Shi, L.; Zhao, T.; Xu, A.; Wei, Z., Unraveling the Catalytic Mechanism of Rutile RuO_2 for the Oxygen Reduction Reaction and Oxygen Evolution Reaction in Li–O_2 Batteries. *ACS Catal.* **2016,** *6* (9), 6285-6293.

193. Yilmaz, E.; Yogi, C.; Yamanaka, K.; Ohta, T.; Byon, H. R., Promoting Formation of Noncrystalline Li_2O_2 in the Li–O_2 Battery with RuO_2 Nanoparticles. *Nano Lett.* **2013,** *13* (10), 4679-4684.

194. Yang, C.; Wong, R. A.; Hong, M.; Yamanaka, K.; Ohta, T.; Byon, H. R., Unexpected Li_2O_2 Film Growth on Carbon Nanotube Electrodes with CeO_2 Nanoparticles in Li–O_2 Batteries. *Nano Lett.* **2016,** *16* (5), 2969-2974.

195. Lu, J.; Jung Lee, Y.; Luo, X.; Chun Lau, K.; Asadi, M.; Wang, H. H.; Brombosz, S.; Wen, J.; Zhai, D.; Chen, Z.; Miller, D. J.; Sub Jeong, Y.; Park, J. B.; Zak Fang, Z.; Kumar, B.; Salehi–Khojin, A.; Sun, Y. K.; Curtiss, L. A.; Amine, K., A lithium–oxygen battery based on lithium superoxide. *Nature* **2016,** *529* (7586), 377-382.

196. Yadegari, H.; Norouzi Banis, M.; Lushington, A.; Sun, Q.; Li, R.; Sham, T. K.; Sun, X., A bifunctional solid state catalyst with enhanced cycling stability for Na and Li–O_2 cells: revealing the role of solid state catalysts. *Energy Environ. Sci.* **2017,** *10* (1), 286-295.

197. Guo, Z.; Zhou, D.; Dong, X.; Qiu, Z.; Wang, Y.; Xia, Y., Ordered Hierarchical Mesoporous/Macroporous Carbon: A High–Performance Catalyst for Rechargeable Li–O_2 Batteries. *Adv. Mater.* **2013,** *25* (39), 5668-5672.

198. Liu, C.; Younesi, R.; Tai, C. W.; Valvo, M.; Edstrom, K.; Gustafsson, T.; Zhu, J., 3–D binder−free graphene foam as a cathode for high capacity Li–O_2 batteries. *J. Mater. Chem. A* **2016,** *4* (25), 9767-9773.

199. Chen, Y.; Freunberger, S. A.; Peng, Z.; Fontaine, O.; Bruce, P. G., Charging a Li–O_2 battery using a redox mediator. *Nat. Chem.* **2013,** *5* (6), 489-494.

200. Bergner, B. J.; Hofmann, C.; Schurmann, A.; Schroder, D.; Peppler, K.; Schreiner, P. R.; Janek, J., Understanding the fundamentals of redox mediators in Li–O_2 batteries: a case study on nitroxides. *Phys. Chem. Chem. Phys.* **2015,** *17* (47), 31769-31779.

201. Bergner, B. J.; Schürmann, A.; Peppler, K.; Garsuch, A.; Janek, J., TEMPO: A Mobile Catalyst for Rechargeable Li–O_2 Batteries. *J. Am. Chem. Soc.* **2014,** *136* (42), 15054-15064.

202. Feng, N.; He, P.; Zhou, H., Enabling Catalytic Oxidation of Li_2O_2 at the Liquid–Solid Interface: The Evolution of an Aprotic Li–O_2 Battery. *ChemSusChem* **2015,** *8* (4), 600-602.

203. Feng, N.; Mu, X.; Zhang, X.; He, P.; Zhou, H., Intensive Study on the Catalytical Behavior of *N*–Methylphenothiazine as a Soluble Mediator to Oxidize the Li_2O_2 Cathode of the Li–O_2 Battery. *ACS Appl. Mater. Interfaces* **2017,** *9* (4), 3733-3739.

204. Kundu, D.; Black, R.; Adams, B.; Nazar, L. F., A Highly Active Low Voltage Redox Mediator for Enhanced Rechargeability of Lithium–Oxygen Batteries. *ACS Cent. Sci.* **2015,** *1* (9), 510-515.

205. Lim, H. D.; Lee, B.; Zheng, Y.; Hong, J.; Kim, J.; Gwon, H.; Ko, Y.; Lee, M.; Cho, K.; Kang, K., Rational design of redox mediators for advanced Li–O_2 batteries. *Nat. Energy* **2016,** *1*, 16066.

206. Kwak, W. J.; Hirshberg, D.; Sharon, D.; Afri, M.; Frimer, A. A.; Jung, H. G.; Aurbach, D.; Sun, Y. K., Li–O_2 cells with LiBr as an electrolyte and a redox mediator. *Energy Environ. Sci.* **2016,** *9* (7), 2334-2345.

207. Lee, C. K.; Park, Y. J., CsI as Multifunctional Redox Mediator for Enhanced Li–Air Batteries. *ACS Appl. Mater. Interfaces* **2016,** *8* (13), 8561-8567.

208. Liang, Z.; Lu, Y. C., Critical Role of Redox Mediator in Suppressing Charging Instabilities of Lithium–Oxygen Batteries. *J. Am. Chem. Soc.* **2016,** *138* (24), 7574-7583.

209. Lim, H. D.; Song, H.; Kim, J.; Gwon, H.; Bae, Y.; Park, K. Y.; Hong, J.; Kim, H.; Kim, T.; Kim, Y. H.; Lepró, X.; Ovalle–Robles, R.; Baughman, R. H.; Kang, K., Superior Rechargeability and Efficiency of Lithium–Oxygen Batteries: Hierarchical Air Electrode Architecture Combined with a Soluble Catalyst. *Angew. Chem. Int. Ed.* **2014,** *53* (15), 3926-3931.

210. Zhang, T.; Liao, K.; He, P.; Zhou, H., A self–defense redox mediator for efficient lithium–O_2 batteries. *Energy Environ. Sci.* **2016,** *9* (3), 1024-1030.

211. Sun, D.; Shen, Y.; Zhang, W.; Yu, L.; Yi, Z.; Yin, W.; Wang, D.; Huang, Y.; Wang, J.; Wang, D.; Goodenough, J. B., A Solution–Phase Bifunctional Catalyst for Lithium–Oxygen Batteries. *J. Am. Chem. Soc.* **2014,** *136* (25), 8941-8946.

212. Yao, K. P. C.; Frith, J. T.; Sayed, S. Y.; Bardé, F.; Owen, J. R.; Shao–Horn, Y.; Garcia–Araez, N., Utilization of Cobalt Bis(terpyridine) Metal Complex as Soluble Redox Mediator in Li–O_2 Batteries. *J. Phys. Chem. C* **2016,** *120* (30), 16290-16297.

213. Bergner, B. J.; Busche, M. R.; Pinedo, R.; Berkes, B. B.; Schröder, D.; Janek, J., How To Improve Capacity and Cycling Stability for Next Generation Li–O_2 Batteries: Approach with a Solid Electrolyte and Elevated Redox Mediator Concentrations. *ACS Appl. Mater. Interfaces* **2016,** *8* (12), 7756-7765.

214. Lee, D. J.; Lee, H.; Kim, Y. J.; Park, J. K.; Kim, H. T., Sustainable Redox Mediation for Lithium–Oxygen Batteries by a Composite Protective Layer on the Lithium–Metal Anode. *Adv. Mater.* **2016,** *28* (5), 857-863.

215. Salikhov, K. M.; Zavoiskaya, N. E., Zavoisky and the Discovery of EPR. *Resonance* **2015,** *20* (11), 963-968.

216. Freed, J. H., Electron Spin Resonance. *Annu. Rev. Phys. Chem.* **1972,** *23* (1), 265-310.

217. Freunberger, S. A., Batteries: Charging ahead rationally. *Nat. Energy* **2016,** *1*, 16074.

218. Buhrmester, C.; Moshurchak, L.; Wang, R. L.; Dahn, J. R., Phenothiazine Molecules: Possible Redox Shuttle Additives for Chemical Overcharge and Overdischarge Protection for Lithium–Ion Batteries. *J. Electrochem. Soc.* **2006,** *153* (2), A288-A294.

219. Ottakam Thotiyl, M. M.; Freunberger, S. A.; Peng, Z.; Bruce, P. G., The Carbon Electrode in Nonaqueous Li–O_2 Cells. *J. Am. Chem. Soc.* **2013,** *135* (1), 494-500.

220. Park, J. B.; Lee, S. H.; Jung, H. G.; Aurbach, D.; Sun, Y. K., Redox Mediators for Li–O_2 Batteries: Status and Perspectives. *Adv. Mater.* **2018**, 30, 1704162.

221. Paduszek, B.; Kalinowski, M. K., Redox behaviour of phenothiazine and phenazine in organic solvents. *Electrochim. Acta* **1983,** *28* (5), 639-642.

222. Izutsu, K., Properties of Solvents and Solvent Classification. In *Electrochemistry in Nonaqueous Solutions*, Wiley-VCH Verlag GmbH & Co. KGaA: 2009; pp 1-25.

223. Izutsu, K., Solvation and Complex Formation of Ions and Behavior of Electrolytes. In *Electrochemistry in Nonaqueous Solutions*, Wiley-VCH Verlag GmbH & Co. KGaA: 2009; pp 27-61.

224. Izutsu, K., Acid–Base Reactions in Nonaqueous Solvents. In *Electrochemistry in Nonaqueous Solutions*, Wiley-VCH Verlag GmbH & Co. KGaA: 2009; pp 63-87.

225. Izutsu, K., Redox Reactions in Nonaqueous Solvents. In *Electrochemistry in Nonaqueous Solutions*, Wiley-VCH Verlag GmbH & Co. KGaA: 2009; pp 89-110.

226. Mukherjee, S.; Vannice, M. A., Solvent effects in liquid–phase reactions: I. Activity and selectivity during citral hydrogenation on Pt/SiO_2 and evaluation of mass transfer effects. *J. Catal.* **2006,** *243* (1), 108-130.

227. Bae, Y.; Yun, Y. S.; Lim, H. D.; Lee, H.; Kim, Y. J.; Kim, J.; Park, H.; Ko, Y.; Lee, S.; Kwon, H. J.; Kim, H.; Kim, H. T.; Im, D.; Kang, K., Tuning the Carbon Crystallinity for Highly Stable Li–O_2 Batteries. *Chem. Mater.* **2016,** *28* (22), 8160-8169.

228. Liu, J.; Zhao, X.; Al–Galiby, Q.; Huang, X.; Zheng, J.; Li, R.; Huang, C.; Yang, Y.; Shi, J.; Manrique, D. Z.; Lambert, C. J.; Bryce, M. R.; Hong, W., Radical–Enhanced Charge Transport in Single–Molecule Phenothiazine Electrical Junctions. *Angew. Chem.* **2017,** *129* (42), 13241-13245.

229. Soo Kang, Y.; A. Jung, J.; Kevan, L., Electron paramagnetic resonance and electron nuclear double resonance studies of photoinduced charge separation from *N*–methylphenothiazine doped into poly(ethylene oxide) and poly(propylene oxide) polymer matrices. *J. Chem. Soc. Faraday Trans.* **1998,** *94* (21), 3247-3250.

230. Padilla, A. G. Study of 10–Methylphenothiazine Cation Radical Chemistry. Texas Tech University, 1975.

231. Aurbach, D.; Gofer, Y.; Langzam, J., The Correlation Between Surface Chemistry, Surface Morphology, and Cycling Efficiency of Lithium Electrodes in a Few Polar Aprotic Systems. *J. Electrochem. Soc.* **1989,** *136* (11), 3198-3205.

232. Lee, H.; Lee, D. J.; Lee, J. N.; Song, J.; Lee, Y.; Ryou, M. H.; Park, J. K.; Lee, Y. M., Chemical aspect of oxygen dissolved in a dimethyl sulfoxide–based electrolyte on lithium metal. *Electrochim. Acta* **2014,** *123*, 419-425.

233. Alcolea Palafox, M.; Gil, M.; Núñez, J. L.; Tardajos, G., Study of phenothiazine and *N*–methyl phenothiazine by infrared, raman, ^{1}H–, and ^{13}C–NMR spectroscopies. *Int. J. Quantum Chem.* **2002,** *89* (3), 147-171.

234. Ismail, I.; Noda, A.; Nishimoto, A.; Watanabe, M., XPS study of lithium surface after contact with lithium–salt doped polymer electrolytes. *Electrochim. Acta* **2001,** *46* (10–11), 1595-1603.

235. Kanamura, K.; Tamura, H.; Shiraishi, S.; Takehara, Z. i., XPS Analysis of Lithium Surfaces Following Immersion in Various Solvents Containing $LiBF_4$. *J. Electrochem. Soc.* **1995,** *142* (2), 340-347.

236. Gilman, H.; Dietrich, J. J., Lithium Cleavages of Some Heterocycles in Tetrahydrofuran. II. *J. Am. Chem. Soc.* **1958,** *80* (2), 380-383.

237. Uddin, J.; Bryantsev, V. S.; Giordani, V.; Walker, W.; Chase, G. V.; Addison, D., Lithium Nitrate As Regenerable SEI Stabilizing Agent for Rechargeable Li/O_2 Batteries. *J. Phys. Chem. Lett.* **2013,** *4* (21), 3760-3765.

238. Sharon, D.; Hirsberg, D.; Afri, M.; Chesneau, F.; Lavi, R.; Frimer, A. A.; Sun, Y. K.; Aurbach, D., Catalytic Behavior of Lithium Nitrate in $Li–O_2$ Cells. *ACS Appl. Mater. Interfaces* **2015,** *7* (30), 16590-16600.